UNIVERSIDAD NACIONAL AUTÓNOMA DE MEXICO
PROGRAMA DE MAESTRÍA Y DOCTORADO EN CIENCIAS MATEMÁTICAS Y DE
LA ESPECIALIZACIÓN EN ESTADÍSTICA APLICADA

MODELOS NO LOCALES EN LA TEORÍA DE ONDAS EN AGUAS
SOMERAS CON PROFUNDIDAD VARIABLE

TESIS
QUE PARA OPTAR POR EL GRADO DE:
DOCTORA EN CIENCIAS

PRESENTA:
ROSA MARIA VARGAS MAGAÑA

TUTOR O TUTORES PRINCIPALES

DR. PANAYOTIS PANAYOTAROS
INSTITUTO DE INVESTIGACIÓN EN MATEMÁTICAS APLICADAS Y EN SISTEMAS
UNIVERSIDAD NACIONAL AUTÓNOMA DE MÉXICO

MIEMBROS DEL COMITÉ TUTOR

DR. ARTURO OLVERA CHÁVEZ
INSTITUTO DE INVESTIGACIÓN EN MATEMÁTICAS APLICADAS Y EN SISTEMAS
UNIVERSIDAD NACIONAL AUTÓNOMA DE MÉXICO

DR. ANTONIO CAPELLA KORT
INSTITUTO DE MATEMÁTICAS
UNIVERSIDAD NACIONAL AUTÓNOMA DE MÉXICO

CIUDAD DE MÉXICO, JUNIO DE 2017

Modelos no locales en la teoría de ondas en aguas someras con profundidad variable.

T E S I S

Que para obtener el grado de:

DOCTOR EN CIENCIAS MATEMÁTICAS

Presenta

Rosa María Vargas Magaña

Director de la Tesis: Dr. Panayotis Panayotaros

ii

Contents

4 Discussion and future work 93

List of Figures

List of Tables

Chapter 1

Introduction

La descripción precisa de la propagación de ondas en la superficie de un fluido es un tema de gran interés para físicos y matemáticos.

En el siglo XIX d'Alambert, Euler, Lagrange y Bernoulli establecieron el sistema de ecuaciones que gobierna el movimiento de las ondas de superficie en un fluido perfecto e irrotacional bajo el efecto de la gravedad.

Desde entonces existe una profunda investigación dedicada al estudio de las ondas en agua en una amplia gama de problemas que van desde los que atañen a la ingeniería costera, la geofísica etc., hasta los que abordan aspectos teóricos de las ecuaciones diferenciales parciales y del comportamiento cualitativo y cuantitativo de sus soluciones.

En años recientes el progreso en el estudio teórico y computacional del problema de ondas en agua obedece directamente a cuatro factores que, bajo distintos niveles de interacción a lo largo del tiempo, han generado una rica y basta teoría de ondas de superficie en fluidos.

A continuación se expone brevemente la naturaleza y la relevancia de estos aspectos. Además, cuando corresponde, se indican las contribuciones que dentro de esta tesis se realizan a los mismos.

I. El primer aspecto del que haremos mención corresponde a la derivación de *Modelos simplificados de ondas en agua.*

   Diversos científicos e ingenieros se han enfocado en la derivación de modelos simplificados de las ecuaciones de ondas en agua los cuales resultan ser excelentes aproximaciones cualitativas y cuantitativas para el estudio de problemas bajo diferentes regímenes físicos.

   Ejemplos de estos modelos en aguas someras son las ecuaciones: Korteweg-de Vries (1895) [33], Boussinesq (1871) [34], Benjamin et al. (1972) [35],

1

Serre (1953) [36], Green and Naghdi (1976) [37], Camassa and Holm (1993) [38], Kadomtsev - Petviashvili (1970) [39] entre muchos otros.

Estos modelos son fruto de una abstracción e idealización del fenómeno físico que se desea estudiar y que obedece a las leyes que rigen la materia y a la basta teoría de la mecánica de fluidos y principalmente al desarrollo del análisis matemático, del cálculo variacional y de métodos asintóticos.

La relevancia de la derivación de estos modelos radica en que con cada uno de ellos es posible capturar características escenciales del fenómeno que se desea estudiar permitiento abstraer y discernir las cantidades importantes que rigen el movimiento de las ondas en diversos ambientes físicos y también bajo distintos tipos de longitud de onda.

▶ En la *Sección* 2.1 se introduce un modelo que describe la propagación bidireccional de ondas en agua con profundidad variable. El modelo descrito por (2.26) es un modelo, no local, que se enmarca en la teoría de ondas en aguas someras, mantiene el término de dispersión exacta obtenido de la linearización de las ecuaciones de Euler y describe los efectos de variaciones de orden grande de la profundidad variable, relativo a la profundidad media del fluido.

La introducción de dicho modelo es el punto de partida de la investigación y en general puede afirmarse que la derivación y estudio de nuevos modelos de ondas en agua ha sido un factor clave para la solución de problemas que atañen desde fenómenos geofísicos hasta aspectos teóricos sobre el comportamiento de las ecuaciones diferenciales parciales y sus soluciones.

II. Otro aspecto que ha sido muy relevante para el progreso de la teoría de ondas en agua corresponde con el desarrollo del *Análisis Asintótico de los operadores y de las soluciones.*

Gran parte de los modelos que surgen en diversas aplicaciones a problemas de la vida real están descritos en terminos de ecuaciones diferenciales parciales y estas ecuaciones raramente pueden resolverse analíticamente.

En ciertos casos, cuando pueda encontrarse una fórmula de la solución, no existe en general una forma directa de analizarla y/o de calcularla. Consecuentemente, los métodos y análisis asintóticos para el análisis del comportamiento de las soluciones y la discretización de los operadores e integradores que están envueltos en las ecuaciones diferenciales parciales se han convertido en procedimietos necesarios para el progreso en el entendimiento de los fenómenos que modelan dichas ecuaciones.

Ejemplos de este tipo de análisis los podemos encontrar en la derivación y validación de ecuaciones como Korteweg-de Vries y la ecuación no lineal de Schrodinger las cuales describen diferentes aspectos de la propagación de ondas no lineales en diferentes contextos como la óptica no lineal y los plasmas.

▶ El modelo que se introduce en esta tesis se enmarca en la formulación Hamiltoniana del problema de ondas en agua la cual involucra al operador, no local, Dirichlet-Neumann que presentamos en la *Sección* 1.2 y *Sección* 2.1.

Un problema que debe afrontarse al abordar dicha formulación es que no existe una fórmula explícita de dicho operador para dominios con topografía variable. Es por ello que el papel de la teoría de onda larga presentada en la *Sección* 1.3 junto con la teoría de perturbación estándar del Hamiltoniano son las herramientas matemáticas que se utilizan para derivar diversas aproximaciones de onda larga de dicho operador y con ello dar origen a los modelos de onda larga clásicos que se conocen para fondo plano.

Dicho enfoque fue la base formal que dio origen a la aproximación propuesta en esta tesis para el caso de profundidad variable del operador Dirichlet Neumann (2.25). El operador propuesto se construyó de tal manera que satisface características estructurales que caracterizan el operador Dirichlet-Neumann para fondo plano. Algunas de estas propiedades se muestran en forma análitica y otras numéricamente en la *Sección* 2.2.

Una contribución muy importante y crucial para la continuación de la investigación fue la discretización en el espacio de Fourier del operador (2.25) la cual se muestra en la *Sección* 2.1 y se desarrolla detalladamente en el *Apéndice* **A** ubicado en 2.5.

III. Otro aspecto que ha acompañado el desarrollo de la teoría y que ha sido promotor y testigo de enormes progresos en el entendimiento del comportamiento de las ondas en agua corresponde con el *desarrollo de métodos de medición, recolección y tratamiento de datos de laboratorio.*

La sofisticación de las herramientas para la medición de datos, ya sea en el laboratorio en donde se puede reproducir de forma controlada el fenómeno de interés observado en la naturaleza o bien *in situ*, ha hecho posible la reproducción de fenómenos y la recolección de las cantidades cuantificables del fenómeno observado a un orden de error casi imperceptible

Algunos ejemplos de estos métodos que han resultado muy útiles para medir la propagación de las ondas en agua son, el *Método de Schlieren sintético* y la *Perfilometría por Transformada de Fourier*. Ello representa un progreso enorme para dar certeza y respaldo a los modelos teóricos y métodos asintóticos mencionados en el aspecto anterior.

IV. Finalmente y no de menor importancia haremos mención de un aspecto que desde finales del siglo pasado hasta la actualidad se ha destacado en el desarrollo de la teoría de ondas en agua, esto es, la *Modelación computacional.*

La enorme capacidad de cómputo que existe en la actualidad aunado a la eficiencia, precisión y estabilidad de esquemas numéricos así como al desarrollo de lenguajes de programación, han hecho posible la integración de las ecuaciones que gobiernan la evolución de las ondas de superficie para un fluido perfecto en un dominio con batimetría variable bajo determinadas condiciones iniciales por periodos largos de tiempo.

Esta realidad computacional se perfila para los años venideros en una herramienta muy poderosa para adentrarse en problemas que superan la teoría y la reproducción controloda de los fenómenos en el laboratorio permitiéndonos abordar cuestiones de muy diversa índole en el campo de la ciencia reduciendo costos y esfuerzos.

▶ En la *subsección* 2.4 se presentan los resultados de un análisis espectral del operador (2.25) para diferentes batimetrías. En la *Sección* 2.5 se presentan los resultados de la integración numérica del sistema Whitham Boussinesq para diferentes batimetrías. Las ecuaciones de evolución así como su discretización en el espacio de Fourier, se desarrolla en la *Subsección* 2.1.2 y en el *Apéndice* **A** ubicado en 2.5.

▶ Otro problema clásico de la teoría de ondas en agua que se aborda en la tesis, en donde el cálculo numérico juega un papel crucial, es la existencia de soluciones correspondientes a modos transversales y modos atrapados para geometrías no triviales del dominio del fluido, el cual corresponde a un problema clásico en el área que abordaron Lamb, Kelland, Ursell y más recientemente Packhman, Greenhill, Groves, Evans, Minzoni, Linton, Mei, Garipov, Zhevandrov etc.

En la *Sección* 3.2 se muestra la comparación del cómputo de soluciones exactas existentes para canales rectos infinitos con seccion transversal triangular, con los modos calculados numéricamente con nuestro operador aproximado (3.12). Ver los resultados presentados en la *Sección* 3.2.

► En la *Sección* 3.3.2 se aborda el estudio de ondas atrapadas en la superficie de una plataforma continental que se extiende en una dirección espacial en el dominio no acotado del fluido. Se presentan detalladamente las comparaciones entre los resultados numéricos que se obtienen del operador aproximado para este problema y las soluciones explícitas que presenta Mei desde su enfoque de aguas someras.

De lo expuesto anteriormente se puede apreciar que en esta tesis se muestran contribuciones principalmente en el primero, segundo y tercer aspecto. Sin embargo los investigadores experimentales han empezado a mostrar interés en probar el modelo en su laboratorio, esta oportunidad abre la posibilidad de una colaboración en un futuro cercano y de esta manera cubrir el espectro de aplicación y extensión del impacto del trabajo de investigación desarrollado en esta tesis con:

✳ La introducción de un modelo, que provee una idealización del fenómeno de propagación de ondas de agua en un fondo variable,

✳ las predicciones numéricas y los resultados que arroja el modelo propuesto ante diversos cuestionamientos del fenómeno observado y finalmente,

✳ la posibilidad de probar el modelo con mediciones reales del laboratorio o en la misma naturaleza lo cual es muy satisfactorio en este problema pues las preguntas en los dominios de geometrías no triviales que se desea estudiar y comprender trascienden el marco del análisis matemático formal.

1.1 Problema de ondas en agua

El problema de ondas en agua para un fluido ideal consiste en la descripción del movimiento de la superficie libre y la evolución del campo de velocidades de un fluido perfecto, incompresible e irrotacional bajo la influencia de la gravedad. El fluido ocupa un dominio simplemente conexo bidimensional donde h_0 es la profundidad media del dominio de fluido, $\beta(x)$ es fijo y denota el perfil de variación del fondo desde este valor y $\eta(x,t)$ representa a la superficie libre del fluido y mide la amplitud de la onda. El potencial de velocidad es una función armonica y en el fondo del dominio el movimiento del fluido es tangencial. En la superficie libre, las condiciones de frontera están dadas por la ecuación cinemática y la condición de Bernoulli.

Consideramos un fluido incompresible, irrotacional y sin viscosidad. Suponemos que la única fuerza externa que actúa sobre él es la fuerza de gravedad. Suponemos además que la presión en la superficie del fluido es constante $p = 0$.

Definimos y denotamos al dominio del fluido por :

$$D_t(\beta, \eta) := \{(x, y) : x \in \mathbb{R} - h_0 + \beta(x) < y < \eta(x, t)\} \tag{1.1}$$

y a la frontera por:

$$\partial D_t(\beta, \eta) := \{(x, y) : y = \eta(x, t) \wedge y = -h_0 + \beta(x)\}, \tag{1.2}$$

y suponemos que $\beta(x) < h_0$ para todo $x \in \mathbb{R}$. Dada la condición de incompresibilidad:

$$\operatorname{div} \overline{u} = 0 \text{ en } D_t(\beta, \eta), \tag{1.3}$$

y por la condición de irrotacionalidad, el gradiente del potencial de velocidades, φ, nos determina el campo de velocidades del fluido:

$$\overline{u} = \nabla\varphi \text{ en } D_t(\beta, \eta), \tag{1.4}$$

de esta manera obtenemos el sigiente sistema de ecuaciones mejor conocido como ecuaciones de Euler.

$$\Delta\varphi(x, y) = 0 \text{ on } D_t(\beta, \eta), \tag{1.5}$$

con las condiciones de frontera

$$\nabla\varphi \cdot N(\beta) = 0 \tag{1.6}$$

en $y = -h_0 + \beta(x)$ con $N(\beta) = (1 + (\partial_x\beta)^2)^{-\frac{1}{2}}(-\partial_x\beta, 1)$ es el vector normal exterior en la frontera rígida y las condiciones en la superficie libre son:

$$\eta_t + \eta_x\varphi_x - \varphi_y = 0 \tag{1.7}$$

$$\varphi_t + \frac{1}{2}(\varphi_x^2 + \varphi_y^2) + g\eta = 0 \tag{1.8}$$

en $y = \eta(x, t)$. Para una presentación más detallada de lacondición de cinemática y de la ecuación de Bernoulli ver libro de Lamb, [42] y libro de Whitham, [68].

En esta tesis abordaremos la versión periódica en la variable espacial de las ecuaciones (1.5)-(1.6). Por ello proponemos las siguientes condiciones de frontera $\eta(x + L, t) = \eta(x, t)$ and $\varphi(x + L, y, t) = \varphi(x, y, t)$ para algún periodo $L > 0$. La razón de considerar este marco periódico se explica principalmente por dos motivos, el más importante es la representación explícita que podemos obtener del operador Dirichlet-Neumann para dominios periódicos y del cual hablaremos más adelante. La segunda razón es la implementación y simulación numérica de las ecuaciones de evolución por medio de un método espectral de Fourier.

Definimos

$$\xi(x, t) = \varphi(x, \eta(x, t), t)$$
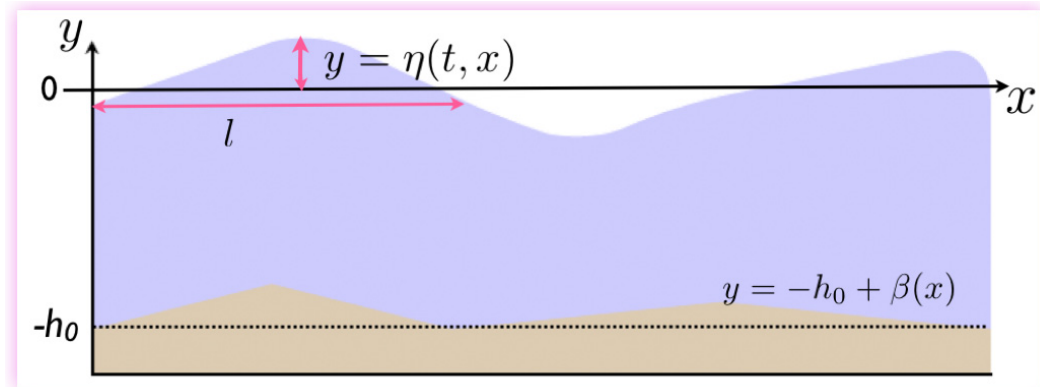
Figure 1.1: Gráfico del problema de ondas en agua.

como el potencial definido en la superficie del fluido en el tiempo t.

Una de las mayores dificultades que se presentan al intentar resolver el problema de valor inicial para las ondas en agua es que se trata de un problema de frontera libre. Respecto a este problema debe notarse que, en cada tiempo t, el dominio D_t está definido por la forma funcional de la superficie libre $\eta(x, t)$. De este modo si a un tiempo t están dados tanto $\eta(x, t)$ como ϕ en $y = \eta(x, t)$, el potencial φ en todo el dominio D_t al tiempo t queda determinado unívocamente al resolverse la ecuación de Laplace para ϕ en D_t tomando como condición de Dirichlet el potencial en la superficie libre: $\varphi(x, \eta(x, t)) = \xi(x, t)$ y como condición de Neumann la relación (1.6).

Para las ondas en agua dos dimensionales (2D), donde la superficie evoluciona como función de una variable espacial y del tiempo, hay varias técnicas que pueden utilizarse para eliminar la coordenada vertical espacial y reducir el problema a la evaluación del movimiento de la altura de la onda y del potencial de velocidad en la superficie libre.

Métodos que han probado su efectividad en el problema 2D incluyen los mapeos conformes y ecuaciones con integrales singulares que hacen uso de técnicas de análisis complejo, ver A. Nachbin and G. Papanicolaou (1994) [57], B. Fornberg (1980) [15], J. Dold (1992) [14], Zakharov (1968) [70], Radder (1992) [59].

1.1.1   Estado del arte de la formulación Hamiltoniana

Uno de los avances más relevantes que ha tenido el problema de ondas en agua en épocas recientes se atribuye al descubrimiento de Zakharov en 1968 [70] de que las ecuaciones que gobiernan el movimiento de un flujo irrotacional bajo la influencia de la gravedad en un domino en dos y tres dimensiones poseen estructura Hamiltoniana. Más tarde Broer [5] y Miles (1977) [54] obtuvieron de forma

independiente el mismo resultado.

Zakharov mostró que la altura de la onda, η, y el potencial de velocidad, φ, evaluado en la superficie libre son variables canónicas conjugadas y formuló las ecuaciones de ondas en agua como un sistema Hamiltoniano. Este derivación no es otra cosa que la formalización de la idea de que dada la naturaleza del flujo potencial, es suficiente conocer la evolución del perfil del fluido $\eta(x,t)$ en todo tiempo y el potencial de velocidades en la frontera, $\xi(x,t)$ a cada instante t para determinar el flujo en todo el dominio del fluido en el instante t. Craig and Sulem en [10] emplearon estas variables e introdujeron el operador Dirichlet-Neumann $G(\beta, \eta)$ asociado con el potencial de velocidad en la frontera explícitamente en el Hamiltoniano, el cual elimina la coordenada vertical de la formulación.

Algunas generalizaciones y planteamientos relacionados también se deben a Benjamin y Olver [3] quienes además aplicaron dicho formalismo para encontrar las constantes de movimiento para el flujo potencial de frontera libre.

En trabajos relacionados, Radder [59] y Yoon y Liu [69] presentan expresiones análogas para el flujo 2-D con topografía variable.

Expresiones análogas para el operador Dirichlet- Neumann en fondo variable fueron derivadas más recientemente por Craig, Guyenne, Nicholls y Sulem en [12], en este artículo del año 2005 los autores presentan una expansión del operador Dirichlet Neumann lineal, (i.e. para un dominio con superficie plana que se generaliza a 3D) y con variaciones del fondo. Suponiendo la validéz de la expansión del operador Dirichlet-Neumann para amplitudes pequeñas, realizan el cálculo recursivo del operador Dirichlet-Neumann para amplitudes de ondas arbitrarias, en términos del operador Dirichlet-Neumann lineal para topografías arbitrarias del fondo.

La formulación Hamiltoniana de las ondas de agua ha sido extendida a fluidos invíscidos con superficie libre que no son necesariamente flujos potenciales por Lewis, Montgomery, Marsden y Ratiu ver,[46] y también a fluidos estratificados con voriticidad ver T.S. Haut y M. J. Ablowitz [25].

Muchos autores han investigado la estructura Hamiltoniana de los modelos de ondas de agua somera de forma independiente a la formulación descrita por Zakharov. De hecho, la ecuación Korteweg-de Vies que discutimos brevemente en la *Sección 1.3* fue escrita en un principio como un sistema Hamiltoniano por Gardner [16], y resultados análogos son conocidos para otros modelos. Craig y Groves [11] mostraron que la estructura Hamiltoniana para varios modelos de este tipo (Kd-V, Boussinesq, shallow water) se derivan de la formulación hamiltoniana del flujo potencial de frontera libre. Sin embargo, como fue observado por Magri [47], la ecuación Kd-V y otros modelos integrables poseen más de una estructura Hamiltoniana

1.2 Formulación Hamiltoniana y Operador Dirichlet-Neumann

En 1968, Zakharov mostró en [70], que el sistema descrito anteriormente en (1.5)-(1.7), podía reformularse como un sistema Hamiltoniano de dimensión infinita en términos de las variables de superficie η y ξ con las ecuaciones de Hamilton:

$$\begin{cases} \eta_t = \frac{\delta H}{\delta \xi} \\ \xi_t = -\frac{\delta H}{\delta \eta} \end{cases} \tag{1.9}$$

En 1993, W. Craig y C. Sulem en [10] introdujeron el operador Dirichlet-Neumann $G(\beta, \eta)$, explícitamente en el Hamiltoniano del sistema de ondas en agua.

$$H = \frac{1}{2} \int_{\mathbb{R}} (\xi G(\beta, \eta)\xi + g\eta^2) dx \tag{1.10}$$

El operador Dirichlet-Newmann, $G(\beta, \eta)$ es definido como sigue:

$$(G(\beta, \eta)\xi)(x) = (1 + (\partial_x \eta(x))^2)^{\frac{1}{2}} \nabla \varphi(x, \eta(x)) \cdot N(\eta(x)), \tag{1.11}$$

donde $N(\eta(x)) = (1 + (\partial_x \eta(x))^2)^{-\frac{1}{2}}(-\partial_x \eta(x), 1)$, $x \in \mathbb{R}$ y φ es la solución del problema con condiciones de frontera:

$$\Delta \varphi(x, y) = 0, \quad \text{para } (x, y) \in D_t \eta, \tag{1.12}$$

$$\varphi(x, \eta(x)) = \psi(x), \quad \text{para } x \in \mathbb{R}, \tag{1.13}$$

$$\frac{\partial \varphi}{\partial \hat{n}}(x, -h_0 + \beta(x)) = 0, \quad \text{para } x \in \mathbb{R}. \tag{1.14}$$

De esta forma el operador $G(\beta, \eta)$ transforma la condición de Dirichlet sobre la superficie libre en una condición de Neumann la cual dicta la evolución del perfil de onda inicial.

Finalmente las ecuaciones de evolución para el potencial en la superficie libre, ξ, y para la evolución del perfil de la frontera libre, η, en la forma siquiente:

$$\eta_t = G(\beta, \eta)\xi, \tag{1.15}$$

$$\xi_t = -\frac{1}{2(1 + \eta_x^2)}(\xi_x^2 - (G(\beta, \eta)\xi)^2 + 2\eta_x \xi_x G(\beta, \eta)\xi) - g\eta. \tag{1.16}$$

R. Coifman y Y. Meyer derivaron en [6] una expansión analítica del operador $G(\beta, \eta)$ en potencias de η:

$$G(\beta, \eta) = G_0(\beta, \eta) + G_1(\beta, \eta) + G_2(\beta, \eta) + ..., \tag{1.17}$$

donde $G_j(\beta, \eta)$ es homogéneo de grado j en η.

Los operadores G_j involucran operadores pseudodiferenciales que podemos definir como sigue:

$$Op_\sigma[\xi](x) = \int_{\mathbb{R}} \sigma(x,k)\hat{\xi}_k e^{ikx} dk. \tag{1.18}$$

donde $\sigma(x,k)$ es una función que depende de las variables espaciales x y las variables espectrales k. Podemos pensar al símbolo $\sigma(x,k)$ como una prescripción de cómo modificamos la función ξ simultáneamente en espacio físico y en el espacio de números de onda.

A esta la representación del operador pseudiferencial Op_σ se le conoce como la representación de Kohn-Nirenberg, ver libro de J. J. Kohn, y L. Nirenberg, (1965) en [29]. Algunos ejemplos sencillos que ilustran la forma que adquiere el operador para determinados funciones del símbolo son:

  i. Con $\sigma(x,k) \equiv 1$ obtenemos $Op_1 = Id$

  ii. Con $\sigma(x,k) \equiv \lambda$ obtenemos $Op_\lambda = \lambda Id$

  iii. Con $\sigma(x,k) = m(x)$ obtenemos $(Op_m f)(x) = m(x)f(x)$.

  iv. Con $\sigma(x,k) = \hat{g}(k)$ obtenemos $(Op_{\hat{g}})f = (g * f)(x)$.

De los ejemplos enunciados anteriormente es fácil observar que todo está bien definido para $f \in L^2(\mathbb{R})$.

Un operador pseudodiferencial generaliza la noción de operador diferencial, los cuales son aquellos que poseen símbolos de la forma polinomial en la variable de Fourier k:

$$\sigma(x,k) = b_0(x) + b_1(x)k + b_2(x)k^2 + ... + b_m(x)k^m. \tag{1.19}$$

Una característica importante que debe cumplir el símbolo es que éste no debe oscilar mucho, esto es que las derivadas del símbolo deben de estar acotadas para concluir heuristicamente que el operador así definido tiene sentido para cualquier función $f \in \mathbb{S}$ y cualquier elección razonable de σ (incluidas distribuciones temperadas). Coloquialmente hablando, queremos que $\sigma(x,k)$ se comporte como un polinomio de algún orden m en la variable k, así esperamos que el orden de crecimiento decrezca cuando diferenciamos en k. Más precisamente decimos que $\sigma(x,k)$ es un símbolo de orden m y escribimos $\sigma \in S^m$ si la función y todas sus derivadas son del orden específico:

$$\partial_x{}^\alpha \partial_k{}^\beta \sigma(x,k) \sim o(|\,k\,|^{m-|\beta|}) \text{ cuando } k \longrightarrow \infty$$

Existe una amplia literatura que clasifica a dichos operadores con base al símbolo y sus propiedades de orden de derivación respecto a las variables x y k, ver M.E. Taylor [63], M-A. Shubin [61], L. Hormander [26].

Un aspecto muy importante derivado en el artículo de W. Craig, P. Guyenne, D. P. Nicholls y C. Sulem. en [12] son las expresiones de los términos en la expansión $G_k(\beta, \eta)$;

$$
\begin{align}
G_0(\beta, \eta) &= D\tanh(h_0 D) + DL(\beta), \tag{1.20}\\
G_1(\beta, \eta) &= D\eta D - G_0\eta G_0, \tag{1.21}\\
G_2(\beta, \eta) &= \frac{1}{2}(G_0 D\eta^2 D - D^2\eta^2 G_0 - 2G_0\eta G_1), \tag{1.22}
\end{align}
$$

donde $D = -i\partial_x$.

El operador $L(\beta)$, que actúa sobre la frontera libre $\xi(x)$, se escoge de tal forma que la expresión

$$
\varphi(x, y) = \frac{\cosh((y + h_0)D)}{\cosh(h_0 D)}\xi(x) + \sinh(yD)(L(\beta)\xi)(x), \tag{1.23}
$$

es una solución al problema dado por la ecuaciones (1.5)- (1.8). Y de esta forma podemos deducir una forma implícita de dicho operador como:

$$
L(\beta) = -B(\beta)A(\beta), \tag{1.24}
$$

donde

$$
\begin{align}
A(\beta)\xi &= \int_{\mathbb{R}} e^{ikx}\sinh(\beta(x)k)\text{sech}(hk)\hat{\xi}(k)dk, \tag{1.25}\\
C(\beta)\xi &= \int_{\mathbb{R}} e^{ikx}\cosh((-h_0 + \beta(x))k)\hat{\xi}(k)dk, \tag{1.26}
\end{align}
$$

y

$$
B(\beta) = C(\beta)^{-1}. \tag{1.27}
$$

El inverso $B(\beta)$ del operador $C(\beta)$ está bien definido, ver W. Craig, P. Guyenne, D. P. Nicholls y C. Sulem. en [12].

Estos operadores $A(\beta)$ y $B(\beta)$ así como también el operador D-N introducido anteriormente entran en la clase de OPD's definidos en (3.80) . En el *Capítulo 2* de esta tesis se introducirá una definición de este tipo de operadores en dominios periódicos.

En el trabajo realizado por W. Craig, P. Guyenne, D. P. Nicholls y C. Sulem. en [12], obtienen expresiones explícitas aproximadas para el operador $L(\beta)$ a partir de una expansión del mismo:

$$
L(\beta) = \Sigma_{j=0}^{\infty}L_j(\beta) = L_0(\beta) + L_1(\beta) + L_2(\beta) + ..., \tag{1.28}
$$

en donde $L_j(\beta)$ es homogéneo en β de orden j.

$$L_0(\beta) = 0, \tag{1.29}$$
$$L_1(\beta) = -\text{sech}(h_0 D)\beta D\text{sech}(h_0 D), \tag{1.30}$$
$$L_2(\beta) = \text{sech}(h_0 D)\beta D \sinh(h_0 D)L_1(\beta). \tag{1.31}$$

Aquí observamos lo siguiente, al expandir en su serie de Taylor $\text{sech}(h_0 D)$, esto es, $\text{sech}(h_0 D) = 1 - \frac{(h_0 D)^2}{2} + ...$ obtenemos:

$$DL(\beta) = -D\beta D + O(\gamma^2) \tag{1.32}$$

donde $\gamma = \frac{\beta}{h_0}$

Más adelante hablaremos de un modelo derivado siguiendo esta expansión, presentado en [1].

1.3   Teoría de onda larga

Un abordaje que ha mostrado ser muy prolífico en el estudio del problema de ondas en agua es el régimen de onda larga, dicho escalamiento corresponde a ondas en agua que poseen una longitud de onda que es grande en comparación con la profundidad media del dominio del fluido.

Este escalamiento es accesible experimentalmente y es de gran interés para la ingeniería costera y los flujos geofísicos de gran escala, cabe mencionar que un *tsunami* se estudia como una onda en aguas someras, para este ejemplo y muchos más ver: P. H. LeBlond y L. A. Mysak, [45], C.C. Me, M. Stiassnie y D. K. P. Yue, [52], M. S. Longuet-Higgins, [44], M.C. Lin, W.J. Juang y T.K. Tsay [43] y Klapp, J., Sigalotti, L. D. G., Medina, A., López, A., y Ruiz-Chavarría, G. [30].

Estos modelos han sido ampliamente estudiados para el caso de profundidad constante, las ecuaciónes Korteweg-de Vries y Kadomtsev-Petviashvili, son ejemplos que describen la formación de solitones y sus interacciones.

Para entender dicho escalamiento es preciso realizar un proceso de adimensionalización de las ecuaciones que consite en escribir las ecuaciones de ondas en agua, luego entonces al operador $G(\beta, \eta)$, de forma adimensional. El primer paso es discernir las cantidades importantes que rigen el movimiento de las ondas en el ambiente físico que enmarca el problema y los cuales denotaremos como parámetros adimensionales. Éstos son: la amplitud y longitud típica de la onda y la profundidad media del fluido. En el caso de profundidad variable también se observan las cantidades típicas del perfil de batimetría del dominio del fluido, como la amplitud media del perfil batimétrico.
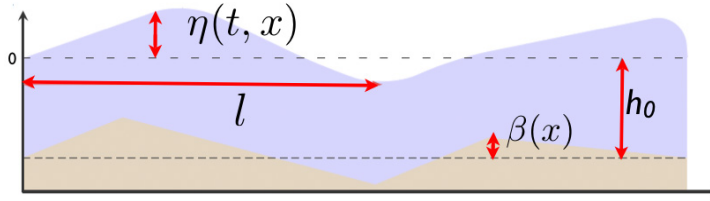
Figure 1.2: Cantidades típicas del problema de ondas en agua.

Definimos los siguientes parámetros adimensionales a partir de las cantidades típicas del problema que se muestran en la Figure 1.2:

$$\delta = \frac{h_0^2}{l^2}, \ \epsilon = \frac{\eta}{h_0}, \ \gamma = \frac{\beta}{h_0} \tag{1.33}$$

donde h_0 es la profundidad media del agua, l es la escala horizontal típica, η es un valor característico de la amplitud de las ondas, $c_0 = \sqrt{gh_0}$ y $T = \frac{l}{c_0}$, c_0 es la velocidad de las ondas lineales en el límite de ondas largas $l \longrightarrow 0$, siendo entonces T un tiempo característico en la propagación de ondas largas.

Se define así a las variables adimensionales $\tilde{x}, \tilde{t}, \tilde{\eta}, \tilde{\phi}$ y al operador $\tilde{D}$ como

$$\tilde{x} = \frac{x}{l}, \ \tilde{\eta} = \frac{\eta}{h_0}, \tilde{t} = \frac{t}{T} \tag{1.34}$$

$$\tilde{\eta} = \frac{1}{\epsilon} \left(\frac{\eta}{h_0} \right), \ \tilde{\phi} = \frac{1}{\epsilon} \left(\frac{\phi}{c_0 l} \right), \ \tilde{D} = -i\frac{\partial}{\partial x^*} \tag{1.35}$$

Con estas variables y dado que conocemos la expansión del operador, $G(\beta, \eta)$, es posible obtener diferentes Hamiltonianos que aproximan al Hamiltoniano asociado al problema de ondas en agua mediante la sustitución del operador $G(\beta, \eta)$ por aproximaciones del mismo dentro del Hamiltoniano y finalmente mediante las ecuaciones canónicas pueden obtenerse modelos aproximados de las ecuaciones de ondas en agua .

Lo que haremos a continuación será usar la expansión de $G(\beta, \eta)$ en potencias de η que fueron desarrolladas por W. Craig, P. Guyenne, D. P. Nicholls y C. Sulem. en [12] y expuestas en (1.20) -(1.22), con ello obtendremos los distintos modelos de ecuaciones de ondas de agua somera para fondo variable en concordancia con el trabajo de W. Craig and M. D. Groves en [11].

De acuerdo a la expansión analítica del operador $G(\beta, \eta)$ expuesta anteriormente y retomando únicamente los términos de G_0 y el primer término de G_1 de la expansión, proponemos las siguientes aproximaciones del operador $G(\beta, \eta)$ bajo distintas consideraciones en las variaciones del fondo.

i) Suponiendo **fondo plano**, esto es, $\beta \equiv 0$. Consideramos G_0 exacto más la aproximación de onda larga, ($\frac{\eta}{h_0} = \frac{h_0^2}{l^2}$, l, la longitud típica de la onda), para
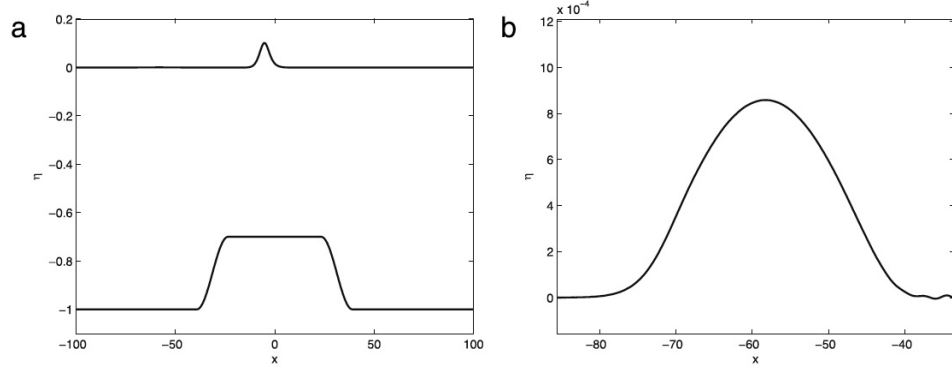
Figure 1.3: a) Onda tipo solitón al tiempo $t = 75.103$, moviendose a la derecha. b) Se muestra un acercamiento de la parte derecha del soliton en la Figura $1.3b$. Figura extraída del artículo de P. Acévez-Sánchez, A.A. Minzoni y P. Panayotaros en [1].

G_1. Así obtenemos la aproximación Boussinesq clásica, ver D. Moldabayev, H. Kalisch, y D. Dutykh en [49].

$$G_{Aprox_1} = D\tanh(h_0 D) + D\eta D \qquad (1.36)$$

ii) Suponiendo una **perturbación pequeña y suave** en la topografía del fondo, β, podemos hacer una expansión de Taylor del operador $L(\beta)$ que aparece en el término G_0. De esta forma obtenemos una expresión explícita del mismo, además del término correspondiente a la aproximación de onda larga para G_1. Obtenemos el modelo propuesto en [1].

$$G_{Aprox_2} = D\tanh(h_0 D) - D\beta D + D\eta D \qquad (1.37)$$

La necesidad de introducir un nuevo modelo como el presentado en (2.25) se justifica principalmente por los motivos que ilustramos a continuación

La primer motivación surge de que en el modelo propuesto por Aceves, Minzoni, Panayotaros presentado en (1.37), no se observan fuertes efectos en la onda de superficie, los efectos visibles están muy atenuados, tal como se ilustra en la imágenes Figure 1.3 y Figure 1.4 extraídas del artículo de los mismos autores en [1]

Los autores en [1] concluyen que dicha expansión de primer orden en β no es muy útil para el estudio de este tipo de fenómenos. Así mismo, otras opciones que han estudiado diversos autores, entre ellos podemos citar a P. Guyenne y D. Nicholls en [23], para desarrollar modelos de ondas en aguas someras con profundidad variable involucran expansiones de mayor orden en β lo que conlleva a la derivación de ecuaciones más complicadas que a su vez acarrea las complicaciones inherentes a los términos con derivadas más grandes por la dificultad de integrarlos numéricamente y de controlar la estabilidad de los esquemas numéricos.
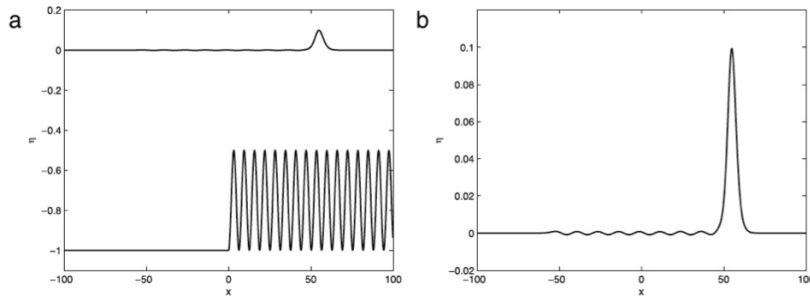
Figure 1.4: a) Onda tipo solitón al tiempo $t = 125.103$, sobre un fondo de variación rápida. Los autores promediaron la variación del fondo para poder introducir un perfil de esta manera en su modelo. b) Se muestra un acercamiento a la Figura $1.4b$. Figura extraída del artículo de P. Acévez-Sánchez, A.A. Minzoni y P. Panayotaros en [1].

1.4   Modelo Whitham-Boussinesq de onda larga para profundidad variable.

En este trabajo proponemos un modelo Hamiltoniano no local para la propagación bidireccional de ondas en aguas someras que involucra operadores pseudodiferenciales que simplifican al operador lineal Dirichlet-Neumann en profundidad variable. Nuestro análisis tiene su origen en la teoría general de profundidad variable expuesta brevemente antes de [12], y a su vez a su simplificación a una ecuación del tipo Boussinesq para onda larga y para pequeñas variaciones del fondo expuesta en [1].

En [1] la componente de profundidad constante en la parte lineal de la ecuación es también reemplazada por el término de dispersión exacta derivado de la linealización de las ecuaciones de Euler, ello da lugar a la obtención de unas ecuaciones que corresponden a un análogo bidireccional de la ecuación de Whitham, para un análisis más detallado de dichas ecuaciones ver tambien, G. B. Whitham, [68], Zakharov, [71] y D. Moldabayev, H. Kalisch, y D. Dutykh, [49].

Las ecuaciones de tipo Whitham para profundidad constante han recibido una atención especial en años recientes, ver [49], y hay resultados en esas ecuaciones que sugieren que un término en las ecuaciones que obedece a dispersión de onda más débil, produce comportamiento más realistas de las ondas con amplitudes más altas. Las distintas versiones de modelos Whitham-Boussinesq poseen además la otra ventaja de que evitan el problema del sistema de ecuaciones lineales tipo Boussinesq de ser un problema *mal planteado* en el formalismo de las ecuaciones diferenciales parciales.

En [1] los autores muestran que las correcciones de orden menor al operador Dirichlet-Neumann en fondo variable en general sólo capturan efectos muy atenu-

ados y poco concluyentes de la topografía en la propagación de las ondas.

Para la obtención de mejores resultados uno podría considerar expresiones más complicadas del operador Dirichlet-Neumann tales como expansiones de mayor orden del perfil de variación del fondo, ver Guyenne y Nicholls [23, 24] y Gouin et al. [18] para una implementación reciente, y [12] para expresiones semi-explicit adionales.

De forma alternativa, nosotros proponemos un operador que posee una expresión relativamente simple y que satisface algunas propiedades estructurales del operador lineal Dirichlet Neumann exacto $G_0(\beta)$, con β la función que describe la variación de la profundidad. El operador $\mathcal{A}_{G_0} = \mathsf{Approx}(G_0(\beta))$ que estamos proponiendo es de la forma $\mathcal{A}_{G_0} = \mathsf{sym}(D\tanh(h(x)D))$. El sistema Whitham-Boussinesq correspondiente a este operador se encuentra definido en la *Sección* 2.1. Este operador es claramente una simplificación *ad-hoc* del operador lineal Dirichlet-Neumann, pero es lo suficientemente sencilla, y se reduce a la expresión de profundidad constante. En la *Sección* 2.1 discutiremos algunas propiedades estructurales generales que debemos pedir al operador $\mathcal{A}_{G_0}$ tales como simetría, positividad y que su comportamiento asíntotico para frecuencias de onda altas tengan un comportamiento como el que describen en el operador de profundidad constante. Estas propiedades son verificadas analíticamente o bien numéricamente en la *Sección* 2.2.

El análisis espectral realizado numéricamente a la matriz que obedece a una discretización de la aproximación del operador lineal Dirichlet-Neumann $\mathcal{A}_{G_0}$ para distintos perfiles (periódicos) de la variación del fondo muestra dos efectos significativos de la topografía sobre los modos normales. El primer efecto visible es que los perfiles de los modos normales, en presencia de batimetría no trivial, muestran una mayor pendiente. Los modos en los que este efecto es visible se encuentran en el rango de frecuencias de baja a intermedia. Otro efecto visible es la modulación en la amplitud directamente relacionada con la topografía. Esta modulación es reportada en frecuencias intermedias.

La integración numérica con del sistema Whitham-Boussinesq para profundidad constante de dos ejemplos expuestos en [10] muestra una enorme similitud cualitativa con la evolución de las ondas modelada por Craig y Sulem en [10] usando términos de mayor orden de la amplitud pequeña en la expansión del operador Dirichlet Neumann. Para el caso de profundidad variable vemos que la velocidad de las crestas de onda se sigue de las variaciones en la profundidad del fondo. También vemos como este efecto modifica la forma de los trenes de ondas de Stokes.

En síntesis, el modelo que introducimos en esta tesis, incluye efectos de topografía variable y es lo suficientemente simple para motivar futuros estudios teóricos de las ondas de agua. Su validación requiere de comparaciones con

modelos más precisos y/o con soluciones exactas que se conozcan en la literatura para otros modelos. Uno de los objetivos del siguiente capítulo de esta tesis va precisamente en esta dirección. También en un futuro a corto plazo se pretende realizar un análisis análitico mas profundo de las ecuaciones y la comparación de nuestro modelo aproximado con el modelo semi-explícito propuesto por Craig, Guyenne, Nicholls y Sulem en [12].

1.5 Modos transversales y modos atrapados en geometrías no triviales.

En el *Capítulo* 3 usaremos el modelo no local para la propagación bidireccional de ondas en aguas someras para profundidad variable que obedece a una simplificación del operador lineal Dirichlet-Neumann introducido en el *Capítulo* 2 de esta tesis y en [65] por Vargas-Magaña y Panayotaros.

El análisis numérico espectral de la matriz asociada al operador $\mathcal{A}_{G_0}$, una aproximación de caracter *ad-hoc* al operador lineal Dirichlet-Neumann y que es presentado en el *Capítulo* 2 para diferentes perfiles,periódicos, de la variación de la profundidad del fondo, muestra efectos significativos de la topografía en la forma de los modos normales.

Esta nueva formulación Hamiltoniana del problema de ondas de agua para profundidad variable ha demostrado ser muy apropiada debido a la versatilidad y simplicidad para la inclución de variaciones fuertes y de orden grande de la topografía del fondo y a su vez por la relativa simplicidad para medir sus efectos en la propagación de las ondas.

Otro factor interesante de este enfoque es que involucra un operador pseudodiferencial (PDO) cuyo símbolo considera el perfil batimétrico exacto. En el *Capítulo* 2, calculamos los modos normales derivados del análisis espectral de dicho operador para distintas topografías y comparamos los resultados con los ampliamente conocidos resultados para profundidad constante, ver R.M. Vargas-Magaña y P. Panayotaros [65]. Se muestran varios resultados muy reveladores sobre la deformación de los modos normales que sugen cuando variamos el perfil topográfico en el símbolo del operador. Dicho análisis ha abierto la posibilidad de explorar esta maquinaria en dos problemas clásicos muy interesantes acerca de modos normales y modos atrapados en geometrías particulares.

El primer problema que estudiamos en éste *Capítulo* 3 son las soluciones correspondientes a los modos transversales en canales largos de longitud infinita con sección transversal uniforme. Estos son modos normales que son independientes de la dimensión transversal del canal, *i. e.* son modos normales bidimensionales, ver [65]. Las soluciones que se conocen para este problema son muy pocas y se

restringen a algunas secciones transversales particulares, como son las secciones con lados inclinados a un ángulo de $45°$ y $30°$ con la horizontal, más recientemente Evans y Linton en [13], ver también Groves [22], obtuvieron el conjunto completo de modos transversales para canales con secciones transversales semicirculares.

Las investigaciones con respecto a la propagación de ondas largas en canales con sección transversal triangular uniforme fueron hechas por P. Kelland [31]. Más tarde Greenhill, [19] investigó la propagación de ondas en canales triangulares con una inclinación de $30°$ con respecto a la horizontal. El asunto fue tratado sistematicamente por Macdonald más adelante en [51] quien estableció que una solución con la propiedad de ser una onda plana existe sólo para los ángulos $\gamma = 45°$ y $\gamma = 30°$.

Este hallazgo no excluye la posibilidad de la existencia de un tipo de ondas periódicas progresivas con frente de onda curvo para otros ángulos, sin embargo las ondas no podrán ser descritas con la misma forma para el potencial Φ presentado aquí, ver J. V. Wehausen y E.V. Laitone, [67].

En el *Capítulo* 3 introdujimos un nuevo camino para el cálculo de modos transversales para canales de diferentes secciones transversales, presentamos aquí resultados para secciones triangulares de ángulos $45°$ y $30°$ y comparamos dichos resultados con las soluciones exactas derivadas por Macdonald en [51], Lamb en [42] *artículo 261*, Packhman en [58], y presentadas más recientemente por Groves en [22]. Referimos al lector en este respecto al artículo [65] para el caso más sencillo de un canal de sección transversal rectangular. Una vez que damos la formulación de los problemas que abordamos en este capítulo y que mostremos la posibilidad de abordar el problema de una variedad de canales de perfiles diferentes en términos de un operador pseudodiferencial que corresponde con el operador lineal Dirichlet-Neumann estudiado en [65], la primer parte del capítulo retoma el análisis hecho para este caso pero ahora en el nuevo marco del problema que nos interesa abordar en este capítulo.

El segundo problema que estudiamos en el *Capítulo* 3 de esta tesis es sobre la existencia y el cálculo de cierto tipo de soluciones que corresponde a ondas armónicas propagándose en la dirección z sobre la sección transaversal y con decaimiento de la solución fuera de dicha región.

Los modos atrapados de ondas en la superficie libre de un fluido homogéneos han sido ampliamente estudiados y son bien conocidos. El primer tratamiento matemático de las ondas de agua atrapadas sobre un fondo inclinado nos remite a Stokes, quien proveyó una solución explícita para los modos atrapados, o mejor conocidos como, ondas de orilla sobre un fondo inclinado en [62], ver también [40], Ursell (1952) [64] y Munk [56] quienes generaliza la solución de Stokes a un conjunto infinito de modos discretos, incluyendo a las 'ondas de orilla de Stokes como los modos fundamentales. Es bien sabido también que una cresta submarina puede atrapar ondas de agua ver nuevamente el trabajo pionero de Ursell [64],

Garipov [17], A.M. Marín, R.D. Ortíz, R. D. and P. Zhevandrov. [48], M. I. Romero Rodríguez and P. Zhevandrov, [60] y más recientemente Bonnet-Ben et. al. [4].

Calcularemos numéricamente los modos atrapados como las eigenfunciones que corresponden a eigenvalores puntuales debajo del espectro contínup del operador que aproxima al operador Dirichlet-Neumann para el operador modificado de Helmholtz en presencia de topografía no trivial del fondo. Esta aproximación *ad-hoc* se sigue de las ideas expuestas en [65] y que se enuncian en esta tesis como una extension del operador Dirichlet-Neumann para dominios con fondo plano.

Existen pocos resultados generales sobre la naturaleza exacta del espectro en dominios no acotados y dichos resultados involucran herramientas de análisis profundo, y esta es la razón por la que el estudio de modos atrapados ha llamado la atención a muchos matemáticos. Existen numerosos artículos de investigación que abordan el estudio de ondas atrapadas desde diversos enfoques, podemos encontrar artículos en donde se reporta por mediciones via satelite la presencias de este tipo de ondas alrededor del mundo, tambien los hay sobre los diversos tipos de ondas de agua, tales como, ondas de orilla, ondas atrapadas por encima de cilindro verticales y horizontales de diferente radio o bien sobre distintos tipos de protuberancias en el fondo, ver [40]. En muchos de esos artículos se trata de abordar la existencia de este tipo de ondas atrapadas así como también la busqueda de cierto tipo de cotas en las frecuencias que permitan la presencia de este tipo de ondas de orilla y modos atrapados. El objetivo de este capítulo es el de mostrar un nuevo método para calcular estos modos atrapados de una forma sencilla para cualquier geometría imaginable y que los resultados numéricos den certeza del tipo de onda que se está calculando.

Unos de los principales objetivos de este capítulo recae en el hecho de que todos los resultados que en el se presentan, más allá de su importancia en oceanografá e ingeniería nos arrojan elementos sólidos para la validación y la trascendencia de este nuevo modelo, que es lo suficientemente sencillo para motivar más estudios teóricos en ondas de agua y también es lo suficientemente preciso y eficiente numéricamente para superar pruebas más fuertes con estudios experimentales de ondas de agua en el laboratorio.

1.6 Agradecimientos

Mi primer agradecimiento es para mi asesor el Dr. Panayotis Panayotoras quien sin duda es un artífice más de esta tesis. Este proyecto de investigación es fruto de un constante aprendizaje, retroalimentación, colaboración, dirección, revisión, y edición que recibí de su parte. Su sobresaliente entendimiento y visión de un amplio espectro de las matemáticas y de la física fueron cruciales para dar cause, construir y finalizar esta tesis, sus inagotables sugerencias e ideas para encontrar

inspiración por la incansable curiosidad y búsqueda de soluciones que lo hacen pionero en el descubrimiento de bellísimos e importantes fenómenos no lineales que podemos observar en la atmósfera, en la óptica y en el océano.

Un agradecimiento muy particular al Dr. Walter Craig de quien primero leí y estudié sus interesantes artículos sobre la formulación Hamiltoniana del problema de ondas en agua y con los cuales desarrollé esta fascinación por su estudio. Más adelante, durante mis estudios de doctorado tuve la fortuna de conocerlo personalmente e interactuar con él en varias ocasiones lo cual enalteció más mi admiración y agradecimiento ante un científico que destella conocimiento, simpatía y motivación por hacer matemáticas, hablar de matemáticas y compartir conocimiento. Sobra decir que su contribución en el área es de tal relevancia y calidad que sus artículos y su nombre son un referente en la disciplina.

Un agradecimiento al Dr. Arturo Olvera quien fungió como un mentor en el área de la mecánica y análisis numérico transmitiendo siempre su fascinación por la física y de los sistemas dinámicos, es sin duda una fuente de inspiración y dedicación al quehacer científico, académico y a la construcción de una convivencia humana activa con gran calidez y gran valor académico. Muchas gracias por ser un pilar en la construcción de esta tesis.

Un agradecimiento al Dr. Antonio Capella quien fungió como parte de mi comité de estudios de doctorado, realizando recomendaciones a lo largo de todo el periodo que sin duda ayudaron al mejoramiento del proyecto de investigación y me alentaron a profundizar en el objeto de estudio.

Me gustaría agradecer al Dr. Gilberto Flores Gallegos y al Dr Gustavo Cruz Pacheco quienes siempre fueron un soporte muy importante en mi formación doctoral, me brindaron sin mesura su tiempo para escucharme en innumerables ocasiones y momentos de flaquezas pero también compartí momentos de alegría e interesantes conversaciones. Al Dr. Gilberto Flores Gallegos le agradezco sus enseñanzas, entereza, integridad, calidez humana, inteligencia y profundo dedicación a la academia, al departamento de Matemáticas y Mecánica del IIMAS y a la preparación de estudiantes y científicos de gran nivel, su labor tiene y tendrá un gran impacto en las futuras generaciones.

Quiero agradecer al CONACyT por haber otorgado la beca con número 213696 para realizar mis estudios de doctorado en la Universidad Nacional Autónoma de México.

Por último y fundamentalmente quisiera agradecer a mi mamá, a mi papá, a Marianita, a Germancito y a Sebastian, por estar VIVOS, por reír, sonreír, sentir, aprender, discutir, reflexionar, por estar cerca de mí, por poder contar con ustedes incondicionalmente, por ser una fuente de inspiración, por ser tan bellos seres humanos, tan pensantes y soñadores por compartir conmigo sus inmensas alegrías e innegables tristezas, por quererme tanto y por ser un ejemplo de lucha, de empatía, de implacable curiosidad y de incesante transformación.

1.7   Contribuciones de la Tesis

⁕ La derivación y el estudio de un nuevo modelo no local para la propagación de ondas en aguas someras con profundidad variable en la teoría de onda larga. Al modelo se le llamó: *Modelo des ondas en agua Whitham -Boussinesq para dominios con profundidad variable.*

⁕ La discretización de una familia muy importante de operadores Pseudodiferenciales que aparecen en diversas ecuaciones de la física y de la Geometría, somo lo son los operadores que se denotan como $a(x, D)$, donde x es la variable física, D es el operador $D = \frac{1}{i}\partial_x$ cuyo símbolo es de la foma $\sigma(x, \kappa)$, donde κ es la variable de Fourier.

⁕ La elaboración de un código numérico espectral para el cómputo de operadores pseudodiferenciales con símbolo $\sigma(x, \kappa)$ y $\sigma(x, \kappa, \lambda_0)$ donde λ_0 está fijo.

⁕ La obtención por medio de un análisis asintótico de la segunda aproximación al tren de ondas periódico para la ecuación Whitham-Boussinesq para fondo plano. Dicha onda se le conoce como *Ondas de Stokes.*

⁕ La elaboración de un código numérico espectral para la integración en el tiempo de las ecuaciones diferenciales parciales de segundo orden con un término no local que involucra el cómputo de operadores pseudodiferenciales.

⁕ El análisis espectral del operador pseudodiferencial para diversas batimetrías no triviales.

⁕ Cálculo de modos transversales para geometrías no triviales.

⁕ Cálculo de $Modos Atrapados$, los cuales se presentan en dominios no acotados y consisten en ondas armónicas que se propagan sobre cordilleras inmersas en el agua, con sección transversal uniforme. Dichas ondas no se atenuan o distorsionan al propagarse en la dirección de la cordillera y poseen decaimiento exponencial fuera del área de la cordillera.

⁕ La exposición de la derivación analítica de los modos transversales para las geometrías no triviales que se abordan en esta tesis y el modelado de las mismas con la obtención explícita de los parámetros que las determinan.

⁕ Una extensión y simplificación de las ecuaciones de la teoría de ondas de agua someras abordada por Mei para el estudio de ondas atrapadas en la

superficie de una plataforma continental desde el enfoque del modelo de ondas de agua somera y el modelado de las mismas para la obtención explícita de los parámetros que las determinan.

✳ Análisis del operador que describimos en el inciso anterior, calculo numérico de las eigenfunciones que corresponden a dicho operador. Planteamiento como modelo base para la calibración de nuestro modelo pseudodiferencial.

Chapter 2

A Whitham-Boussinesq water waves model over variable depth

In this chapter we study the propagation of water waves in a channel of variable depth using the long-wave asymptotic regime. We use the Hamiltonian formulation of the problem in which the non-local Dirichlet-Neumann operator appears explicitly in the Hamiltonian, and propose a Hamiltonian model for bidirectional wave propagation in shallow water that involves pseudo-differential operators that simplify the variable-depth Dirichlet-Neumann operator. The model generalizes the Boussinesq system, as it includes the exact dispersion relation in the case of constant depth. Analogous models were proposed by Whitham for unidirectional wave propagation. We first present results for the normal modes and eigenfrequencies of the linearized problem. We see that variable depth introduces effects such as a steepening of the normal modes with the increase in depth variation, and a modulation of the normal mode amplitude. Numerical integration also suggests that the constant depth nonlocal Boussinesq model can capture qualitative features of the evolution obtained with higher order approximations of the Dirichlet-Neumann operator. In the case of variable depth we observe that wave-crests have variable speeds that depend on the depth. We also study the evolutions of Stokes waves initial conditions and observe certain oscillations in width of the crest and also some interesting textures and details in the evolution of wave-crests during the passage over obstacles.

The organization of this chapter is as follows. In *Section 2* we present the Hamiltonian formulation of the water wave problem and propose the Whitham-Boussinesq model for variable depth. In *Section 3* we discuss some general ideas for simplifying the Dirichlet-Neumann operator and present a numerical spectral analysis of the particular choice we use for different depth profiles. In *Section 4* we present numerical simulations of the Whitham-Boussinesq equations with constant and variable depths.

2.1   Hamiltonian formulation of the free surface problem and Whitham-Boussinesq models

We consider an ideal fluid, *i.e.* incompressible and inviscid, where the flow is assumed to be irrotational and surface tension is neglected. The fluid occupies a two dimensional time-dependent simply connected domain $\mathcal{D}_t$, given by

$$\mathcal{D}_t(\beta, \eta) := \{(x, y) : x \in \mathbb{R}, -h_0 + \beta(x) < y < \eta(x, t)\},$$

whose boundaries are given by

$$\partial\mathcal{D}_t(\beta, \eta) := \{(x, y) : y = \eta(x, t) \text{ and } y = -h_0 + \beta(x)\}, \tag{2.1}$$

where h_0 is the mean depth, $\beta(x)$ is the variation of the depth from this value, and η measures the perturbation of the free surface of the fluid from $y = 0$. We assume $\beta(x) < h_0$ for every $x \in \mathbb{R}$.

We also assume that the only bulk force acting on the fluid mass is gravity and that the pressure p at the free surface fluid is constant, $p = 0$. The Euler equations for free surface potential flow is then

$$\Delta\varphi(x, y) = 0 \qquad \text{in } D_t(\beta, \eta), \tag{2.2}$$

$$\partial_t\eta = \partial_y\varphi - (\partial_x\eta)(\partial_x\varphi) \qquad \text{in } y = \eta(x, t) \tag{2.3}$$

$$\partial_t\varphi = -\frac{1}{2}|\nabla\varphi|^2 - g\eta \qquad \text{in } y = \eta(x, t) \tag{2.4}$$

$$\nabla\varphi \cdot N(\beta) = 0 \qquad \text{in } y = -h_0 + \beta(x), \tag{2.5}$$

where φ is the velocity potential and the velocity is given by $u = \nabla\varphi$. $g > 0$ is the gravitational constant. Moreover $N(\beta)$ is the exterior unit normal on the rigid boundary.

With the aim to apply a numerical analysis on the study of these equations we will consider the spatially periodic version of equations (2.2)-(2.5), hence we will assume periodic boundary conditions $\eta(x + L, t) = \eta(x, t)$ and $\varphi(x + L, y, t) = \varphi(x, y, t)$ for some period $L > 0$.

V. Zakharov [70] showed that the water wave problem (2.2)-(2.5) can be restated as a Hamiltonian system with infinitely degrees of freedom in terms of surface quantities, the wave amplitude $\eta(x, t)$ and surface potential $\xi(x, t) = \varphi(x, \eta(x, t), t)$, namely as

$$\partial_t \begin{pmatrix} \eta \\ \xi \end{pmatrix} = \begin{pmatrix} 0 & I \\ -I & 0 \end{pmatrix} \begin{pmatrix} \frac{\delta H}{\delta \eta} \\ \frac{\delta H}{\delta \xi} \end{pmatrix}. \tag{2.6}$$

The Hamiltonian can be expressed explicitly in terms of η and ξ as

$$H = \frac{1}{2} \int_{\mathbb{R}} (\xi G(\beta, \eta)\xi + g\eta^2)dx, \tag{2.7}$$

see [11], where the operator $G(\beta, \eta)$ is defined as follows: consider the elliptic problem

$$\Delta\varphi(x, y) = 0, \quad \forall\, (x, y) \in D_t\eta, \tag{2.8}$$

$$\varphi(x, \eta(x)) = \xi(x), \quad \forall\, x \in \mathbb{R}, \tag{2.9}$$

$$\frac{\partial\varphi}{\partial\hat{n}}(x, -h_0 + \beta(x)) = 0, \quad \forall\, x \in \mathbb{R}. \tag{2.10}$$

If η and ξ are sufficiently smooth and decay at infinity, then (2.8)- (2.10) admits a unique solution and we can compute the normal derivative of the solution at the surface $y = \eta$. The Dirichlet-Neumann operator $G(\beta, \eta)$ is then defined by

$$(G(\beta, \eta)\xi)(x) = (1 + (\partial_x\eta(x))^2)^{\frac{1}{2}} \nabla\varphi(x, \eta(x)) \cdot N(\eta(x)), \tag{2.11}$$

where $N(\eta(x)) = (1 + (\partial_x\eta(x))^2)^{-\frac{1}{2}}(-\partial_x\eta(x), 1)$, $x \in \mathbb{R}$, is the exterior unit normal at the free surface. The Dirichlet-Neumann operator $G(\beta, \eta)$ is a linear operator on ξ and is symmetric. A similar definition applies to the periodic problem.

In [12], Craig, Guyenne, Nicholls and Sulem give an expansion of this operator in the presence of non-trivial bottom topography

$$G(\beta, \eta) = G_0(\beta, \eta) + G_1(\beta, \eta) + G_2(\beta, \eta) + ..., \tag{2.12}$$

where the G_j are homogeneous of degree j in η. The first terms are

$$G_0(\beta, \eta) = D\tanh(h_0 D) + DL(\beta), \tag{2.13}$$

$$G_1(\beta, \eta) = D\eta D - G_0\eta G_0, \tag{2.14}$$

$$G_2(\beta, \eta) = \frac{1}{2}(G_0 D\eta^2 D - D^2\eta^2 G_0 - 2G_0\eta G_1), \tag{2.15}$$

where $D = -i\partial_x$. The operators G_j involve formal pseudo-differential operators of the form

$$a(x, D)\xi(x) = \int_{\mathbb{R}} a(x, k)\hat{\xi}(k)e^{ikx}dk. \tag{2.16}$$

where the function $a(x, k)$ is the *symbol* of $a(x, D)$.

At higher order, the G_j, $j > 2$, are similarly obtained from G_0, using a recursion formula. The recursion formula for the G_j is the one obtained for a flat bottom, where $G_0(0, \eta) = D\tanh(h_0 D)$, see [11]. Variable depth effects are thus encoded in the pseudo-differential operator $L(\beta)$.

The operator $L(\beta)$ acting on the boundary data $\xi(x)$, can be written in the semi-explicit form, see [12]

$$L(\beta) = -B(\beta)A(\beta), \tag{2.17}$$

where the operators $A(\beta)$ and $C(\beta)$ are defined by

$$A(\beta)\xi = \int_{\mathbb{R}} e^{ikx}\sinh(\beta(x)k)\text{sech}(hk)\hat{\xi}(k)dk, \tag{2.18}$$

$$C(\beta)\xi = \int_{\mathbb{R}} e^{ikx}\cosh((-h_0 + \beta(x))k)\hat{\xi}(k)dk, \tag{2.19}$$

and $B(\beta) = C(\beta)^{-1}$. The inverse $B(\beta)$ of the operator $C(\beta)$ is well defined, see Craig, *et. al.* in [12].

An alternative expression for $L(\beta)$ is in powers of the depth variation β as $L(\beta) = \Sigma_{j=0}^{\infty}L_j(\beta)$, where the $L_j(\beta)$ are homogeneous of order j in β, and are computed recursively, see [12]. The first two terms in the expansion are

$$L_0(\beta) = 0, \tag{2.20}$$
$$L_1(\beta) = -\text{sech}(h_0 D)\beta D\text{sech}(h_0 D). \tag{2.21}$$

2.1.1 Long-wave approximations of the operator $G(\beta, \eta)$

We now consider different approximations of the operator $G(\beta, \eta)$ in the Hamiltonian (2.7) and obtain different Hamiltonian shallow water wave models.

i) Assuming constant depth, $\beta \equiv 0$, we consider the operator G_0 in its exact form and we add the long wave approximation for G_1 considering $\epsilon = \delta^2$, where $\epsilon = \frac{\eta}{h_0}$ and $\delta = \frac{h_0^2}{l^2}$, with l the typical wavelength. We then obtain a modification of the classical Boussinesq scaling regime, see [68],

$$G_{Aprox_0} = \frac{\tilde{D}}{\sqrt{\epsilon}}\tanh(h_0\sqrt{\epsilon}\tilde{D}) + \epsilon\tilde{D}\tilde{\eta}\tilde{D}, \tag{2.22}$$

where $\tilde{D} = \frac{1}{l}D$ and $\tilde{\eta} = \frac{\eta}{a}$. We may call the resulting equation a "Whitham-Boussinesq" model.

ii) Assuming smooth and small depth variations, *i.e.* $\beta \sim O(\epsilon)$, it is possible to use an explicit expression of the $L(\beta)$ operator as an expansion in powers of β, see [12]. The long-wave limit uses (2.21),

$$\text{sech}(h_0 D) = 1 - \frac{(h_0 D)^2}{2} + \dots,$$

and we derive

$$\frac{h_0}{\delta}\tilde{D}L(\tilde{\beta}) = -h_0\tilde{D}\tilde{\beta}\tilde{D} + O(\gamma^2), \tag{2.23}$$

with $\gamma = \frac{\beta}{h_0}$.

Then we add the long-wave approximation of G_1 described above, see P. Acéves-Sáchez, A. A. Minzoni and P. Panayotaros in [1].

$$G_{Aprox_1} = \frac{\tilde{D}}{\sqrt{\epsilon}} \tanh(\sqrt{\epsilon}\tilde{D}) - \tilde{D}\tilde{\beta}\tilde{D} + \epsilon\tilde{D}\tilde{\eta}\tilde{D}, \qquad (2.24)$$

with $\tilde{\beta} = \frac{\beta}{h_0}$, assuming $\gamma \sim \beta \sim \epsilon$. This model was studied in [1].

Another option is to approximate numericaly (2.17)-(2.19). This direction seems to require some care due to the apparent cancelations of the exponentially increasing and decreasing symbols in the product of (2.17). We hope to examine this in future work.

iii) Assuming depth variations of order larger than $O(\epsilon)$, we introduce a pseudo-differential operator with a functional form that is similar to G_0 and takes into account the explicit function $\beta(x)$, again using the long- wave approximation of G_1 above. In particular, we propose

$$G_{Aprox_2} = \textbf{\textit{Sym}}(\frac{\tilde{D}}{\sqrt{\epsilon}} \tanh(\sqrt{\epsilon}(1 - \beta(x))\tilde{D})) + \epsilon\tilde{D}\tilde{\eta}\tilde{D}, \qquad (2.25)$$

where $-1 + \tilde{\beta}(x)$ is the vertical coordinate of the bottom, and Sym refers to the symmetrized operator, discussed in more detail in the next section. The linear part reduces to that of the Whitham-Boussinesq equation of (2.22) for $\beta \equiv 0$.

The Hamiltonians arising from using G_{Aprox_0}, G_{Aprox_1}, and G_{Aprox_2} in (2.7) will be denoted by H_0, H_1, and H_2 respectively.

For instance

$$H_2 = \frac{1}{2} \int_{\mathbb{R}} [\xi^*(\textbf{\textit{Sym}}(\frac{\tilde{D}}{\sqrt{\epsilon}} \tanh(\sqrt{\epsilon}h(x^*)\tilde{D})) + \epsilon\tilde{D}\tilde{\eta}\tilde{D})\xi^* + \eta^{*2}]dx^*, \qquad (2.26)$$

where $\xi^* = \frac{\xi}{\epsilon c_0 l}$, $x^* = \frac{x}{l}$ and $\eta^* = \frac{\eta}{a}$.

REMARK

Note that the symmetrization of G_0 appears naturally in Hamilton's equations of motion. For instance, consider formally Hamilton's equations $\dot{z} = \mathcal{J}\nabla H$, $\mathcal{J}$ the canonical form, with the quadratic Hamiltonian $H = \frac{1}{2}z^T E z$. Then Hamilton's equations are $\dot{z} = \frac{1}{2}(E + E^T)z$.

2.1.2 Spectral formulation and Galerkin truncations

As the Hamiltonians above involve pseudo-differential operators, it is natural to consider Fourier spatial discretizations.

Let $\eta(x,t)$ and $\xi(x,t)$ be 2π-periodic real functions, $\hat{\eta}_k$, $\hat{\xi}_k$, $k \in \mathbb{Z}$, their respective Fourier coefficients. Then Hamilton's equations become

$$\begin{cases} \partial_t \hat{\eta}_k = \frac{\partial H}{\partial \hat{\xi}_{-k}} \\ \partial_t \hat{\xi}_k = -\frac{\partial H}{\partial \hat{\eta}_{-k}} \end{cases}, \ k \in \mathbb{Z} \ . \tag{2.27}$$

It is possible to assume $k \in \mathbb{Z} \setminus \{0\}$ in these equations, since $\hat{\eta}_0 = \hat{\xi}_0 = 0$ imply $\partial_t \hat{\eta}_0 = 0$, $\partial_t \hat{\xi}_0 = 0$. Thus $\hat{\eta}_0 = \hat{\xi}_0 = 0$ define an invariant subspace of (2.27).

Since η, ξ are real-valued functions, we also have $\hat{\eta}_{-k} = \hat{\eta}_k^*$ and $\hat{\xi}_{-k} = \hat{\xi}_k^*$. Then we can make the change of variables from $\{\hat{\eta}_k, \hat{\xi}_k \mid k \in \mathbb{Z} \setminus \{0\}\}$, to the variables $\{\hat{\eta}_k, \hat{\eta}_k^*, \hat{\xi}_k, \hat{\xi}_k^* \mid k \in \mathbb{Z}^+\}$, $\forall k \in \mathbb{Z}$, and write (2.27) as

$$\begin{cases} \partial_t \hat{\eta}_k = \frac{\partial H}{\partial \hat{\xi}_k^*} \\ \partial_t \hat{\xi}_k = -\frac{\partial H}{\partial \hat{\eta}_k^*} \end{cases}, \quad k \in \mathbb{Z}^+ \ . \tag{2.28}$$

Galerkin truncations are obtained by considering

$$\begin{cases} \partial_t \hat{\eta}_k = \frac{\partial H}{\partial \hat{\xi}_k^*} \\ \partial_t \hat{\xi}_k = -\frac{\partial H}{\partial \hat{\eta}_k^*} \end{cases}, \ k \in J_M, \text{ with } J_M = \{1, \ldots, M\} \ . \tag{2.29}$$

2.2 Spectral analysis for the operator $Sym(D\tanh(h(x)D)$

The main goal of this section is to present some numerical results on the spectral analysis of the linear part of the Dirichlet-Neumann operator of the model (2.25). We first present some general considerations leading to (2.25). The idea is to define an operator that has a relatively simple expression and satisfies some structural properties of the exact linear Dirichlet-Neumann operator. Specifically, one may define n model Dirichlet-Neumann operator, denoted by $\mathcal{A}_{G_0} = \mathsf{Approximate}(G_0(\beta))$, that satisfies

  i. $(\mathcal{A}_{G_0})[f](x)$ is real if f is real.

  ii. $\mathcal{A}_{G_0}$ is a formally symmetric operator, that is $\langle f, \mathcal{A}_{G_0} g \rangle = \langle \mathcal{A}_{G_0} f, g \rangle$, where $\langle f, g \rangle = \int_{\mathbb{R}} f \, g \, dx$ is the standard L^2-inner product, $\langle f, g \rangle = \int_0^{2\pi} f \, g \, dx$ for 2π-periodic boundary conditions. f and g are in the domain of $\mathcal{A}_{G_0}$, see iii.

iii. The high frequency spectral asymptotics of $\mathcal{A}_{G_0}$ are those of the constant depth case. We make this more precise in the periodic case, requiring that the generalized dispersion relation $\omega_\kappa = \sqrt{\lambda_\kappa}$ v.s. κ, where the λ_κ is the κ–th eigenvalue of $\mathcal{A}_{G_0}$ in increasing order, approach the constant depth dispersion relation $\omega_\kappa = \sqrt{g\kappa \tanh(\kappa h)}$ as $k \longrightarrow \infty$. A similar convergence condition should apply to the eigenfunctions.

iv. $\mathcal{A}_{G_0}$ is a positive operator, that is $\langle f, \mathcal{A}_{G_0} f \rangle \geq c\|f\|^2$.

When $\beta = 0$ all properties i)-iv) are satisfied by $\mathcal{A}_{G_0} = D \tanh(h_0 D)$.

The simple generalization of this operator $\mathcal{A}_{G_0} = D \tanh(h(x)D)$ is not in general symmetric, but can be symmetrized to satisfy ii). Property i) is verified below. Properties iii) and iv) are verified numerically below.

In the 2π-periodic framework we let $a(x, k)$ be 2π-periodic function in the variable x and define $a(x, D)$ as

$$a(x, D)[\xi](x) = \frac{1}{2\pi} \sum_{k=-\infty}^{\infty} a(x, k)\hat{\xi}_k e^{ikx}. \tag{2.30}$$

Also

$$a(x, k) = \sum_{\lambda \in \mathbb{Z}} e^{i\lambda x} \hat{a}_\lambda(k), \tag{2.31}$$

where $\hat{a}_\lambda(k)$ are the Fourier coefficients in the x variable

$$\hat{a}_\lambda(k) = \int_0^{2\pi} a(x, k)e^{-i\lambda x}\, dx, \quad \lambda \in \mathbb{Z}. \tag{2.32}$$

Then the quadratic form $K_{a(x,D)}$, defined as

$$K_{a(x,D)} = \frac{1}{2} \int_0^{2\pi} \xi a(x, D)\xi\, dx, \tag{2.33}$$

becomes

$$\begin{aligned}
K_{a(x,D)} &= \frac{1}{2} \int_0^{2\pi} \xi a(x, D)\xi dx = \frac{\pi}{2} \sum_{[k,\lambda] \in \mathbb{Z}^2} \hat{\xi}_{-k-\lambda} \hat{\xi}_k \hat{a}_\lambda(k) \\
&= \frac{\pi}{2} \sum_{[k,\lambda] \in \mathbb{Z}^2} \hat{\xi}_k \hat{\xi}_\lambda \hat{a}_{-k-\lambda}(\lambda).
\end{aligned} \tag{2.34}$$

Also, if ξ is real-valued then $[a(x, D)]\xi$ is also real-valued. Then $[a(x, D)]\xi = \overline{\alpha(x, D)\xi}$, and

$$a(x, \mu) = \overline{a(x, -\mu)}, \quad \forall x, \mu \in \mathbb{R} \tag{2.35}$$

$$\hat{a}_\lambda(k) = \overline{\hat{a}_\lambda(k)} = \hat{a}_\lambda(-k), \quad \hat{a}_{-\lambda}(k) = \overline{\hat{a}_\lambda(-k)} = \overline{\hat{a}_\lambda(k)}, \quad \forall \lambda, k \in \mathbb{Z}. \qquad (2.36)$$

It follows that, if $a(x, D)\xi$ is real, then the quadratic form $K_{Sym(a(x,D))}$ is

$$K_{Sym(a(x,D))} = \frac{1}{4\pi} \sum_{[k,\lambda] \in \mathbb{Z}^2} \hat{\xi}_k [\hat{a}_{\lambda-k}(k) + \overline{\hat{a}_{k-\lambda}(\lambda)}] \hat{\xi}_\lambda^*. \qquad (2.37)$$

We also describe the Galerkin truncations of the quadratic forms obtained from $a(x, D)$ and its symmetrization. We will use real and imaginary parts to obtain real, symmetric bilinear forms. Let $\hat{\xi}^M = (\hat{\xi}_1, ..., \hat{\xi}_M)$ as in (2.29), and consider the Galerkin truncation $K_{a(x,D)}^M$ of $K_{a(x,D)}$,

$$
\begin{aligned}
K_{a(x,D)}^M &= \frac{1}{4\pi} \sum_{[k_1,k_2] \in J_M^2} \left[\hat{\xi}_{k_1} \hat{\xi}_{k_2} \hat{a}_{k_1+k_2}^*(k_2) + \hat{\xi}_{k_1}^* \hat{\xi}_{k_2}^* \hat{a}_{k_1+k_2}(k_2) \right] \\
&+ \frac{1}{4\pi} \sum_{[k_1,k_2] \in J_M^2} \left[\hat{\xi}_{k_1} \hat{\xi}_{k_2}^* \hat{a}_{-k_1+k_2}(k_2) + \hat{\xi}_{k_1}^* \hat{\xi}_{k_2} \hat{a}_{-k_1+k_2}^*(k_2) \right] \\
&= \frac{1}{4\pi} ((\hat{\xi}^M)^T, ((\hat{\xi}^M)^*)^T) \begin{pmatrix} P^* & S \\ S^* & P \end{pmatrix} \begin{pmatrix} \hat{\xi}^M \\ (\hat{\xi}^M)^* \end{pmatrix}, \qquad (2.38)
\end{aligned}
$$

with P, S defined implicitly by (2.38), (2.38). P^*, S^* are the complex conjugates of P, S respectively. To clearify what the matrix blocks P and S refer to, see Appendix B.

Letting $\hat{\xi}^M = \theta + i\zeta$, $\theta, \zeta \in \mathbb{R}^M$, we have $K_{a(x,D)}^M$ is equal to

$$\frac{1}{4\pi}(\theta^T, \zeta^T) \begin{pmatrix} Re(P^* + S^* + P + S) & -Im(P^* - S^* + S - P) \\ -Im(P^* + S^* - S - P) & -Re(P^* - S^* - S + P) \end{pmatrix} \begin{pmatrix} \theta \\ \zeta \end{pmatrix} \quad (2.39)$$

Letting

$$\mathcal{M} = \frac{1}{4\pi} \begin{pmatrix} Re(P^* + S^* + P + S) & -Im(P^* - S^* + S - P) \\ -Im(P^* + S^* - S - P) & -Re(P^* - S^* - S + P) \end{pmatrix}, \qquad (2.40)$$

and $\mathcal{M}_{Sym} = \frac{1}{2}(\mathcal{M} + \mathcal{M}^T)$, we then have

$$K_{Sym(a(x,D))}^M = (\theta^T, \zeta^T) \mathcal{M}_{Sym} \begin{pmatrix} \theta \\ \zeta \end{pmatrix}. \qquad (2.41)$$

2.3 Second order Stokes waves

We present an asymptotic analysis for the computation of the second order traveling wave solutions of the travelling Whitham-Boussinesq equations, better known

in the water-wave literature as the second order *Stokes waves train*. This project has been started with the colaboration of Dr. Carlos Garcia Azpeitia and the aim to compute these waves is because as a further project we would like to present an analysis of the global bifurcation of waves for the Whitham-Boussinesq equations.

As was shown by V. Zakharov [70] the water wave problem (2.2)-(2.5) can be restated as a Hamiltonian system (2.6) with infinitely degrees of freedom in terms of surface quantities, the wave amplitude $\eta(x,t)$ and surface potential $\xi(x,t) = \varphi(x,\eta(x,t),t)$. Substituting (2.22) in (2.7) we get the Whitham-Boussinesq equations for flat bottom topography

$$
\begin{aligned}
-\xi_t &= g\eta + \frac{1}{2}(\xi_x)^2 \\
\eta_t &= -K_0\xi_{xx} - (\eta\xi_x)_x.
\end{aligned}
\tag{2.42}
$$

We impose the periodic boundary conditions in x. Hereafter, in the nondimensionalized equation $g = 1$.

Looking for $2\pi/\nu$-periodic solutions of the equations (2.42) is equivalent to the zeros of the operator

$$
\begin{aligned}
F(\eta,\xi;\nu) = -J\nu\frac{d}{dt}\begin{pmatrix}\eta\\\xi\end{pmatrix} + \nabla H(\eta,\xi) = \begin{pmatrix}-\nu\eta_t - K_0\xi_{xx} - (\eta\xi_x)_x\\\nu\xi_t + g\eta + \frac{1}{2}(\xi_x)^2\end{pmatrix} \\
: H^2(T^2;\mathbb{R}^2) \to L^2(T^2;\mathbb{R}^2).
\end{aligned}
\tag{2.43}
$$

Looking for traveling waves of the form $(\eta,\xi)(\tau)$, where $\tau = \nu t + x$ leads us to the equations

$$
\begin{aligned}
-\nu\xi' &= g\eta + \frac{1}{2}(\xi')^2, \\
\nu\eta' &= -K_0\xi'' - (\eta\xi')'.
\end{aligned}
\tag{2.44}
$$

Actually, traveling waves of the form (2.44) are zeros of (2.43).

Indeed, the zeros of the operator

$$
f(\eta,\xi;\nu) = \begin{pmatrix}\nu\xi' + g\eta + \frac{1}{2}(\xi')^2\\-\nu\eta' - K_0\xi'' - (\eta\xi')'\end{pmatrix} : H^2(S^1;\mathbb{R}^2) \to L^2(S^1;\mathbb{R}^2).
\tag{2.45}
$$

correspond to solutions of equations (2.44).

Let

$$
f(\xi;\nu) = K_0\xi'' - \nu^2\xi'' - N(\xi) = 0,
$$

where

$$
N(\xi) = \nu\xi'\xi'' - (\eta\xi')' = 3(\nu\xi''\xi' + \xi'^2\xi''/2).
$$

The aim is to find the next approximation to the linear periodic wavetrain for the Whitham-Boussinesq equation. This solution corresponds to an expansion in

a power series ε. We look for a solution of the above equation as expansions of ξ and ν in power series

$$\xi(\tau) = \varepsilon\xi_1(\tau) + \varepsilon^2\xi_2(\tau) + \varepsilon^3\xi_3(\tau) + \mathcal{O}(\varepsilon^4),$$
$$\nu = \nu_0 + \varepsilon\nu_1 + \varepsilon^2\nu_2 + \mathcal{O}(\varepsilon^3).$$

We then obtain

$$\nu^2\xi'' = \nu_0^2\xi_1''\varepsilon + \left(\xi_2''\nu_0^2 + 2\nu_1\xi_1''\nu_0\right)\varepsilon^2 + \left(\xi_3''\nu_0^2 + 2\xi_2''\nu_0\nu_1 + 2\nu_2\xi_1''\nu_0 + \xi_1''\nu_1^2\right)\varepsilon^3 + \mathcal{O}(\varepsilon^4)$$

and

$$N(\xi) = 3\nu_0\xi_1'\xi_1''\varepsilon^2 + \left(\frac{3}{2}(\xi_1')^2\xi_1'' + 3\nu_0\xi_1'\xi_2'' + 3\nu_0\xi_2'\xi_1'' + 3\nu_1\xi_1'\xi_1''\right)\varepsilon^3 + \mathcal{O}(\varepsilon^4).$$

We use the inner product in $L_{2\pi}^2$ as

$$\langle u, v \rangle = \frac{1}{\pi}\int_0^{2\pi} uv\,d\tau,$$

such that

$$\langle \sin k\tau, \sin j\tau \rangle = \delta_{k,j}.$$

To order ε:

$$K_0\xi_1'' - \nu_0^2\xi_1'' = 0.$$

The operator K_0 has eigenvalues

$$\lambda_k = \frac{1}{k}\tanh(h_o k) \tag{2.46}$$

and eigenfunctions $\sin k\tau$ for $k \in \mathbb{N}$. Then, the solutions are $\xi_1'' = \sin k\tau$,

$$\xi_1 = -\frac{1}{k^2}\sin k\tau, \qquad \nu_0 = \sqrt{\lambda_k}.$$

To $O(\varepsilon^2)$:
$$(K_0 - \nu_0^2)\xi_2'' - 2\nu_1\nu_0\xi_1'' - 3\nu_0\xi_1'\xi_1'' = 0.$$

Taking the inner product with ξ_1'', we obtain

$$\left\langle (K_0 - \nu_0^2)\xi_2'', \xi_1''\right\rangle - 2\nu_1\nu_0\left\langle \xi_1'', \xi_1''\right\rangle - 3\nu_0\left\langle \xi_1'\xi_1'', \xi_1''\right\rangle = 0.$$

Since $(K_0 - \nu_0^2)$ is self adjoint, we have

$$\left\langle (K_0 - \nu_0^2)\xi_2'', \xi_1''\right\rangle = \left\langle \xi_2'', (K_0 - \nu_0^2)\xi_1''\right\rangle = 0.$$

Moreover, since

$$\langle \xi_1' \xi_1'', \xi_1'' \rangle = -\frac{1}{2\pi k} \int_0^{2\pi} \sin(2k\tau)\sin(k\tau)d\tau = 0,$$

we have $2\nu_1\nu_0 \langle \xi_1'', \xi_1'' \rangle = 0$, and that

$$\nu_1 = 0.$$

To obtain ξ_2, we consider

$$(K_0 - \nu_0^2)\xi_2'' = -3\nu_0\xi_1'\xi_1'' = \frac{3}{2}\frac{\nu_0}{k}\sin 2k\tau.$$

Thus, the solution ξ_2 is of the form

$$\xi_2'' = B\sin 2k\tau.$$

Using the equation (2.46), we have

$$B = \frac{3}{2}\frac{\nu_0}{k}(\lambda_{2k} - \lambda_k)^{-1} = \frac{3\nu_0}{\tanh(h_o 2k) - 2\tanh(h_o k)}.$$

To $O(\varepsilon^3)$, using $\nu_1 = 0$, we have

$$K_0\xi_3'' - \nu_0^2\xi_3'' = 2\nu_2\xi_1''\nu_0 + \frac{3}{2}(\xi_1')^2\xi_1'' + 3\nu_0\xi_1'\xi_2'' + 3(1+\nu_0)\xi_2'\xi_1''.$$

On taking the inner product with ξ_1'', we have

$$\left\langle 2\nu_2\xi_1''\nu_0 + \frac{3}{2}(\xi_1')^2\xi_1'' + 3\nu_0\xi_1'\xi_2'' + 3(1+\nu_0)\xi_2'\xi_1'', \xi_1'' \right\rangle = 0.$$

Since $\langle \xi_1'', \xi_1'' \rangle = 1$, we have

$$2\nu_0\nu_2 + \frac{3}{2}\left\langle (\xi_1')^2\xi_1'', \xi_1'' \right\rangle + 3\nu_0 \left\langle \xi_1'\xi_2'', \xi_1'' \right\rangle + 3(1+\nu_0) \left\langle \xi_2'\xi_1'', \xi_1'' \right\rangle = 0.$$

The inner products can be calculated, to give

$$\left\langle (\xi_1')^2\xi_1'', \xi_1'' \right\rangle = \frac{1}{4k^2}\frac{1}{\pi} \int_0^{2\pi} \sin^2(2k\tau)d\tau = \frac{1}{4k^2}.$$

$$\left\langle \xi_1'\xi_2'', \xi_1'' \right\rangle = -\frac{B}{2k}\frac{1}{\pi} \int_0^{2\pi} \sin^2(2k\tau)d\tau = -\frac{B}{2k}$$

$$\langle \xi_2' \xi_1'', \xi_1'' \rangle = \frac{B}{4k} \frac{1}{\pi} \int_0^{2\pi} \cos(2k\tau)\left(\cos(2k\tau) - 1\right) d\tau = \frac{B}{4k}.$$

Therefore, we obtain

$$\nu_2 = -\frac{3}{4\nu_0} \left[\langle (\xi_1')^2 \xi_1'', \xi_1'' \rangle + 2\nu_0 \langle \xi_1' \xi_2'', \xi_1'' \rangle + 2(1 + \nu_0) \langle \xi_2' \xi_1'', \xi_1'' \rangle \right]$$

$$= -\frac{3}{4\nu_0} \left(\frac{1}{4k^2} - \nu_0 \frac{B}{k} + (1 + \nu_0)\frac{B}{2k} \right) = -\frac{3}{4\nu_0} \left(\frac{1}{4k^2} + (1 - \nu_0)\frac{B}{2k} \right).$$

We conclude that at second order, the approximation of Stoke's waves is

$$\xi(\tau) = \varepsilon \frac{-1}{k^2} \sin(k\tau) + \varepsilon^2 \frac{-B}{4k^2} \sin(2k\tau) + \mathcal{O}(\varepsilon^3)$$

$$c = \frac{\nu}{k} = \frac{\sqrt{\tanh k}}{k\sqrt{k}} - \varepsilon^2 \frac{3}{4\nu_0} \left(\frac{1}{4k^2} + (1 - \nu_0)\frac{B}{2k} \right) + \mathcal{O}(\varepsilon^3).$$

Moreover,

$$\xi'(\tau) = \frac{-\varepsilon}{k} \cos(k\tau) - \frac{\varepsilon^2 B}{2k} \cos(2k\tau).$$

From equation (2.42) we obtain the surface elevation as

$$-\eta = (\nu_0 + \varepsilon^2 \nu_2) \left(\frac{-\varepsilon}{k} \cos(k\tau) - \frac{\varepsilon^2 B}{2k} \cos(2k\tau) \right)$$

$$+ \frac{1}{2} \left(\frac{\varepsilon}{k} \cos(k\tau) + \frac{\varepsilon^2 B}{2k} \cos(2k\tau) \right)^2 + \mathcal{O}(\varepsilon^3),$$

or

$$\eta = \frac{\varepsilon \nu_0}{k} \cos(k\tau) + \frac{\nu_0 \varepsilon^2 B}{2k} \cos(2k\tau) - \frac{\varepsilon^2}{2k^2} \cos^2(k\tau) + \mathcal{O}(\varepsilon^3). \qquad (2.47)$$

2.4   Numerical spectra of $Sym(D \tanh(h(x)D))$ for different depth profiles

We now study the linear system corresponding to the quadratic part $H_{2,Q}$ of the Hamiltonian H_2 of (2.26) with $2\pi-$periodic boundary conditions. We have

$$H_{2,Q} = \frac{1}{2} \int_0^{2\pi} [\xi(\textit{Sym}(D \tanh(\sqrt{\epsilon}h(x)D))\xi + \eta^2] dx. \qquad (2.48)$$

The first term (the quadratic part of the kinetic energy) is of the form $K_{Sym(a(x,D))}$, with $Sym(a(x, D))$ the model Dirichlet-Neumann operator $\mathcal{A}_{G_0} = G_0(\beta)$. We
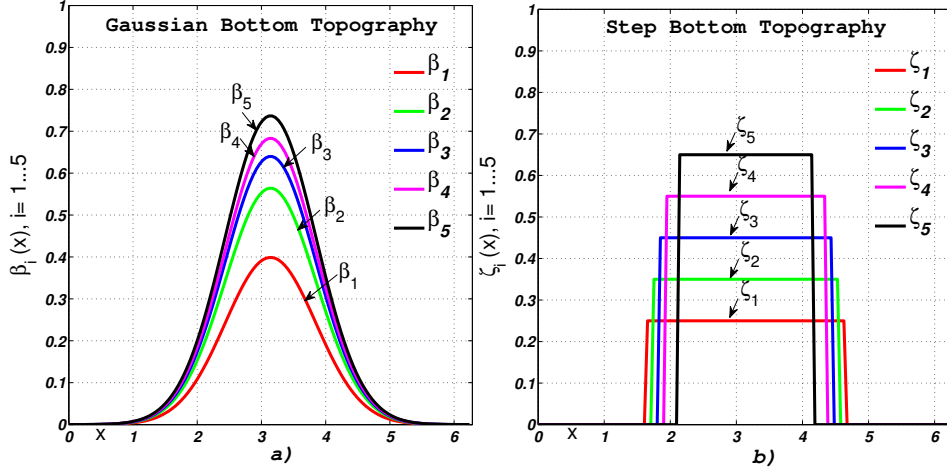
Figure 2.1: a) *Gaussian* family depth profile, and b) *Step* family depth profile.

have that every $\lambda \in \sigma(G_0(\beta))$ corresponds to a frequency $\omega(\lambda) = \sqrt{\lambda}$ of the linear system for (2.48).

In the numerical study below we use the Galerkin truncations given in (2.29), but using real variables, see *Appendix B* in (2.5) formulation. The model Dirichlet-Neumann operator $\mathcal{A}_{G_0}$ is then represented by the matrix $\mathcal{M}_{Sym}$ of (2.41). We use

$$a(x, k) = \frac{1}{\sqrt{\epsilon}} \tanh(\sqrt{\epsilon}(1 - \beta(x))k))k, \tag{2.49}$$

and the following depth profiles: the one-parameter *Gaussian* family

$$\beta(x) = \beta_i(x) = \frac{1}{\sqrt{a_i}} e^{-(x-\pi)^2}, \tag{2.50}$$

with $a_1 = 2\pi$, $a_2 = \pi$, $a_3 = \pi - 0.7$, $a_4 = \pi - 1$, $a_5 = \pi - 1.3$, see Figure 2.1a, and the *Step* family

$$\zeta_i(x) = \begin{cases} 0 & \text{for } 0 \le x < \pi - d_i, \\ b_i & \text{for } \pi - d_i \le x < \pi + d_i, \\ 0 & \text{for } \pi + d_i \le x \le 2\pi, \end{cases} \tag{2.51}$$

with $b_1 = 0.25$, $b_2 = 0.35$, $b_3 = 0.45$, $b_4 = 0.5$, $b_5 = 0.65$, and $d_1 = 1.5$, $d_2 = 1.4$, $d_3 = 1.3$, $d_4 = 1.2$, $d_5 = 1.5$, see Figure 2.1b.

Figure 2.2a and Figure 2.2b show a visual representation of the size of the entries of $\mathcal{M}_{Sym}$ for the β_5 and ζ_5 bottom profiles of the *Gaussian* and *Step* families, respectively, in a gray intensity color scale. We have used $k_{Max} = 2^6$ positive

modes. The matrix $\mathcal{M}_{Sym}$ for $\beta \equiv 0$ is diagonal. Since we consider the real and imaginary parts of every mode, M_{Sym} is $2M \times 2M$.

In Figure 2.2a and Figure 2.2b we see that for variable depth $\mathcal{M}_{Sym}$ is not diagonal. The larger entries are on the diagonal and the decay from the diagonal is related to the amplitude and smoothness of $\beta(x)$ of (2.50) and (2.51). As the depth β becomes flatter we recover the diagonal matrix seen for constant depth.

In Figure 2.2c and Figure 2.2d we show the matrices $\mathcal{M}_{sym}$ for the β_5 and ζ_5 profiles of *Gaussian* and *Step* families respectively with $k_{Max} = 2^{10}$. We see an enlargement around the diagonal that finishes in a line, first the bright region "opens" and then "closes" around the diagonal for larger k. This suggests that the symbol of the constant depth operator dominates the behavior for large k. In other words, the high frequencies do not feel the bottom topography. This behaviour, can be expected, roughly speaking, from the asymptotic behaviour of the function $\tanh(kh)$ for k, large enough.

In Figure 2.3 we show the generalized dispersion relation for different depths. We plot $\omega_\kappa = \sqrt{\lambda_\kappa}$ v.s. κ, where the λ_κ is the $\kappa-$th eigenvalue of $\mathcal{M}_{sym}(\beta)$. In each figure we also plot the constant depth dispersion relation $\omega_\kappa = \sqrt{g\kappa \tanh(h\kappa)}$. As β approaches the constant depth profile in each of the two families considered in Figure 2.3 we see that the eigenvalues approach the constant depth dispersion relation in a monotonic way. Figure 2.3b and Figure 2.3d also indicate that the ω_κ obtained for different depth profiles are much closer for large enough κ, i.e. for large enough κ we recover the constant depth dispersion.

We now indicate some effects of the topography on the eigenmodes of $\mathcal{M}_{Sym}$ for different bottom profiles. The main effects are:

A. Steepening. In Figure 2.4 we plot the normal modes corresponding to the first three eigenvalues of $\mathcal{M}_{sym}$ for the *Gaussian* topography β_5, see (2.50). Each eigenvalue λ_κ of $\mathcal{M}_{Sym}$ gives rise to two eigenmodes, one odd and one even. We also compare these eigenmodes with the constant depth eigenmodes, $\cos(\kappa x)$ and $\sin(\kappa x)$, $\kappa = 1, 2, 3....$ In Figure 2.5 the profile we see the steepening of the first mode with increasing depth variation β_i of (2.50). The shapes are close but topography leads steeper profiles. The steepening effect is observed for all lower to intermediate modes. Truncating with $k_{Max} = 2^6$, we calculated that for modes larger than $\kappa = 37$ this effect is almost imperceptible. **B. Modulation.** In Figure 2.6 we show the amplitude modulation of the $\kappa = 15$ mode, using $k_{Max} = 2^7$. The range of wavelengths where this effect is clearly visible is roughly from $\kappa = 6$ to $\kappa = 30$. Using $k_{Max} = 2^6$, the effect is seen from $\kappa = 5$ to $\kappa = 18$. In both cases the effect is seen for lower to intermediate modes. This locked range is around the peak of the Fourier transform of β. High frequencies are not affected in this way by the bottom topography. In Figure 2.7 we see the Fourier amplitudes of the $\kappa = 1, 3, 5,$ and 7 modes, corresponding to *Gaussian* profile β_5. As κ increases,
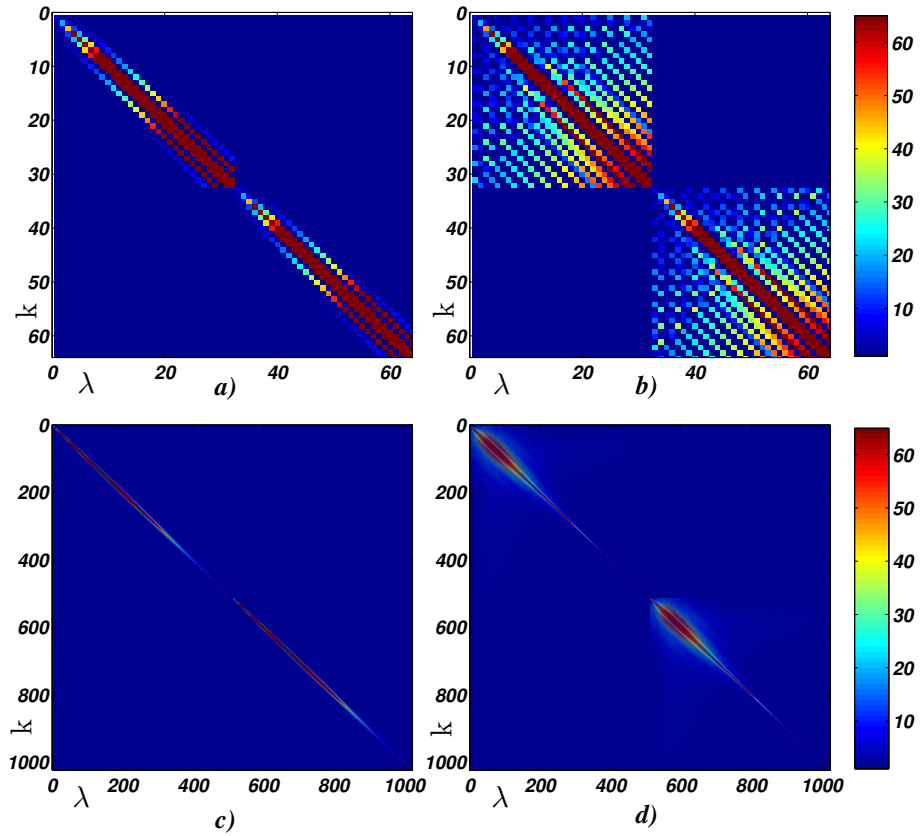
Figure 2.2: Colormatrix representation of matrix $\mathcal{M}_{Sym}(\lambda, k)$. Figure a) shows $\mathcal{M}_{Sym}(\beta_5)$ and b) $\mathcal{M}_{Sym}(\zeta_5)$ with $k_{Max} = 2^6$. Figure c) shows $\mathcal{M}_{Sym}(\beta_5)$ and d) $\mathcal{M}_{Sym}(\zeta_5)$ with $k_{Max} = 2^9$, see (2.50), (2.51) for exact analitic expression of bottom profiles.
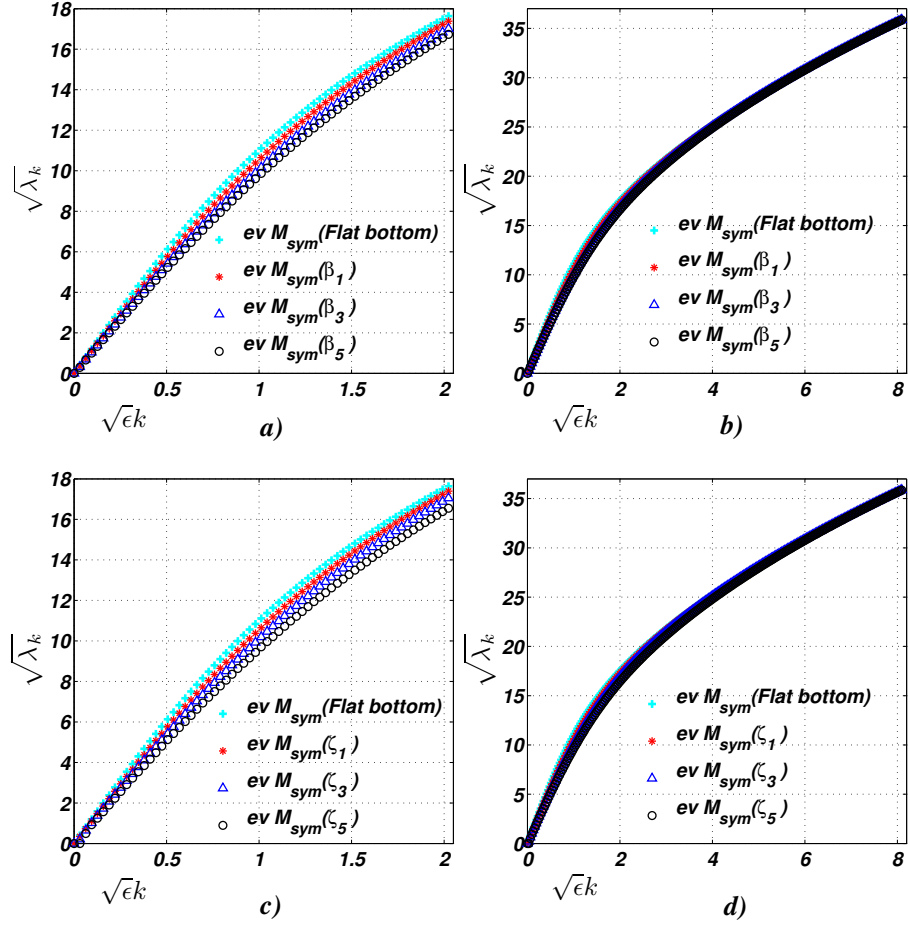
Figure 2.3: *Generalized dispersion relation* for *Gaussian* and *Step* depth profiles compared with constant depth dispersion considering $\epsilon = 0.001$ on $\beta_1, \beta_3, \beta_5$ Figure a) $k_{\mathsf{Max}} = 2^8$ and b) $k_{\mathsf{Max}} = 2^{10}$. $\zeta_1, \zeta_3, \zeta_5$. Figure c) $k_{\mathsf{Max}} = 2^8$ and d) $k_{\mathsf{Max}} = 2^{10}$.
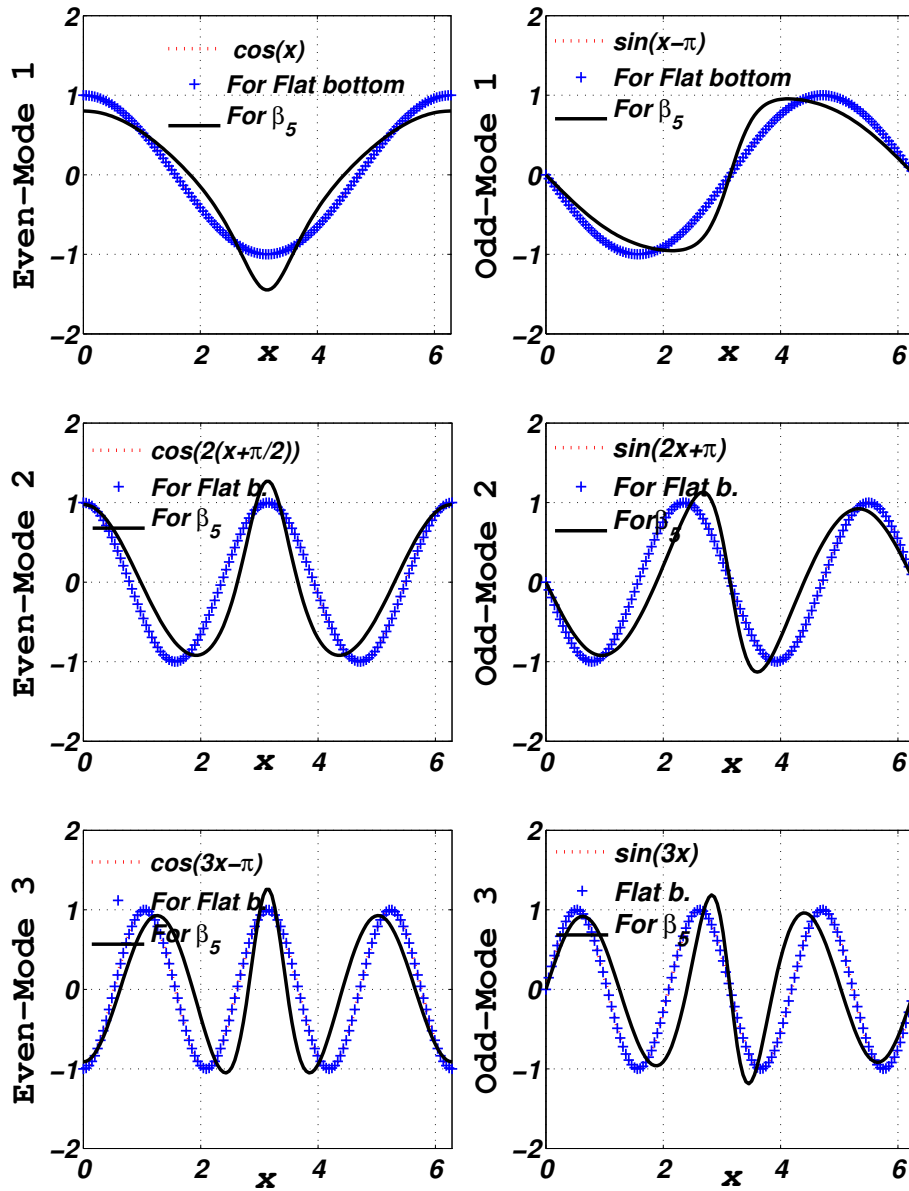
Figure 2.4: The even and odd $\kappa = 1, 2$ and 3 eigenmodes for β_5 *Gaussian* bottom profile, see Figure (1a), with $k_{Max} = 2^6$ and $\epsilon = 0.001$.
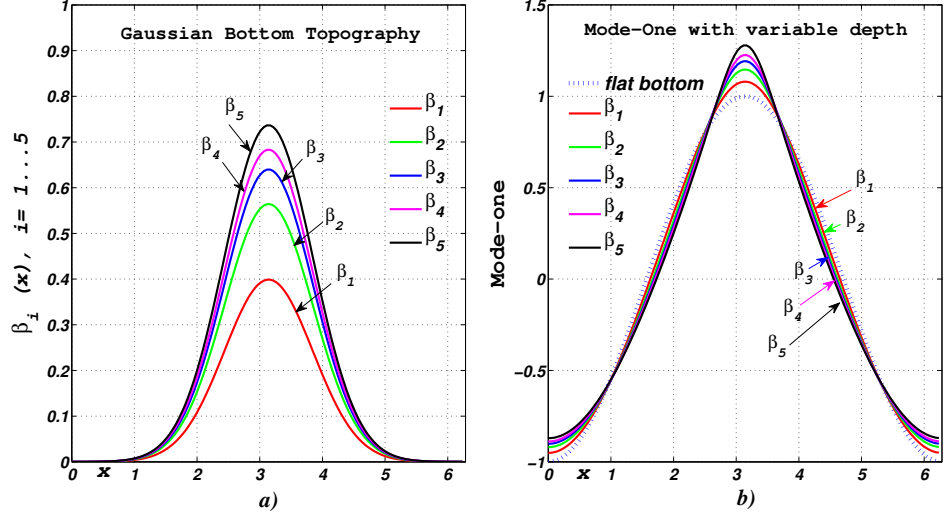
Figure 2.5: Figure b) shows the $\kappa = 1$ eigenmode for the *Gaussian* depth profiles of Figure a), see Figure (1a).

the bandwidth becomes narrower. For instance, the $\kappa = 1$ normal mode has a bandwidth of 17 modes, that is the amplitudes of all the other modes are less than or equal to 10^{-6} (using a truncation with $k_{Max} = 2^6$).

2.5 Numerical integration of the Whitham-Boussinesq model

In this section we integrate numerically the system derived from the Hamiltonian H_2, using the model Dirichlet-Neumann operator G_{Aprox_2} of (2.25). In the constant depth case H_2 reduces to H_0.

We examine two types of experiments, the separation of an initial disturbance into two counter-propagating waves, and the evolution of a Stokes wavetrain. We report first that in the constant depth case, the H_0 model seems to capture qualitatively the results from the higher order model of Craig and Sulem [10]. In the variable depth case we see clear effects of the topography on the evolution of the wave crests and a significant deformation of the Stokes wave.

We discretized the system spatially using the spectral representations introduced in the previous sections. The Galerkin equations of motion are outlined in Appendix A. We comment on the possibility of a more efficient evaluation of the discretized system in Section 5. Numerical integration is performed using a fourth-fifth order Adams-Bashford/Moulton (ABM) predictor-corrector scheme, see [2]. Some
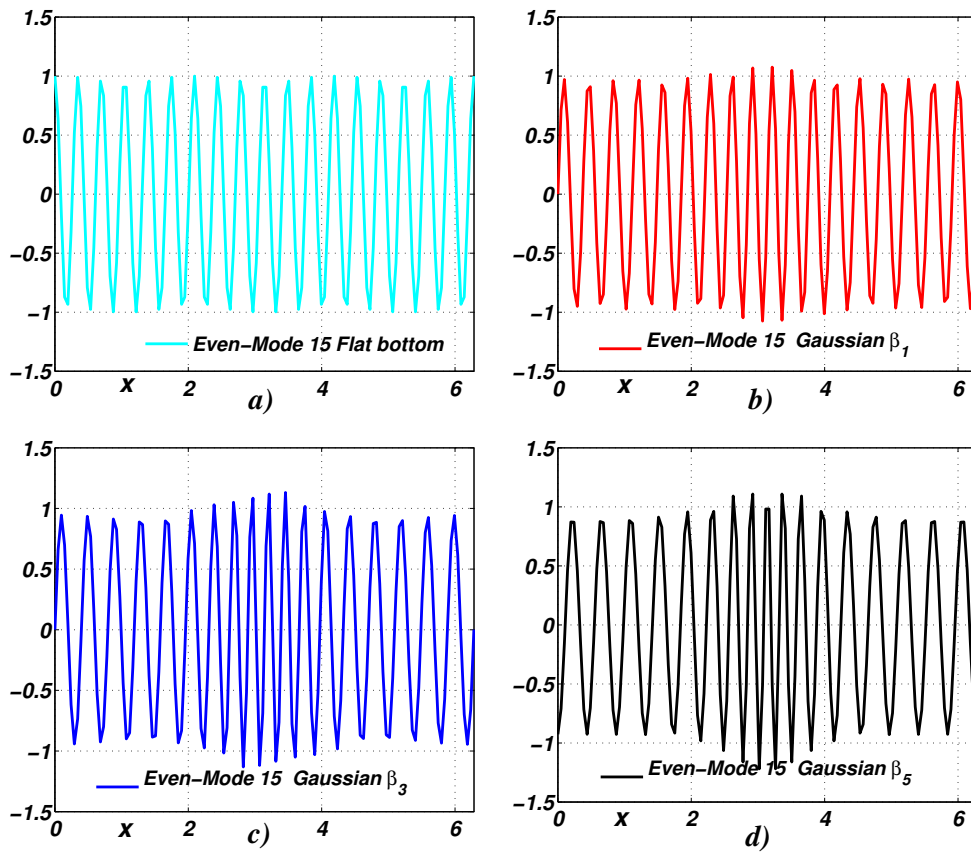
Figure 2.6: The figure shows the $\kappa = 15$ eigenmode for the a) Flat bottom profile b) for the *Gaussian* bottom profile β_1, c) for β_3 and d) for β_5, from equation (2.50), see Figure (1a), with $k_{Max} = 2^6$, $\epsilon = 0.001$.
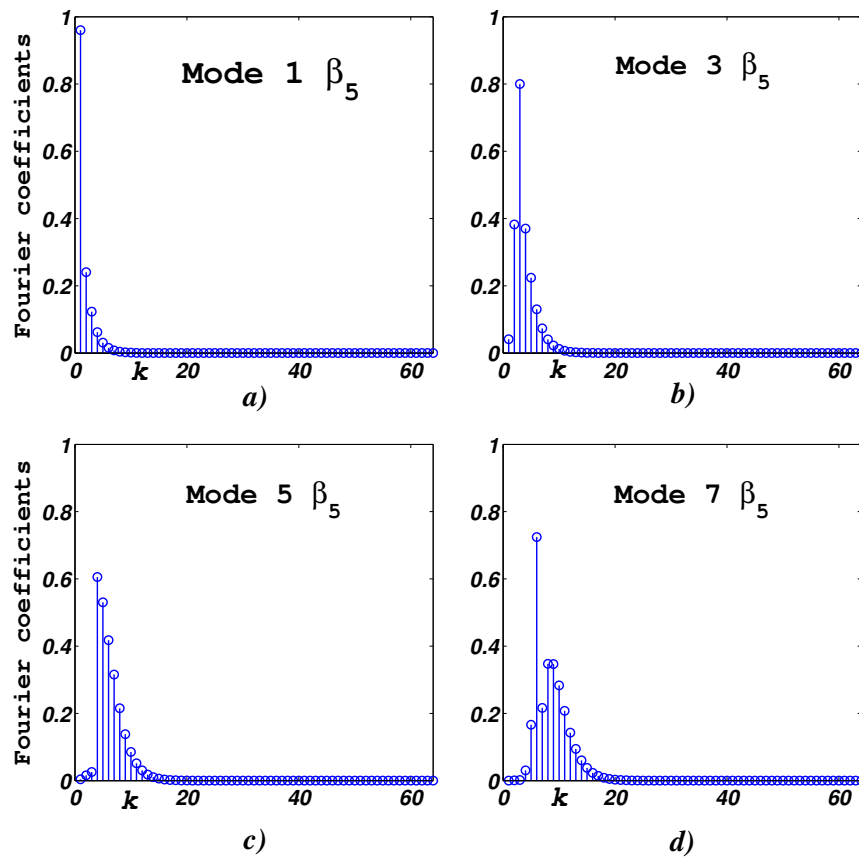
Figure 2.7: Fourier spectrogram of $\kappa = 1, 3, 5$ and 7 eigenmodes for β_5 *Gaussian* profile, see Figure (1a), with $k_{Max} = 2^6$, $\epsilon = 0.001$.

details are in *Appendix A*.

In all the numerical experiments below we consider smooth initial conditions for η and ξ. We choose the time step Δt so that the relative error in the energy vs. t, $\frac{|E_t - E_0|}{E_0}$, is less than 10^{-3}. In the case of variable topography we calibrated the accuracy of the integration using as initial conditions some of the normal modes computed in *Section* 3. The numerical scheme was implemented in MATLAB.

We first consider the propagation of a modulated wave packet using the initial conditions of [10]

$$\eta_0(x) = 0.01 \, e^{-\frac{4}{3}(x-\pi)^2} \cos(10x), \tag{2.52}$$

$$\xi_0(x) = 0, \, \forall x \in [0, 2\pi]. \tag{2.53}$$

The depth is constant at $h = 1$.

In Figure 2.8 we show the evolution of the free surface based on Hamiltonian flow of H_2. Specifically, in Figure (8c) we show $\eta(x,t)$ in the time interval from $t = 0$ to $t = 120$. We use the time step $\Delta t = 0.0001$ and 2^5 Fourier modes. The nonlinearity parameter is $\epsilon = 0.01$ (note that ϵ also appears in the linear terms. This is due to the long-wave scaling).

Figure 2.8a shows the wave profiles $\eta(x,t)$ at $t = 0$ and $t = 120$. We see the splitting of the initial wave profile into two waves traveling in opposite directions. After some time we observe the interference of the two packets due to the periodic boundary conditions. We observe the same qualitative behavior as in the numerical results presented in [10] by Craig and Sulem. The wave-crests in each wave packet have constant speeds. The evolution of the energy is indicated inFigure 2.8b . This quantity is conserved very well throughout the computation, with a relative error of $O(10^{-3})$. The numerical scheme is seen to be slightly dissipative and we need to use a time step that is small enough to result in a small relative error in the energy.

Figure 2.9 shows the evolution of the free surface $\eta(x,t)$ using H_2 and the initial conditions (2.52), (2.53), but now with variable depth β_5, see (2.50). The integration is from $t = 0$ to $t = 120$, and we use $k_{\text{Max}} = 2^5$, time step $\Delta t = 0.0001$, and $\epsilon = 0.01$. Figure 2.9c shows the free surface profile during the propagation through a variable depth channel. As in the constant depth case, we see the splitting of the initial wave profile into two wave-packets traveling in opposite directions. Nevertheless in this case we observe that the wave-crests have variable speed, and travel faster in the regions of higher depths. This behavior was expected because it is well known that the water wave travel faster in depth water than in shallow water.

The second numerical experiment used as initial condition a second-order approximation of the Stokes wavetrain of the full Euler equations used in [10],

$$\eta_0(x) = a\cos(\lambda x) + \mu_2 a^2 \cos(2\lambda x), \tag{2.54}$$

$$\xi_0(x) = \nu_1 a \cosh(\lambda(\eta_0 + h))\sin(\lambda x) + \nu_2 a^2 \cosh(2\lambda(\eta_0 + h))\sin(2\lambda x) \tag{2.55}$$
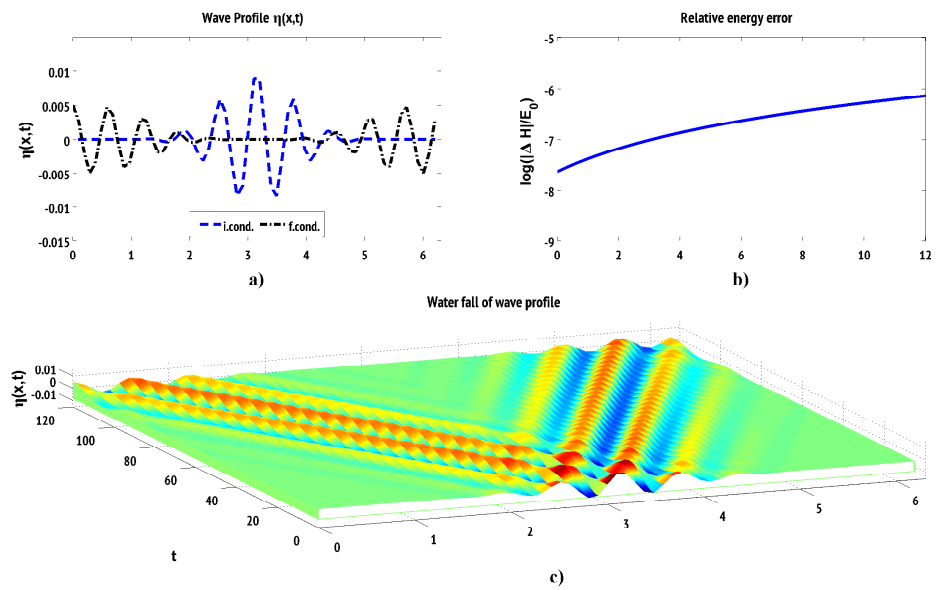
Figure 2.8: a) The dashed line shows the initial wave amplitude profile, the dot-dashed line shows the wave amplitude profile at time $t = 120$. b) The logarithm of the relative energy error from $t = 0$ to $t = 120$. c) Evolution of the free surface $\eta_0(x, t) = 0.01 \, e^{-\frac{4}{3}(x-\pi)^2} \cos(10x)$, $\xi_0(x) \equiv 0$, using H_2, with constant depth $h = 1.0$
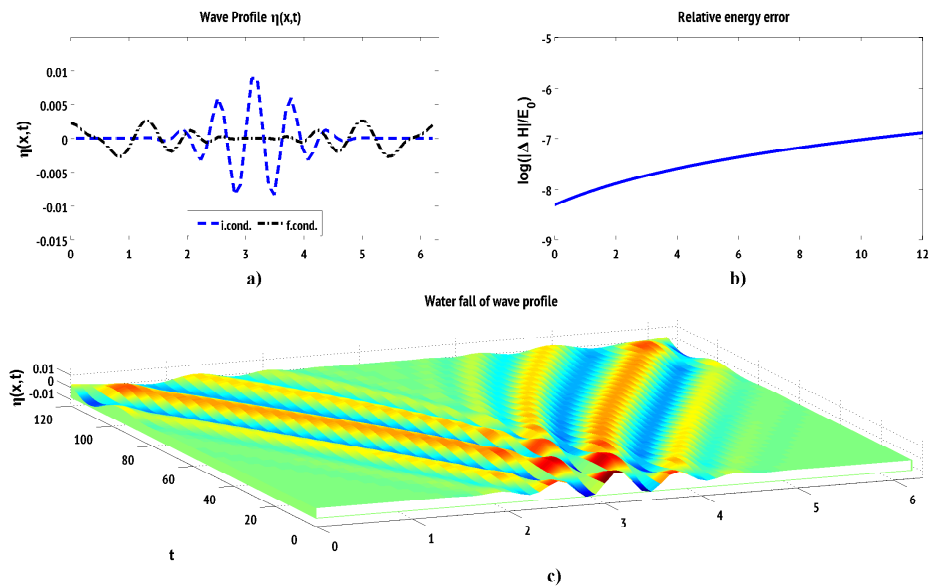
Figure 2.9: a) The dashed line is the initial wave amplitude profile, the dot-dashed line shows the wave amplitude profile at time $t = 120$. b) The logarithm of the relative energy error from $t = 0$ to $t = 120$. c) Evolution of the free surface $\eta_0(x,t) = 0,01e^{-\frac{4}{3}(x-\pi)^2}\cos(10x)$, $\xi_0(x) \equiv 0$, using H_2, and depth profile $\beta_5 = \frac{1}{\sqrt{\pi - 1.3}}e^{-(x-\pi)^2}$ of equation (2.50).
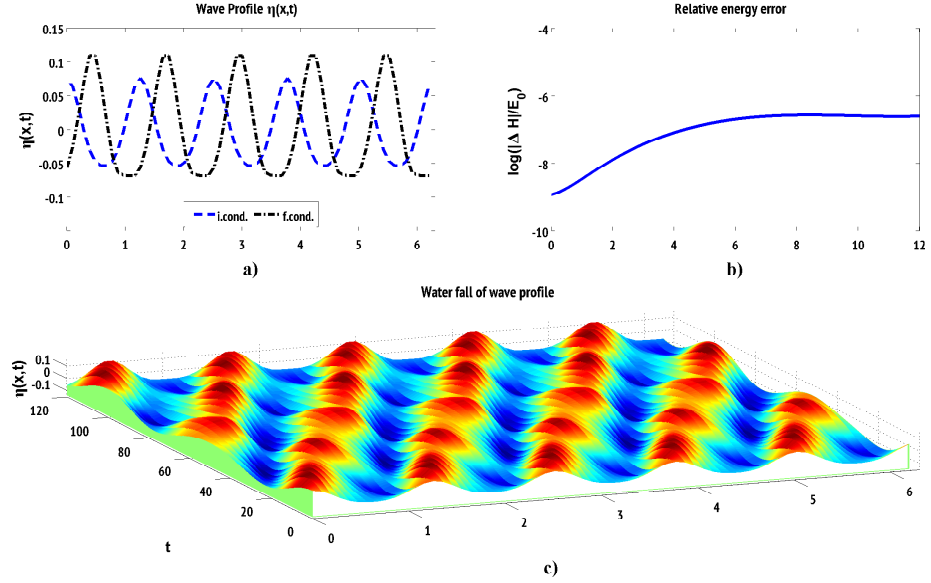
Figure 2.10: a) The dashed line shows the initial wave amplitude profile, the dot-dashed line shows the wave amplitude at time $t = 120$. b) The logarithm of the relative energy error from $t = 0$ to $t = 120$. c) Evolution of the second-order approximation Stokes wavetrain using H_2, and $\lambda = 5$, $a = 0.065$, $h = 1.0$ (constant depth).

where

$$\mu_2 = \frac{1}{2}\lambda\coth(h\lambda)\left(1 + \frac{3}{2\sinh(\lambda h)}\right), \quad \nu_1 = \frac{\omega}{\lambda\sinh(h\lambda)}, \quad \nu_2 = \frac{3}{8}\frac{3\omega}{\sinh^4(h\lambda)}, \tag{2.56}$$

and $a = 0.065$, $\lambda = 5$.

In Figure 2.10 we show $\eta(x,t)$ based on the equations for H_2 with constant depth $h = 1$. Specifically in Figure 2.10c we plot $\eta(x,t)$ in the time interval from $t = 0$ to $t = 120$ in the (x,t)-plane using $\Delta t = 0.0001$. In Figure 2.10a we show the initial wave profile compared to the profile at $t = 120$. The computation was performed with a resolution of 2^5 Fourier modes, using $\epsilon = 0.065$ (this was also the value of the amplitude a of (2.54)). In Figure (10b) we verify the conservation of energy. We observe the same qualitative behavior seen in the numerical results of [10] by Craig and Sulem. The wave amplitude stays near the traveling wave profile, with some oscillations in the width of the crests, as in [10].

Figure 2.11 shows the evolution of the free surface $\eta(x,t)$ using H_2, the same initial condition given by (2.54) and (2.55), but with variable depth β_5, as in (2.50). The time integration is from $t = 0$ to $t = 120$, and we use $k_{\mathsf{Max}} = 2^5$, time step $\Delta t = 0.0001$, and $\epsilon = 0.065$. Figure 2.11 c shows the free surface as the Stokes wavetrain propagates through a channel with the variable *Gaussian* depth profile
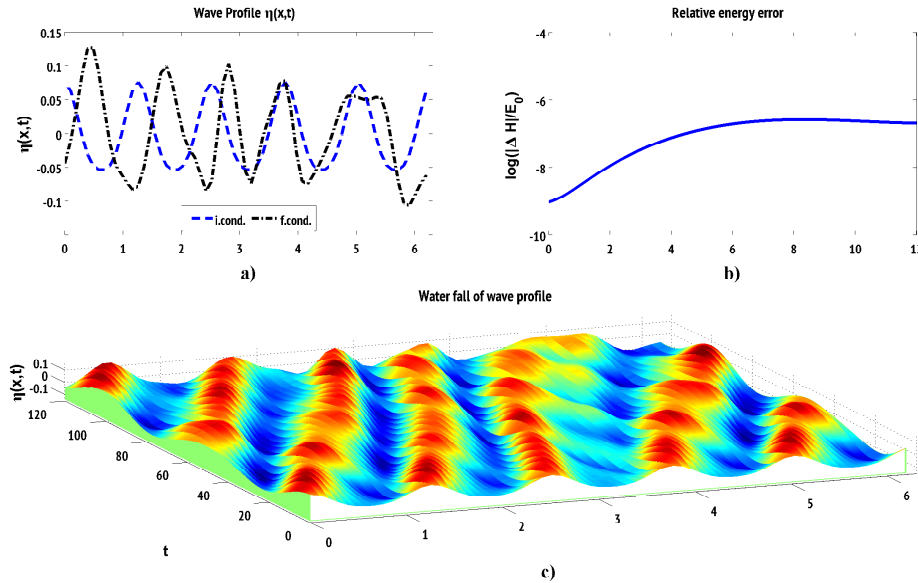
Figure 2.11: a)The dashed line shows the initial wave amplitude profile, the dot-dashed line shows the wave amplitude profile at time $t = 120$. b) The logarithm of the relative energy error from $t = 0$ to $t = 120$. c) Evolution of the second-order approximation Stokes wavetrain using H_2, and $\lambda = 5$, $a = 0.065$, depth profile $\beta_5 = \frac{1}{\sqrt{\pi - 1.3}} e^{-(x-\pi)^2}$, see (2.50).

β_5 of (2.50). At the initial time the solution is a slightly perturbed Stokes wavetrain, and the propagation is shown as in Figure 2.10c. However, as time progresses and the wave starts to feel the bottom topography, it develops stronger deformations that start to destroy its shape. The deformation involves changes in the speed and height of some of the crests which roughly follow the topography.

We conclude with some remarks on the accuracy of the numerical integrations. The dependence of our results on the numerical time step Δt is indicated in Figure 2.12 , where we see the wave profiles at time t=120 obtained using the time steps $\Delta t = 0.01$, $\Delta t = .001$, and $\Delta t = .0001$. The relative energy error decreases noticeably as we decrease the time step. In Figure 2.13 we show the dependence of the results on $k_{Max} = M$. Results obtained with $k_{Max} = 2^6$, $k_{Max} = 2^7$, and $k_{Max} = 2^8$ for the depth profile β_5 are almost identical. Similar results were obtained for the depth profile ζ_5. It then appears that $k_{Max} = 2^6$ gives reliable results, and that decreasing the time step is more important for increasing the accuracy. (Computations with Δt of order 10^{-4}, $k_{Max} = 2^6$ were not possible because of storage limitations in our computer). This is a important reason to move to other programming language different from MATLAB an by this way improve the efficiency of the numerics computations. One of the member of the jury was surpriced
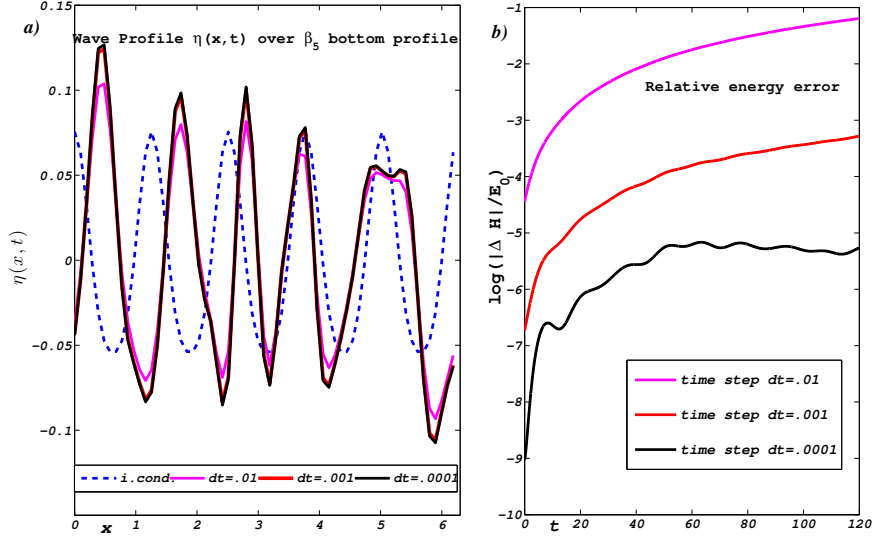
Figure 2.12: a) The dashed line shows the initial wave amplitude profile, the continuous lines in different colors show the wave amplitude at time $t = 120$, with $k_{Max} = 2^6$, and time steps $\Delta t = .01$ (magenta), t=.001(red), Δ t=.0001 (black). Figure b) Shows the logarithm of the relative error from $t = 0$ to $t = 120$ for different time steps $\Delta t = .01$, $\Delta t = .001$, and $\Delta t = .0001$.

with this incovenient, considering that $2^6$is not a large number in computational capacity terms. Nevertheless, we consider that, a time step of 10^{-4} is small enough to overpass the storage of computation in some computers as Macbook Air with lets say 30G available of storage at the moment of our computations.

Appendix A

We now display the equations of motion derived from the Hamiltonians H_2, see Hamiltonian (2.26), and H_1, the corresponding Hamiltonian with (2.24). The corresponding Galerkin approximations, see (2.29)), are denoted by H_2^M and H_1^M, respectively.
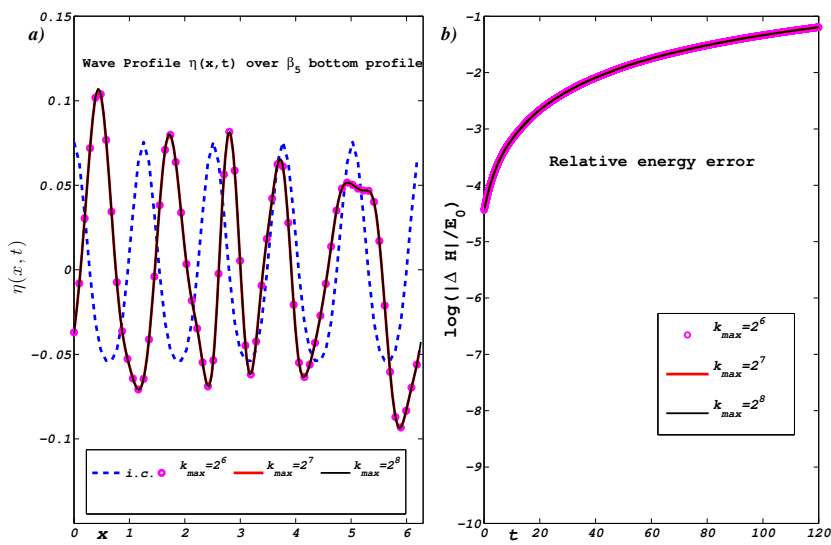
Figure 2.13: a)The dashed line shows the initial wave amplitud profile, the continuous line in different colors shows the wave amplitude at time $t = 120$ with time step $\Delta t = .01$ for $k_{Max} = 2^6$ (magenta), red $k_{Max} = 2^7$ (red), $k_{Max} = 2^8$ (black) Figure b) Shows the logarithm of the relative error from $t = 0$ to $t = 120$ for $k_{Max} = 2^6$, 2^7, and 2^8.

Hamilton's equations for the Hamiltonian H_1^M are

$$
\frac{\partial \hat{\eta}_k}{\partial t} = \frac{k}{\sqrt{\epsilon}} \tanh(\sqrt{\epsilon}k)(\frac{1}{2\pi}\hat{\xi}_k) + \frac{\epsilon}{4\pi^2} \sum_{k_1 \in J_M} (-kk_1\hat{\xi}_{k_1}\hat{\beta}_{-k_1+k} + kk_1\hat{\xi}_{k_1}^*\hat{\beta}_{k+k_1}) \quad (2.57)
$$

$$
+ \; \mathcal{N}_{1,k}(\hat{\eta}^M, (\hat{\eta}^M)^*, \hat{\xi}^M, (\hat{\xi}^M)^*), \tag{2.58}
$$

$$
\frac{\partial \hat{\xi}_k}{\partial t} = -\frac{1}{2\pi}\hat{\eta}_k + \mathcal{N}_{2,k}(\hat{\eta}^M, (\hat{\eta}^M)^*, \hat{\xi}^M, (\hat{\xi}^M)^*), \quad k = 1, \dots, M. \tag{2.59}
$$

$$
\tag{2.60}
$$

The $\mathcal{N}_{i,k}(\hat{\eta}^M, (\hat{\eta}^M)^*, \hat{\xi}^M, (\hat{\xi}^M)^*)$ are the nonlinear terms calculated from (2.29). They are given by

$$
\mathcal{N}_{1,k} = \begin{cases} -\frac{\epsilon}{4\pi^2}(\sum_{k_1=1}^{M-1} k_1\hat{\xi}_{k_1}^*\hat{\eta}_{1+k_1} + \sum_{k_1=2}^{M} k_1\hat{\xi}_{k_1}\hat{\eta}_{-1+k_1}^*), \; k = 1, \\ \frac{\epsilon}{8\pi^2}(-\sum_{k_1=1}^{M-k} kk_1\hat{\xi}_{k_1}^*\hat{\eta}_{k+k_1} + \sum_{k_1=1}^{k-1} k_1k\hat{\xi}_{k_1}\hat{\eta}_{k-k_1} + \\ \sum_{k_1=k+1}^{M} kk_1\hat{\xi}_{k_1}\hat{\eta}_{-k+k_1}^*), \; k = 2, \dots, M-1, \\ \frac{\epsilon M}{4\pi^2}\sum_{k_1=1}^{M-1} k_1\hat{\xi}_{k_1}\hat{\eta}_{M-k_1}, \; k = M \end{cases}, \tag{2.61}
$$

$$
\mathcal{N}_{2,k} = \begin{cases} \frac{\epsilon}{8\pi^2}(\sum_{k_2=1}^{M-1} k_2(1+k_2)\hat{\xi}_{k_2}^*\hat{\xi}_{1+k_2} + \sum_{k_2=2}^{M} k_2(-1+k_2)\hat{\xi}_{k_2}\hat{\xi}_{-1+k_2}^*), \; k = 1, \\ \frac{\epsilon}{8\pi^2}(-\sum_{k_2=1}^{k-1} k_2(k-k_2)\hat{\xi}_{k_2}\hat{\xi}_{k-k_2} + \sum_{k_2=1}^{M-k} k_2(k+k_2)\hat{\xi}_{k_2}^*\hat{\xi}_{k+k_2} + \\ + \sum_{k_2=k+1}^{M} k_2(-k+k_2)\hat{\xi}_{k_2}\hat{\xi}_{-k+k_2}^*), \; k = 2, \dots, M-1, \\ -\frac{\epsilon}{8\pi^2}\sum_{k_2=1}^{M-1} k_2(M-k_2)\hat{\xi}_{k_2}\hat{\xi}_{M-k_2}, \; k = M, \end{cases},
$$

$$
\tag{2.62}
$$

with $\hat{\eta}^M = (\hat{\eta}_1, ..., \hat{\eta}_M)$, $(\hat{\eta}^M)^* = (\hat{\eta}_1^*, ..., \hat{\eta}_M^*)$, similarly for $\hat{\xi}^M$ and $(\hat{\xi}^M)^*$.

Hamilton's equations for H_2 differ from those for H_1^M in the linear part. The spectral representation of H_2^M in the real variables $\rho = Re(\hat{\eta}^M) = Re(\hat{\eta}_1, ..., \hat{\eta}_k, ..., \hat{\eta}_M)$, $\tau = Im(\hat{\eta}^M) = Im(\hat{\eta}_1, ..., \hat{\eta}_k, ..., \hat{\eta}_M)$, $\theta = Re(\hat{\xi}^M) = Re(\hat{\xi}_1, ..., \hat{\xi}_k, ..., \hat{\xi}_M)$, $\zeta = Im(\hat{\xi}^M) = Im(\hat{\xi}_1, ..., \hat{\xi}_k, ..., \hat{\xi}_M)$, $k \in J_M$, yields the following system in $\mathbb{R}^{4M}$:

$$
\begin{bmatrix} \dot{\rho} \\ \dot{\tau} \\ \dot{\theta} \\ \dot{\zeta} \end{bmatrix} = \begin{pmatrix} 0 & M_2 \\ -I & 0 \end{pmatrix} \begin{bmatrix} \rho \\ \tau \\ \theta \\ \zeta \end{bmatrix} + \mathcal{N}^{Real}(\rho, \tau, \theta, \zeta). \tag{2.63}
$$

$\mathcal{N}^{Real}(\rho, \tau, \theta, \zeta)$ denotes the nonlinear terms, as in (2.61), (2.62), and

$$M_2 = \begin{pmatrix} Sym(C_{11}) & -\frac{1}{2}Im((P^*)^T - P^T + P^* - P) \\ -\frac{1}{2}Im((P^*)^T - P^T + P^* - P) & Sym(C_{22}) \end{pmatrix} \quad (2.64)$$

with P, $C_{11} = Re(P^* + S^* + P + S)$, and $C_{22} = -Re(P^* - S^* - S + P)$ as in (2.40). Also, I denotes the $2M \times 2M$ identity matrix. In this case Hamilton's equations for the Hamiltonian H_2^M are written in real variables.

The nonlinear terms in real variables are given by

$$\mathcal{N}_{1,k}^{Real} = \begin{cases} -\frac{\epsilon}{4\pi^2}(\sum_{k_1=1}^{M-1} k_1\theta_{k_1}^*\rho_{1+k_1} + \theta_{k_1}^*\tau_{1+k_1} + \zeta_{k_1}^*\rho_{\eta 1+k_1} + \zeta_{k_1}^*\tau_{1+k_1} + \\ \sum_{k_1=2}^{M} k_1\theta_{k_1}\rho_{-1+k_1}^* + \theta_{k_1}\tau_{-1+k_1}^* + \zeta_{k_1}\rho_{-1+k_1}^* + \zeta_{k_1}\tau_{-1+k_1}^*) \text{ for } k=1 \\ \frac{\epsilon}{8\pi^2}(-\sum_{k_1=1}^{M-k} kk_1(\theta_{k_1}^*\rho_{k+k_1} + \theta_{k_1}^*\tau_{k+k_1} + \zeta_{k_1}^*\rho_{k+k_1} + \zeta_{k_1}^*\tau_{k+k_1} + \\ \sum_{k_1=1}^{k-1} k_1 k\theta_{k_1}\rho_{\eta k-k_1} + \theta_{k_1}\tau_{k-k_1} + \zeta_{k_1}\rho_{k-k_1} + \zeta_{k_1}\beta_{k-k_1} + \\ \sum_{k_1=k+1}^{M} kk_1\theta_{k_1}\rho_{-k+k_1}^* + \theta_{k_1}\tau_{-k+k_1}^* + \\ +\zeta_{k_1}\rho_{-k+k_1}^* + \zeta_{k_1}\tau_{-k+k_1}^*) \text{ for } k=2,...,M-1 \\ \frac{\epsilon M}{4\pi^2}(\sum_{k_1=1}^{M-1} k_1\theta_{k_1}\rho_{M-k_1} + \theta_{k_1}\tau_{M-k_1} + \zeta_{k_1}\rho_{M-k_1} + \zeta_{k_1}\tau_{M-k_1}) \text{ for } k=M \end{cases}$$

$$(2.65)$$

$$\mathcal{N}_{2,k}^{Real} = \begin{cases} \frac{\epsilon}{8\pi^2}(\sum_{k_2=1}^{M-1} k_2(1+k_2)(\theta_{k_2}^*\theta_{1+k_2} + \theta_{k_2}^*\zeta_{1+k_2} + \zeta_{k_2}^*\theta_{1+k_2} + \zeta_{k_2}^*\zeta_{1+k_2}) + \\ \sum_{k_2=2}^{M} k_2(-1+k_2)(\theta_{k_2}\theta_{-1+k_2}^* + \theta_{k_2}\zeta_{-1+k_2}^* + \zeta_{k_2}\theta_{-1+k_2}^* + \zeta_{k_2}\zeta_{-1+k_2}^*) \text{ for } k=1 \\ \frac{\epsilon}{8\pi^2}(-\sum_{k_2=1}^{k-1} k_2(k-k_2)(\theta_{k_2}\theta_{k-k_2} + \theta_{k_2}\zeta_{k-k_2} + \zeta_{k_2}\theta_{k-k_2} + \zeta_{k_2}\zeta_{\xi k-k_2}) + \\ \sum_{k_2=1}^{M-k} k_2(k+k_2)(\theta_{k_2}^*\theta_{k+k2} + \theta_{k_2}^*\zeta_{k+k2} + \zeta_{k_2}^*\theta_{k+k2} + \zeta_{k_2}^*\zeta_{k+k_2}) + \\ \sum_{k_2=k+1}^{M} k_2(-k+k_2)(\theta_{k_2}\theta_{-k+k_2}^* + \theta_{k_2}\zeta_{-k+k_2}^* + \\ +\zeta_{k_2}\theta_{-k+k_2}^* + \zeta_{k_2}\zeta_{-k+k_2}^*), \text{ for } k=2,...,M-1 \\ -\frac{\epsilon}{8\pi^2}(\sum_{k_2=1}^{M-1} k_2(M-k_2)(\theta_{k_2}\theta_{M-k_2} + \theta_{k_2}\delta_{M-k_2} + \zeta_{k_2}\theta_{M-k_2} + \zeta_{k_2}\zeta_{M-k_2}) \text{ for } k=M \end{cases}$$

$$(2.66)$$

To integrate the system of ODE's (2.63) for $y = (\rho, \tau, \theta, \zeta) \in \mathbb{R}^{4M}$ we use a fourth-fifth order Adams-Bashford/Moulton (ABM) predictor-corrector time integra-

tion scheme, initiated by a 4-stage Runge-Kutta scheme, see [2]. Accordingly, the predictor is defined as

$$y_{n+1} = y_n + \frac{\Delta t}{24}(55\dot{y}_n - 59\dot{y}_{n-1} + 37\dot{y}_{n-2} - 9\dot{y}_{n-3}),$$

and the corrector is

$$y_{n+1} = y_n + \frac{\Delta t}{720}(251\dot{y}_{n+1} + 646\dot{y}_n - 264\dot{y}_{n-1} + 106\dot{y}_{n-2} - 19\dot{y}_{n-3}).$$

Appendix B

Let $\hat{\xi}^M = (\hat{\xi}_1, ..., \hat{\xi}_M)$ as in (2.29), and consider the Galerkin truncation $K^M_{a(x,D)}$ of $K_{a(x,D)}$, assuming $\xi_0 = 0$. Moreover by remarks (3.6) and (3.7) we also assume $\hat{a}_{-\lambda}(k) = \hat{a}^*_\lambda(k)$ and $\hat{a}_\mu(-k) = \hat{a}_\mu(k)$ to obtain equation (2.38).
From the second sumation of equation (3.10)

$$\sum_{[k_1,k_2]\in J^2_M} \hat{\xi}^*_{k_1}\hat{\xi}^*_{k_2}\hat{a}_{k_1+k_2}(k_2) \tag{2.67}$$

we obtain the matrix P as

$$P = \begin{pmatrix} \hat{a}_{1+1}(1) & \hat{a}_{1+2}(2) & ... & \hat{a}_{1+(M-2)}(M-2) & \hat{a}_{1+(M-1)}(M-1) & 0 \\ \hat{a}_{2+1}(1) & \hat{a}_{2+2}(2) & ... & \hat{a}_{2+(M-2)}(M-2) & 0 & 0 \\ ... & ... & ... & ... & ... & ... \\ \hat{a}_{(M-2)+1}(1) & \hat{a}_{(M-2)+2}(2) & 0 & 0 & 0 & 0 \\ \hat{a}_{(M-1)+1}(1) & 0 & ... & 0 & 0 & 0 \\ 0 & 0 & 0 & 0 & 0 & 0 \end{pmatrix}$$

From the third sumation of (3.10)

$$\sum_{[k_1,k_2]\in J^2_M} \hat{\xi}_{k_1}\hat{\xi}^*_{k_2}\hat{a}_{-k_1+k_2}(k_2), \tag{2.68}$$

we obtain the matrix S as

$$S = \begin{pmatrix} \hat{a}_{-1+1}(1) & \hat{a}_{-1+2}(2) & ... & \hat{a}_{-1+(M-1)}(M-1) & \hat{a}_{-1+M}(M) \\ \hat{a}_{-2+1}(1) & \hat{a}_{-2+2}(2) & ... & \hat{a}_{-2+(M-1)}(M-1) & \hat{a}_{-2+M}(M) \\ ... & ... & ... & ... & ... \\ \hat{a}_{-M+1}(1) & \hat{a}_{-M+2}(2) & ... & \hat{a}_{-M+(M-1)}(M-1) & \hat{a}_{-M+M}(M) \end{pmatrix}$$

$$= \begin{pmatrix} \hat{a}_0(1) & \hat{a}_1(2) & ... & \hat{a}_{M-2}(M-1) & \hat{a}_{M-1}(M) \\ \hat{a}^*_1(1) & \hat{a}_0(2) & ... & \hat{a}_{M-3}(M-1) & \hat{a}_{M-2}(M) \\ ... & ... & ... & ... & ... \\ \hat{a}^*_{M-1}(1) & \hat{a}^*_{M-2}(2) & ... & \hat{a}^*_1(M-1) & \hat{a}_0(M) \end{pmatrix}$$

Appendix C

Hamiltonian Structure in real variables and evolution equations.

Letting the real variables

- $a_k = Re(\eta_k)$

- $\beta_k = Im(\eta_k)$

- $\gamma_k = Re(\hat{\xi}_k)$

- $\delta_k = Im(\xi_k)$

such that

- $\hat{\eta}_k = \alpha_k + i\beta_k \,, \quad \hat{\xi}_k = \gamma_k + i\delta_k$

- $\hat{\eta}_k^* = \alpha_k - i\beta_k \,, \quad \hat{\xi}_k = \gamma_k - i\delta_k$

that is,

- $\alpha_k = \frac{1}{2}(\hat{\eta}_k + \hat{\eta}_k^*) \,, \quad \beta_k = \frac{1}{2i}(\hat{\eta}_k - \hat{\eta}_k^*)$

- $\gamma_k = \frac{1}{2}(\hat{\xi}_k + \hat{\xi}_k^*) \,, \quad \delta_k = \frac{1}{2i}(\hat{\xi}_k - \hat{\xi}_k^*)$

By chain rule we have

$$\frac{\partial f}{\partial \hat{\eta}_k^*} = \frac{\partial f}{\partial \alpha_k}\frac{\partial a_k}{\partial \hat{\eta}_k^*} + \frac{\partial f}{\partial \beta_k}\frac{\partial \beta_k}{\partial \hat{\eta}_k^*} = \frac{\partial f}{\partial \alpha_k}\frac{1}{2} + \frac{\partial f}{\partial \beta_k}(\frac{-1}{2i}) = \frac{1}{2}\frac{\partial f}{\partial \alpha_k} - \frac{1}{2}i\frac{\partial f}{\partial \beta_k}$$

and

$$\frac{\partial f}{\partial \hat{\xi}_k^*} = \frac{\partial f}{\partial \gamma_k}\frac{\partial \gamma_k}{\partial \hat{\xi}_k^*} + \frac{\partial f}{\partial \delta_k}\frac{\partial \delta_k}{\partial \hat{\xi}_k^*} = \frac{\partial f}{\partial \gamma_k}\frac{1}{2} + \frac{\partial f}{\partial \delta_k}(\frac{-1}{2i}) = \frac{1}{2}\frac{\partial f}{\partial \gamma_k} - \frac{1}{2}i\frac{\partial f}{\partial \delta_k}$$

Moreover,

$$\frac{d}{dt}\hat{\eta}_k = \frac{\partial H}{\partial \hat{\xi}_k^*} \Longleftrightarrow \dot{\alpha}_k + i\dot{\beta}_k = \frac{1}{2}\frac{\partial H}{\partial \gamma_k} - \frac{1}{2}i\frac{\partial H}{\partial \delta_k}$$

$$\frac{d}{dt}\hat{\xi}_k = -\frac{\partial H}{\partial \hat{\eta}_k^*} \Longleftrightarrow \dot{\gamma}_k + i\dot{\delta}_k = -\frac{1}{2}\frac{\partial H}{\partial \alpha_k} + \frac{1}{2}i\frac{\partial H}{\partial \beta_k}$$

Denoting $h = \frac{1}{2}H$ above equations becomes

$$\dot{\alpha}_k + i\dot{\beta}_k = \frac{1}{2}\frac{\partial H}{\partial \gamma_k} - \frac{1}{2}i\frac{\partial H}{\partial \delta_k} \Longleftrightarrow \begin{cases} \dot{\alpha}_k = \frac{\partial h}{\partial \gamma_k} \\ \dot{\beta}_k = -\frac{\partial h}{\partial \delta_k} \end{cases}$$

and

$$\dot{\gamma}_k + i\dot{\delta}_k = -\frac{1}{2}\frac{\partial H}{\partial \alpha_k} + \frac{1}{2}i\frac{\partial H}{\partial \beta_k} \iff \begin{cases} \dot{\gamma}_k = -\frac{\partial h}{\partial a_k} \\ \dot{\delta}_k = \frac{\partial h}{\partial \beta_k} \end{cases}$$

We then obtain

$$\begin{matrix} \dot{\alpha}_k = \frac{\partial h}{\partial \gamma_k} \, , \, \dot{\gamma}_k = -\frac{\partial h}{\partial \alpha_k} \\ \dot{\beta}_k = -\frac{\partial h}{\partial \delta_k} \, , \, \dot{\delta}_k = \frac{\partial h}{\partial \beta_k} \end{matrix} \quad , k \in J_M$$

Thus, the Hamilton equations in real variables are

$$q = \begin{bmatrix} \alpha \\ \beta \end{bmatrix} \, , \, p = \begin{bmatrix} \gamma \\ -\delta \end{bmatrix} \tag{2.69}$$

$$\dot{q}_j = \frac{\partial h}{\partial p_j} \, , \, \dot{p}_j = -\frac{\partial h}{\partial q_j} \, , \, j = 1, ..., 2M \tag{2.70}$$

$$\dot{q}_j = \begin{bmatrix} \dot{\alpha}_j \\ \dot{\beta}_j \end{bmatrix} = \begin{bmatrix} \frac{\partial h}{\partial \gamma_j} \\ -\frac{\partial h}{\partial \delta_j} \end{bmatrix} = \frac{\partial h}{\partial p_j} \, , \, \dot{p}_j = \begin{bmatrix} \dot{\gamma}_j \\ -\dot{\delta}_j \end{bmatrix} = \begin{bmatrix} -\frac{\partial h}{\partial \alpha_j} \\ -\frac{\partial h}{\partial \beta_k} \end{bmatrix} = -\frac{\partial h}{\partial q_j} \quad \text{(2.71)}$$

equation above are defined in $\mathbb{R}^{2(2M)}$

Chapter 3

Transverse and trapped linear modes in nontrivial geometries

In this chapter we study two classical and related linear water waves problems, these are i) the computation of transverse modes of infinite straight channels of bounded constant cross-section with known normal modes, and ii) the existence of trapped modes in domains in infinite channels with unbounded cross-section, and sinusoidal dependence in the third direction, without any attenuation or distorsion and with finite transverse energy.

Both problems can be formulated and stated in the same formal setting. The basis of both problems is the classical linearized theory for the water waves equations for an ideal incompressible and irrotational fluid in a simply-connected domain. We will motivate and justify also the introduction of an appropiate approximation of the Dirichlet-Neumann operator of the modified Helmholtz operator for the computation of trapped modes over continental shelves as the corresponding eigenfunctions of the pseudodifferential operator associated with the desired topography.

We study the transverse modes of oscillation of surface water waves contained in two uniform channels whose cross-section is a symmetric triangle with sides inclined at $45°$ and $60°$ to the vertical, respectively, see Figure 3.1a and 3.1b. We present in this chapter a new method to compute these modes for different geometries using approximations to Dirichlet-Neumann operators given by pseudodifferentials operators, for the computation of transverse modes the approximative operator coincide with the operator derived in [65] and we compare our results with the exact solutions reported in the literaturate for these specific channel configurations described above, presented by Lamb [42], Macdonald [51] , Greenhill [19], Packman [58] and more recently Groves [22].

We also present in this article the computation of trapped waves over the top of a submerged ridge, where the cross-section is a idealistic continental shelf. The examples are studied in the literature see, J.M. Miles [53], A.S. Bonnet and P.

Joly[4], N. Kuznetsov [41], [43] and C.C. Mei, M.Stiassnie and D. K. P. Yue [52].

Using the linearized shallow water theory, and we compare these results to results obtained using a 3-D version of the nonlocal approximation of the Dirichlet-Neumann operator of *Chapter* 2.

The organization of this chapter is as follows. In *Section* 3.1 we present the formulation of the linear water wave problem and propose the approximate Dirichlet-Neumann operators associated with each problem. In *Section* 3.2 we present the special geometries where normal modes can be calculated explicitly. We give a short review of the solutions in the literature. We present the comparison of exact solutions and semi-analytical results of Mei et. al. in [52] to the modes computed with our approximate nonlocal Dirichlet-Neumann operators. In *Section* 3.3 we present a detailed account of the analysis of Mei on trapped waves on the top of a continental shelf. We present an alternative approach to this problem using the aproximate Dirichlet-Neumann operartor of *Chapter 2*.

3.1   Formulation of the problem and approximate Dirichlet-Neumann operators

The problems considered in this chapter come from the classical linearized theory of water waves [42]. To describe the equations we use Cartesian coordinates denoted by (x, y, z), where y is directed vertically upwards, x is measured longitudinally along the channel and z is measured across the channel or across the submarine ridge, see e.g. Figures 3.1a, 3.1b, 3.2.

We define the fluid domain as $\mathcal{D} = \mathbb{R} \times \Omega$, where Ω is the cross section, and we distinguish bounded and unbounded cross sections $\Omega = \Omega_B$, Ω_U respectively, with

$$\Omega_B = \{[z, y] : z \in [0, b], y \in [h_m + \beta(z), h_M], \tag{3.1}$$

$$\Omega_U = \{[z, y] : z \in (-\infty, \infty), y \in [h_m + \beta(z), h_M]. \tag{3.2}$$

The heights $y = h_m$ and $y = h_M$ describe the minimum and maximum elevations respectively, with $h_m < h_M$, and $h_m + \beta(z) \leq h_M$ for all z.

We will assume $\partial \mathcal{D} = \mathbb{R} \times \partial \Omega = \Gamma_F \cup \Gamma_B$, with Γ_F representing the free surface and Γ_B the bottom. In the case $\Omega = \Omega_B$

$$\Gamma_F = \{(x, h_M, z) : x \in \mathbb{R}, 0 \leq z \leq b\} \tag{3.3}$$

and

$$\Gamma_B = \{(x, \beta(z), z) : x \in \mathbb{R}, 0 \leq z \leq b\}. \tag{3.4}$$

We are thus assuming that $\partial \mathcal{D}$ has no lateral walls. In the case $\Omega = \Omega_U$ we are interested in domains with $\beta(z) \to 0$ as $z \to \pm\infty$.

(a) β_{45} (b) $\beta_{30}(z)$
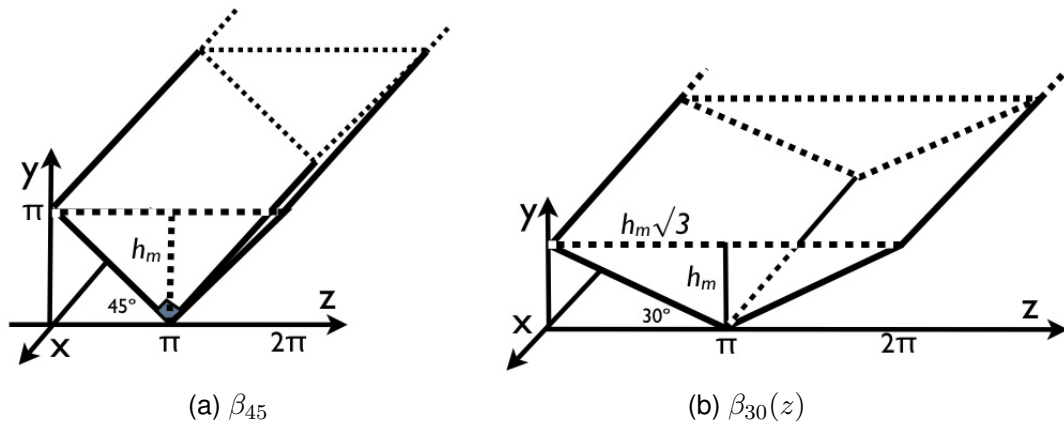
Figure 3.1: Schematics of straight channels with triangular cross-sections Ω and coordinate system
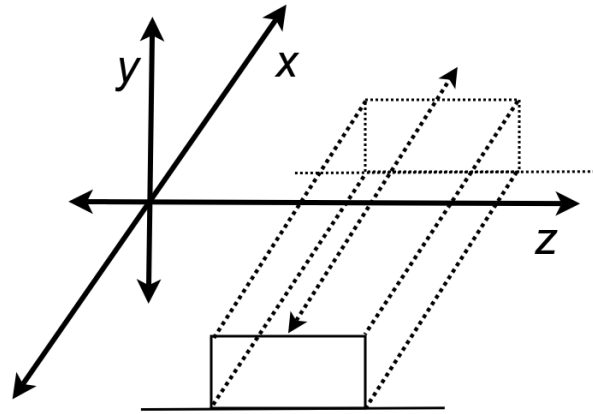
Figure 3.2: Schematics of submerged continental shelf $\beta_{h_i}(z)$ and coordinate system.

To state the problem we introduce a velocity potential $\phi(x, y, z, t)$ and look for solutions of Laplace's equation

$$\phi_{xx} + \phi_{yy} + \phi_{zz} = 0 \text{ in } \mathcal{D}, \tag{3.5}$$

with

$$\begin{cases} \phi_t + g\eta = 0 \text{ on } \Gamma_F \\ \eta_t = \varphi_y \text{ on } \Gamma_F. \\ \frac{\partial \phi}{\partial n} = 0 \text{ on } \Gamma_B, \end{cases} \tag{3.6}$$

see Whitam's book [68].

Equations (3.5) and (3.6) are the linearized Euler equations for free surface flow.

We consider solutions of the following two forms:

A.

$$\phi(x, y, z, t) = \psi(y, z) \cos(\omega t), \tag{3.7}$$

referred to as *transverse modes*, and

B.

$$\phi(x, y, z, t) = \psi(y, z) \cos(\kappa x - \omega t), \tag{3.8}$$

referred to as *longitudinal modes.*

In (3.8) we have a wave of wavelength $\lambda = \frac{2\pi}{\kappa}$ traveling in the $x-$direction with constant *phase velocity* $v_p = \frac{\omega}{\kappa}$.

We reformulate the problem of finding solutions of the above form in terms of the Dirichlet-Neumann operators.

A. Let the fluid domain consist of a straight canal and consider the case $\Omega = \Omega_B$. Consider $f : [0, b] \longrightarrow \mathbb{R}$, and define the Dirichlet-Neumann operator G_0 by

$$g(G_0[f])(z) = \frac{\partial \psi(z, y)}{\partial y}\big|_{y=0}, \tag{3.9}$$

where $\psi : \Omega \to \mathbb{R}$ satisfies

$$\begin{cases} \Delta \psi = 0 \ \text{ at } \Omega, \\ \psi(z, y) = f \text{ at } \Omega \cap \Gamma_F, \\ \frac{\partial \psi}{\partial n} = 0 \ \text{ at } \Omega \cap \Gamma_B \end{cases} \tag{3.10}$$

Then, the problem of finding transverse mode solutions (3.7) of (3.5)-(3.6) is equivalent to the spectral problem

$$(G_0[f])(z) = \omega^2 f. \tag{3.11}$$

Boundary conditions for f must be specified consistently for (3.10) and (3.11). Two possible choices are f of period b, and Dirichlet: $f(0) = f(b) = 0$. Boundary conditions will be further discussed in the next section for specific examples.

The above boundary conditions are mathematically consistent since we expect that the boundary value of the potential at $\Omega \cap \Gamma_F$ can be arbitrary. We note that the "pinned edges" boundary condition

$$\eta(z, 0, t) = \eta(z, b, t), \quad \forall z, t,$$

for the wave amplitude and the first dynamic boundary condition in (3.6) imply Dirichlet boundary conditions for f. Physical systems with pinned edges have been studied theoretically by several authors, see e.g. Groves [11], but are not necessarily physical. The main problem is that the parametrization of the free surface at all times t by the function $\eta(x, t)$, with x defined on a fixed domain, is unlikely to be physical.

Operator G_0 will be approximated by

$$\mathcal{A}_{G_0}[f] = Sym(D\tanh(h(x)D))[f], \tag{3.12}$$

using the notation and definitions of the previous chapter for the periodic case, see also [65]. The Dirichlet case can be defined analogously using a Fourier series.

The approximation of G_0 by $\mathcal{A}_{G_0}$ is consistent with the discussion of the previous chapter, since the transverse modes can be equivalently considered as normal modes of the linearized Dirichlet-Neumann operator for the two dimensional domain Ω. Normal modes for such two dimensional domains were considered in the previous chapter and by [65]. In the next section we will consider domains Ω for which there exist exact solutions of (3.5), (3.6) with sinusoidal time dependence. Such solutions are normal modes.

B. Case Ω_B. Consider $f(z) = \frac{1}{g}\psi(0,z)$, with $z \in [0,b]$ (case $\Omega = \Omega_B$), or $z \in (-\infty,\infty)$ (case $\Omega = \Omega_B$), and define the modified Dirichlet-Neumann operator G_κ by

$$(G_\kappa[f])(z) = \frac{1}{g}\frac{\partial\psi(z,y)}{\partial y}\big|_{y=0} \tag{3.13}$$

where $\psi : \Omega \longrightarrow \mathbb{R}$ satisfies

$$\begin{cases} \Delta\psi = \kappa^2\psi \text{ in } \Omega, \\ \psi(z,y) = f \text{ in } \Omega \cap \Gamma_F, \\ \frac{\partial\psi}{\partial n} = 0 \text{ at } \Omega \cap \Gamma_B. \end{cases} \tag{3.14}$$

The problem of finding longitudinal mode solutions (3.8) of (3.5)-(3.6) is equivalent to the spectral problem

$$(G_\kappa[f])(z) = \omega^2 f. \tag{3.15}$$

In the case of $\Omega = \Omega_B$, the boundary conditions on f are as in the case of the operator G_0 discussed in A.

In the case $\Omega = \Omega_B$ we also want to distinguish between solutions of that satisfy decay properties at infinity, and solutions that do not decay at infinity. Decaying solutions will be referred to as trapped (or Ursell) modes, see [64]. For instance a typical decay condition in the literature, see [4][40] for longitudinal mode solutions (3.8) of (3.5)-(3.6) is

$$\int_\Omega (|\psi(y,z)|^2 + |\nabla\psi(y,z)|^2)dy\,dz < +\infty. \tag{3.16}$$

The operator G_k of (3.13) will be approximated by the operator

$$\mathcal{A}_{G_\kappa}(\beta) = \mathsf{Sym}[\sqrt{\kappa^2 + D^2} \tanh(h(z)\sqrt{\kappa^2 + D^2})], \qquad (3.17)$$

with $h(z) = h_0 - \beta(z)$, $h_0 = h_M - h_m > 0$ and $D = -i\partial_z$. We are here using the notation and definitions for the approximation of G_0 above, with x replaced by z, see the previous chapter and [65].

The approximate operator $\mathcal{A}_{G_\kappa}(\beta)$ of (3.17) is defined heuristically as in the previous chapter, generalizing the case of constant depth. We here review that calculation.

We shall compute this modified Dirichlet-Neumann operator for a simple geometry of constant depth. The calculation is similar to the calculation of the Dirichlet-Neumann operator for a rectangular fluid domain, see [11], which is

$$\Omega(\eta) = \{(z,y) \mid z \in \mathbb{R}, -h_0 < y < \eta(x)\} \qquad (3.18)$$

The set of equations (3.14) for constant depth $-h_0$ are

$$\begin{cases} \Delta\psi(z,y) = \kappa^2\psi \text{ in } \Omega \\ \psi(z,0) = f \text{ in } \Omega \cap \Gamma_F \\ \psi_y(z,-h_0) = 0 \text{ in } \Omega \cap \Gamma_B. \end{cases} \qquad (3.19)$$

We seek expressions for the solution of the elliptic boundary-value problem (3.19) for the undisturbed case, in which the bottom is flat $\Omega(\eta)$.

Applying the Fourier transform in the $z-$variable to the set of equations (3.19), we have

$$\begin{cases} -\widehat{\Delta\psi}(\xi,y) = -\kappa^2\hat{\psi}(\xi,y), \\ \hat{\psi}(\xi,0) = \hat{f}(\xi). \end{cases} \qquad (3.20)$$

By,

$$\widehat{\Delta\psi}(\xi,y) = \widehat{\psi_{yy}}(\xi,y) + \widehat{\psi_{zz}}(\xi,y) = \kappa^2\hat{\psi}(\xi,y) \qquad (3.21)$$

and,

$$\widehat{\psi_{zz}}(\xi,y) = -\xi^2\hat{\psi}(\xi,y), \qquad (3.22)$$

we have,

$$\widehat{\psi_{yy}}(\xi,y)) = \kappa^2\hat{\psi}(\xi,y) + \xi^2\hat{\psi}(\xi,y) = (\kappa^2 + \xi^2)\hat{\psi}(\xi,y) \qquad (3.23)$$

Solving (3.23) we obtain

$$\hat{\psi}(\xi,y) = A(\xi)\sinh(\sqrt{\kappa^2 + \xi^2}y) + B(\xi)\cosh(\sqrt{\kappa^2 + \xi^2}y). \qquad (3.24)$$

Then after straightforward calculation to obtain $A(\xi)$ and $B(\xi)$ we finally obtain

$$\psi(z,y) \;\; = \;\; \int_{\mathbb{R}} \hat{f}(\xi)\frac{\cosh(\sqrt{\kappa^2 + \xi^2}(h+y))}{\cosh((\sqrt{\kappa^2 + \xi^2}h)}e^{i\xi z}d\xi, \qquad (3.25)$$

computing the partial derivative with respect to y of this expression and evaluating it at $y = 0$ we obtain the desired operator

$$\psi_y(z, 0) \;=\; \left(\int_{\mathbb{R}} \hat{f}(\xi) \sqrt{\kappa^2 + \xi^2} \tanh((\sqrt{\kappa^2 + \xi^2} h) e^{i \xi z} d\xi \right) \qquad (3.26)$$

Then the Dirichlet-Neumann operator for the modified Helmholtz operator stated in system (3.19) with κ fixed is

$$\psi_y(z, 0) \;=\; \left[\sqrt{\kappa^2 + D^2} \tanh(h \sqrt{\kappa^2 + D^2}) \right], \qquad (3.27)$$

where $iD = \partial_z$. Therefore

$$G_{\mathcal{A}_\kappa}(0) f \;=\; \left[\sqrt{\kappa^2 + D^2} \tanh(h_0 \sqrt{\kappa^2 + D^2}) \right] f. \qquad (3.28)$$

The operator $\mathcal{A}_{G_\kappa}(\beta)$ of (3.17) is then obtained from the above expression for the constant depth case ($\beta = 0$) by substituting h_0 by $h_0 - \beta(z)$ and symmetrizing, as was done in the previous chapter for the Dirichlet-Neumann operator.

Alternatively, we can consider the three dimensional analogue of the approximate Dirichlet-Neumann operator of the previous chapter of the form

$$\mathcal{A}_{G_0}(\beta) = \mathsf{Sym}[\sqrt{-\Delta} \tanh(h(z) \sqrt{-\Delta})], \qquad (3.29)$$

where Δ is the Laplacian in (x, z), and $h(z) = -h_0 + \beta(z)$, $h_m = -h_0 < 0$. We note that the depth varies only in the z direction. Eigenfunctions of the operator (3.17) of the form $f(z) e^{\pm i \kappa x}$ lead to the spectral problem for the operator $\mathcal{A}_{G_\kappa}(\beta)$ of (3.17). Thus, the ad-hoc approximation of the modified Dirichlet-Neumann in (3.17) is equivalent to a three dimensional generalization of the operator defined in the previous section. This also implies that the operator appearing in the spectral problem for longitudinal modes admits an exact representation in terms of the operators A, B of the previous chapter.

3.2 Exact results and numerical computation of transverse and longitudinal modes in bounded cross-section

Transverse and longitudinal modes can be calculated explicitly only for certain special variable-depth channel cross-sections.

In this section we compare some of exact results of Lamb [42] in *Article 261*, Macdonald [51] , Greenhill [19], Packman [58] and Groves [22] to results obtained using the nonlocal Dirichlet-Neumann operator (3.17).
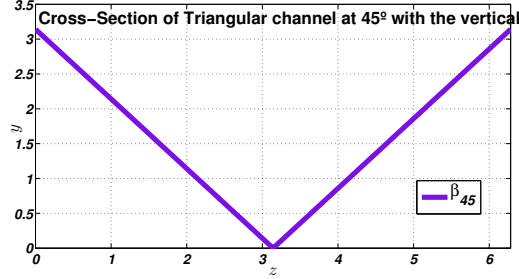
Figure 3.3: Triangular Cross-section of a straight channel see equation (3.30).

3.2.1   Transverse and longitudinal modes for triangular cross-sections

In the following we give the analytic expressions for the channel cross-section profiles that we will consider in this section.

[1.] The first geometry that we will consider corresponds of a uniform straight channel with triangular cross-section with a semivertical angle $45°$, see Figure 3.3. The cross-section $\Omega = \Omega_B$ is as in (3.1) and the bottom is at $y = \beta_{45}(z)$. The channel width is $b = 2\pi$, and the maximum depth is $h_M = \pi$. The cross-section profile is given by,

$$\beta_{45}(z) = \left\{ \begin{array}{l} -z + \pi \ \text{ in } 0 \leq z < \pi \\ z - \pi \ \text{ in } \pi \leq z \leq 2\pi \end{array} \right. , \ z \in [0, 2\pi]. \tag{3.30}$$

Normal modes for this channel were obtained by Kirchhoff, see Lamb [42], *Article 261*, and includes symmetric and antisymmteric modes.

The symmetric modes are given by the potential

$$\phi = A[\cosh(\alpha z) \cos(\beta y) + \cos(\beta z) \cosh(\alpha y)] \cos(\omega t). \tag{3.31}$$

It can be seen that ϕ is symmetric with respect to the $z = \pi$ axis. It is also a harmonic function in the quarter plane $y \geq |z|$ and satisfies the rigid wall boundary condition

$$\frac{\partial \phi}{\partial \hat{n}} = 0 \quad \text{at} \quad y = |z|. \tag{3.32}$$

To impose the boundary condition at the free surface $y = h_M$, we use (3.6) for ϕ as in (3.9) to obtain

$$\omega^2 \phi = \frac{1}{g} \frac{\partial \phi}{\partial y} \quad \text{at} \quad y = h_M. \tag{3.33}$$

Combining with (3.31) we have the conditions

$$\alpha^2 - \beta^2 = 0, \tag{3.34}$$

and

$$\omega^2 \cosh(\alpha h_M) = g\alpha \sinh(\alpha h_M), \tag{3.35}$$

$$\omega^2 \cos(\beta h_M) = -g\beta \sin(\beta h_M) = 0. \tag{3.36}$$

Hence,

$$\alpha h_M \tanh(\alpha h_M) + \beta h_M \tan(\beta h_M) = 0. \tag{3.37}$$

The values of α, β are determined by the intersections of the curves (3.34) and (3.37), see Figure 3.4a. There is an infinite number of solutions, $h_M \alpha_i$ for $i = 0, 2, 4, ...$, with $\alpha_j < \alpha_{j'}$ if $j < j'$. The corresponding frequency ω_j is given by (3.35). The first values of $h_M \alpha_i, \omega_i$ are indicated in Table 3.2.1.

To obtain the antisymmetric modes we use the potential

$$\phi = B(\sinh(\alpha z)\sin(\beta y) + \sin(\beta y)\sinh(\alpha z))\cos(\omega t). \tag{3.38}$$

We check that ϕ satisfies the rigid wall boundary conditions at $y = |y|$ and is harmonic in the quadrant $y \geq |z|$. We also check that ϕ is antisymmetric with respect to the $z = \pi$ axis. Imposing the free surface boundary conditions we obtain (3.33). Then (3.38) leads to the conditions

$$\alpha^2 - \beta^2 = 0 \tag{3.39}$$

and

$$\omega^2 \sinh(\alpha h_M) = g\alpha \cosh(\alpha h_M), \quad \omega^2 \sin(\beta h_M) = g\beta \cos(\beta h_M), \tag{3.40}$$

whence

$$\alpha h \coth(\alpha h_M) = \beta h_M \cot(\beta h_M). \tag{3.41}$$

The values of α, β are determined by the intersections of the curves (3.39) and (3.41), see Figure 3.4b. There is an infinite number of solutions, denoted $h_M \alpha_i$ for $i = 1, 3, 5...$ with $\alpha_j < \alpha_{j'}$ if $j < j'$. The corresponding computation of ω_j given by (3.40) for each case.

By (3.6) the free surface corresponding to the above symmetric and antisymmetric modes is computed by

$$\eta(z) = \frac{1}{g}\left[\frac{\partial \phi}{\partial y}\right]_{y=h_M}. \tag{3.42}$$

In Figure 3.5 and Figure 3.6 we compare the surface amplitude of the exact symmetric and antisymmetric modes found above with the surface amplitudes obtained by computing numerically the eigenfunctions of the approximate Dirichlet-Neumann operator $\mathcal{A}_{G_0}(\beta)$ of (3.12), where $h(z) = h_0 - \beta(z)$, with $h_0 = h_M - h_m$,
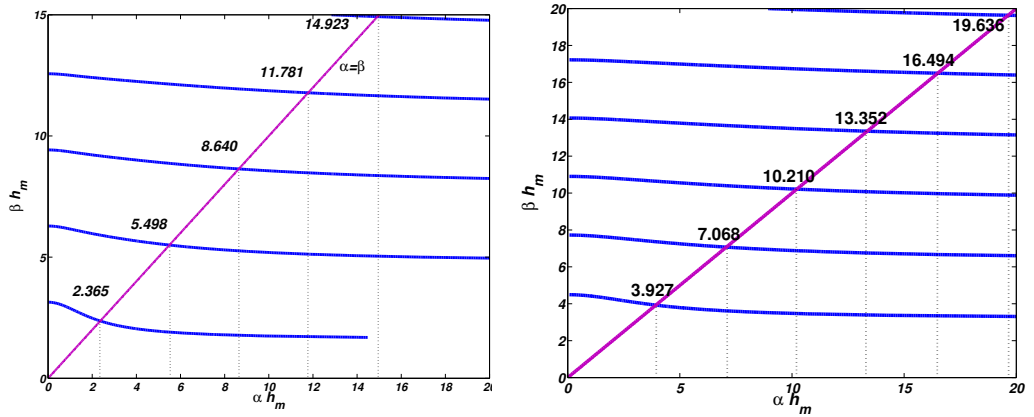
(a) Even modes   (b) Odd modes

Figure 3.4: a) Crossing points of curves (3.39) and (3.41). b) Crossing points of curves: (3.34) and (3.37).

Table 3.1: Locus of Figure 8 associated to Figure 4.

	$i = 0$	$i = 1$	$i = 2$	$i = 3$	$i = 4$	$i = 5$	$\cdots$
$\alpha_i h_M$	2.365	3.927	5.498	10.210	11.781	16.494	$\cdots$
ω_i	4.8624	7.8261	4.1413	5.6445	6.0622	7.1684	$\cdots$

This values are associate to graphic roots in Figure Figure 3.4a
and Figure 3.4b. That correspond to cross section Figure 4. with
$h_M = \pi$

$\beta(z) = \beta_{45}(z)$, see (3.30), and $z \in [0, b]$, $b = 2\pi$. The eigenfunction problem for $\mathcal{A}_{G_0}(\beta)$ is solved numerically with $2\pi-$periodic boundary conditions.

Also, given a computed eigenfunction f we obtain the corresponding surface amplitude η by $\eta = \frac{1}{g}\mathcal{A}_{G_k}(\beta)$, this is analogous to (3.42).

Figure 3.5 also sugests good quantitative agreement for the even modes. For the odd modes we see that the wave amplitudes differ at the boundary, representing the sloping beach. In particular the odd eigenvectors of $\mathcal{A}_{G_\kappa}(\beta)$ have nodes at $z = 0$, $b = 2\pi$, while the exact odd modes do not. It appears that the procedure for obtaining the exact odd modes is obtained from a flow that satisfies the rigid wall boundary condition, and it appears that they do not require of that η be defined in a fixed interval of the variable z. This leads to a more realistic motion of the surface at the sloping beach. In contrast, the odd modes of $\mathcal{A}_{G_\kappa}(\beta)$ correspond to pinned boundary conditions that are not realistic.

[2.] A second geometry with exact normal modes was considered by Macdonald [51], see also Lamb [42], *Article 261*, and corresponds to a uniform straight channel with triangular cross-section with a semivertical angle $60°$, as illustrated Figure 3.7.

We shall now consider the cross-section $\Omega = \Omega_B$, as in (3.1) and the bottom at $y = \beta_{30}$. The channel width is $b = 2\pi$ and the maximum depth maximum depth is $h_M = \frac{\pi}{\sqrt{3}}$. The cross-section profile is given by

$$\beta_{30}(z) = \begin{cases} \frac{-1}{\sqrt{3}}z + \frac{\pi}{\sqrt{3}} & \text{in } 0 \le z < \pi \\ \frac{1}{\sqrt{3}}z - \frac{\pi}{\sqrt{3}} & \text{in } \pi \le z \le 2\pi \end{cases}, \; z \in [0, 2\pi]. \tag{3.43}$$

Following Macdonald, [51], and Lamb [42] *Article 261*. The potential at $y = h_M$ for longitudinal modes with $\kappa > 0$ is given by

$$\psi = P(z)\cos(\kappa x)\cos(\omega t + \epsilon) \tag{3.44}$$

where

$$P(z) = C_0 \left\{ 1 + 2\cosh(\frac{\kappa(z - \pi)\sqrt{3}}{2}\left(\cosh\left(\frac{3\kappa h_M}{2}\right) - \frac{\omega^2}{g\kappa}\sinh\left(\frac{3\kappa h_M}{2}\right)\right)\right\}. \tag{3.45}$$

The quantities ω, h_M, and κ are related by the quadratic equation in $\frac{\omega^2}{g\kappa}$

$$2\left(\frac{\omega^2}{g\kappa}\right)^2 - 3\left(\frac{\omega^2}{g\kappa}\right)\coth\left(3\frac{\kappa h_M}{2}\right) + 1 = 0. \tag{3.46}$$

In the case where the wavelength $\frac{2\pi}{\kappa}$ is large compared with h_M we have

$$\coth\left(\frac{3\kappa h_M}{2}\right) \approx \frac{2}{3\kappa h_M}. \tag{3.47}$$
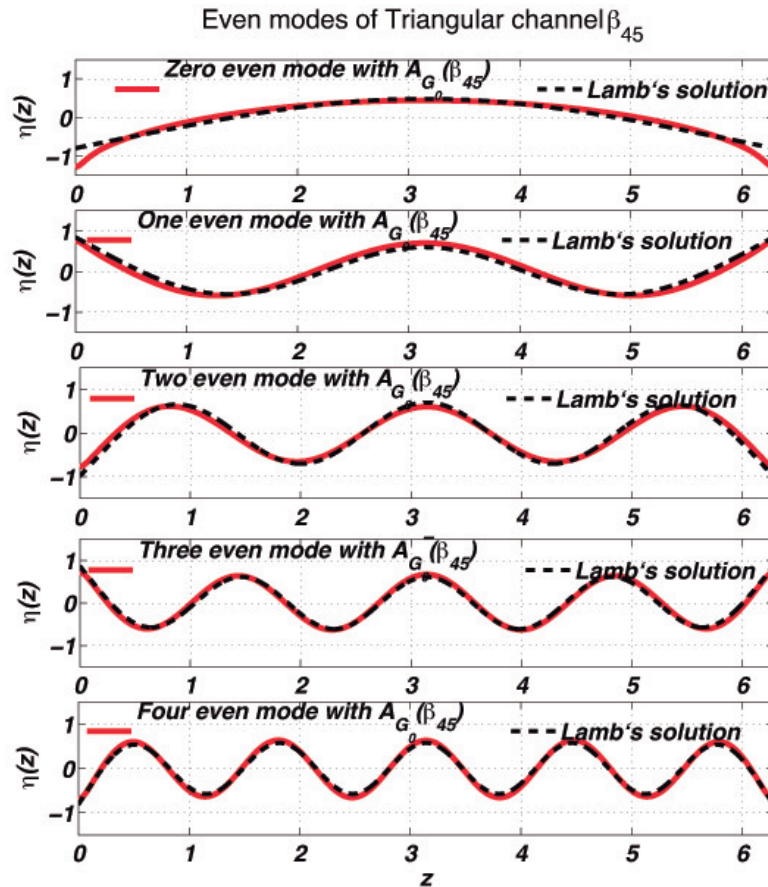
Figure 3.5: Symmetric transverse modes of a channel with triangular cross section illustrated in Figure 3.3. Red lines: operator $\mathcal{A}_{G_0}$, dashed lines: exact solutions from (3.31) and the values in Table 3.2.1.
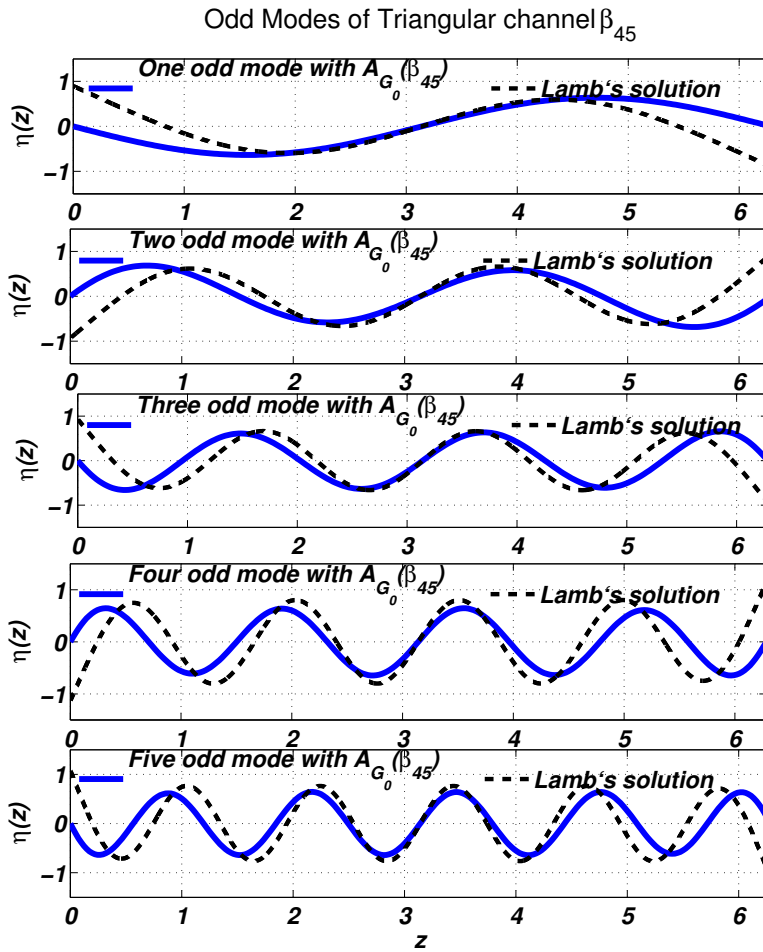
Figure 3.6: Antisymmetric transverse modes of a channel with triangular cross section illustrated in Figure 3.3. Blue lines: operator $\mathcal{A}_{G_0}$, dashed lines: exact solutions using (3.38) and the values in Table 3.2.1.
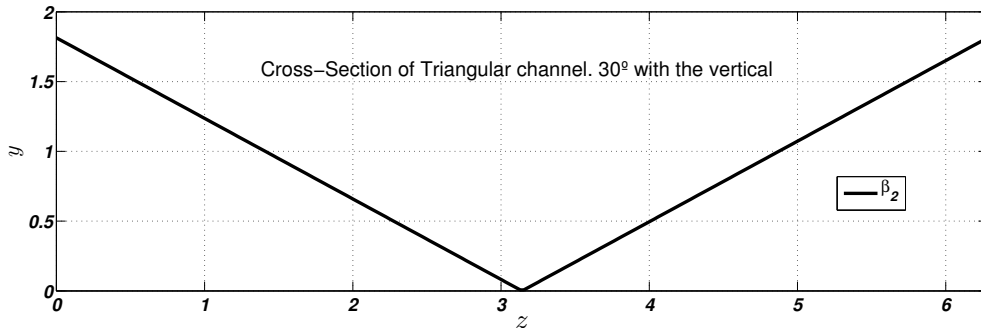
Figure 3.7: Triangular cross-section of a straight channel, see equation (3.43).
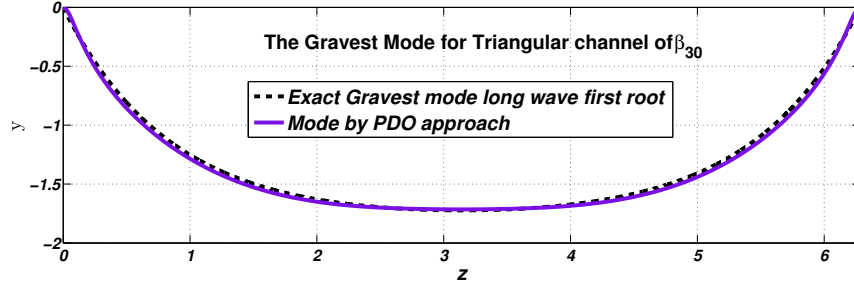
Figure 3.8: Lowest depression mode given by equation (3.48) for the triangular channel given by (3.7).

The roots of (3.46) are then approximated by

$$\frac{\omega^2}{g\kappa} = \frac{1}{2}\kappa_{r1}h_M \text{ and } \frac{\omega^2}{g\kappa_{r2}} = \frac{1}{\kappa_{r2}h_M} \tag{3.48}$$

Figure 3.8 and Figure 3.9 show elevation and depression of lowest modes given by equations (3.47) and (3.48), respectively.

This is another case for which a complete set of modes is known. They have been obtained by Packham [58] and Greenhill [19]. The work of Groves, [22], gives a complete exposition of the remaining symmetric modes described by the velocity potential. In this thesis we limit our analysis to the lowest depression and lowest elevation mode for this cross section and we use the formula of the velocity potential (3.44) presented by Lamb. The cross-section of the wave at a crest is a catenary with its lowest point in the middle of the canal.

A detailed presentation of symmetric and non-symmetric modes, as we did, for example, with the triangular cross-section at $45°$ to the vertical, can be done for this case following the same steps that we did above, but using the corresponding formulas by Groves for this case. From the accurate results we obtained from a channel whose inclined walls are open at $90°$ gives us enough confidence in the computation of these modes in the case of a channel whose inclined walls open at $120°$, as is the case for case b), should be even more accurate due to the slow variation of the bottom in this case.

3.3   Trapped modes over continental shelves profiles: comparison with shallow water theory

In this section we study waves trapped over a submarine shelf by computing longitudinal modes for two approximate models for linear water waves on the surface of fluid of variable depth. We present results for two examples modeling, respectively
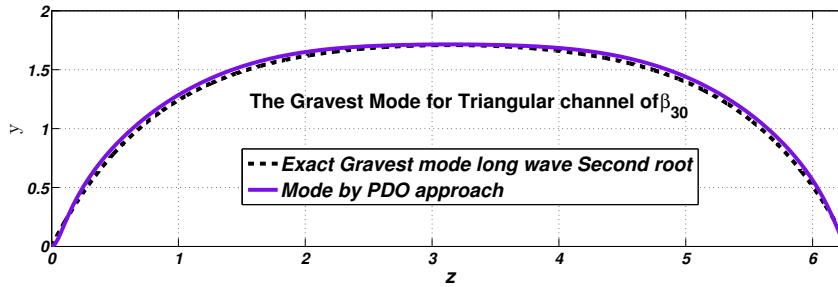
Figure 3.9: Lowest elevation mode given by equation (3.47) for the triangular channel given by (3.7).
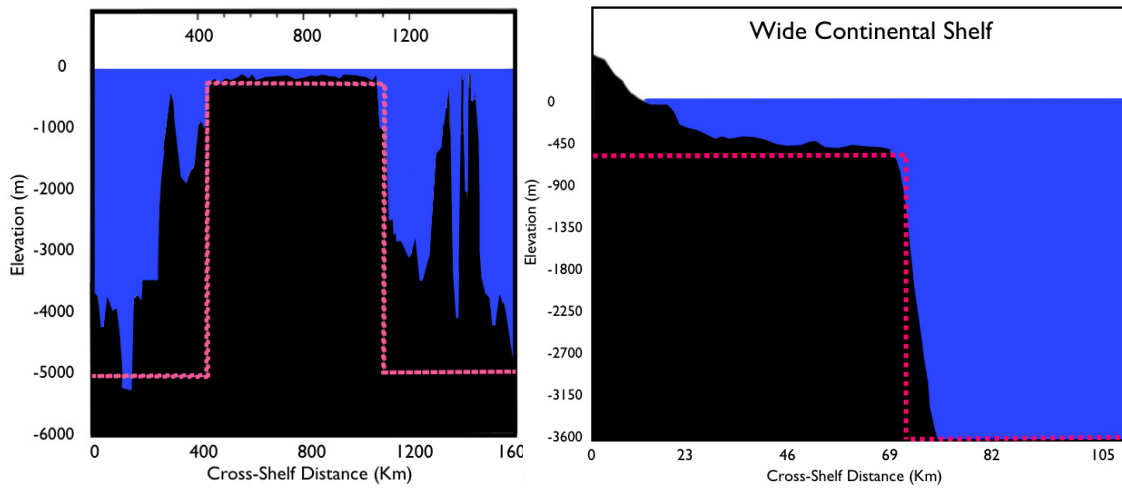
(a) Off coast of Taiwan.

(b) Coast of California.

Figure 3.10: a) Typical topographic profile (a shelf) at a distance of $50km$ off the coast of Taiwan, [43] . b) Typical topographic profile of the California coast, [52, 53]

continental shelves in the off coast of Taiwan and in the off coast of California, see J.M. Miles [53] and C.C. Mei, M. Stiassnie and D.K.P. Yue [52]. These studies consider longitudinal modes for the linearized shallow water equations in an infinite domain Ω_U, see (3.2), with a piecewise constant depth profile $\beta(z)$. The longitudinal modes can be obtained explicitly and we can enumerate all modes which decay in the transverse direction z. The second model is the linear Whitham-Boussinesq equation, whose longitudinal modes lead to the spectral problem for the modified Dirichlet-Neumann $\mathcal{A}_{G_\kappa}(\beta)$ of (3.17). The numerical eigenfunctions of this operator are compared with the trapped modes obtained for the shallow water theory of *Section* 3.1.

The continental shelves will be modeled by domains of the form Ω_U, see (3.2), with a depth that is constant in the longitudinal direction x and only depend on the transverse direction z.

The simplest model of a continental shelf is a plateau of constant minimum depth, h_2, in $a < z < 2a$ terminating in vertical cliffs at $z = a$ and $z = 2a$ plunging down to the deep ocean. Both examples we consider in this thesis are of this shape, but they have different values of a and h_2. And let h_1 the heights besides the shelf equal to the maximum fluid depth. The main interest for a study of this kind of topographies arises directly from its application to nature. We are interested in showing that acceptable results can be obtained even though the bottom slope is not moderate.

We will now state the exact parameters we are considering in each case of the idealized continental shelves.

[I.] *Shelf Off coast of California.* The first example models the continental shelf of the coast of California, following a study by Miles [53] and Mei, [52]. They use an idealized continental shelf model for the California shelf taking $h_2 = 600$m, $h_1 = 3600$m and the total shelf length as $2a = 140km$. The height at the top of the shelf as $h_2 = 1/6$, this value being appropiate for a two step approximation of the typical topographic profile off the coast of Callifornia. We rescale of these quantities for our computations, hence we consider the fluid domain with maximum depth on both sides towards the sea as $h_1 = 1$ equivalent to 3600m, and we obtain the minimum depth over the ridge as $h_2 = \frac{1}{6} = 0.1617$. The rescaled total shelf length is $2a = 12.38\pi$, see formula (3.49) for the corresponding cross-section sketched Figure 3.11.

$$\beta_{\text{Off-California}}(z) = \left\{ \begin{array}{l} 0 \text{ in } 0 \leq z < 4.81\pi, \\ 5/6 \text{ in } 4.81\pi \leq z \leq 17.19\pi, \\ 0 \text{ in } 17.19\pi \leq z < 22\pi. \end{array} \right. \qquad (3.49)$$

Notice that the cross-section profile $\beta_{\text{Off-California}}$ we have written here is the finite computation domain, this is only for numerical purposes. Neverthless this domain in theory is an infinite domain such as has been stated in *Section 3.1*.
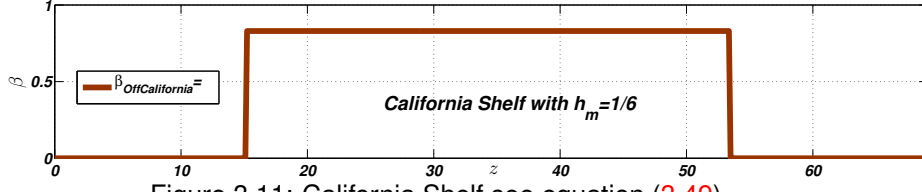
Figure 3.11: California Shelf see equation (3.49).
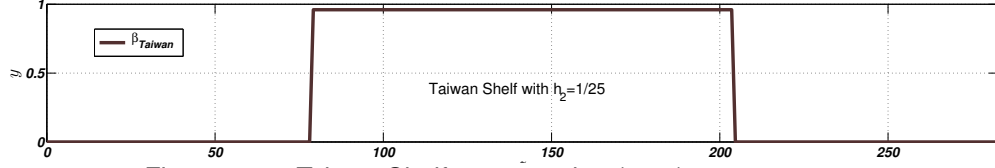
Figure 3.12: Taiwan Shelf see equation (3.50).

[II.]*Shelf Off Coast of Taiwan.* This continental shelf is located on the eastern coast of Taiwan, on the edge of the continental shelf of Asia. Out of the edge submarine slopes plunges down to the deep Pacific Ocean, at a gradient of 1:10 and the ocean reaches a depth of more than 5000 meters about 50 kilometers off the coast, as shown in Figure 3.10a. An idealized model for this shelf uses $h_2 = 80m$ on the shelf and $h_1 = 5000m$ on both sides of the ridge, the total shelf length of $2a = 650km$ is read directly from Figure 3.10a, see [43]. After rescaling for our computations we consider the fluid domain with depth $h_1 = 1$, so we get $h_2 = .0160$ over the ridge $a < z < 2a$ and the total shelf length is $2a = 130$. see formula (3.50) for the corresponding cross-section as shown Figure 3.12.

$$\beta_{\text{Off-Taiwan}}(z) = \left\{ \begin{array}{l} 0 \text{ in } 0 \leq z < 25\pi, \\ 24/25 \text{ in } 25\pi \leq z \leq 65\pi, \\ 0 \text{ in } 65\pi \leq z < 90\pi. \end{array} \right. \qquad (3.50)$$

Notice again here that the cross-section profile $\beta_{\text{Off-Taiwan}}$ written before is considering the finite computation domain, this is only for numerical purposes. Neverthless this domain in theory is an infinite domain such as has been stated in *Section 3.1*.

3.3.1 Longitudinal modes computed with pseudodifferential operator $\mathcal{A}_{G_\kappa}$ with κ fixed.

The first aim of this section is to use the discretized operator $\mathcal{A}_{G_\kappa}(\beta)$ with κ_{Max} and β fixed but, increasing the Fourier resolution of the operator. In order to do that we enlarge the number of eigenvalues and in order to keep the k_{max} constant we enlarge also the length of the domain. Keeping this proportionality we increase the density of the eigenvalues and we keep κ_{Max} constant. This allows us to study the

asymptotic behaviour of the eigenfunctions and spectra of the operator associated with the profile β_{shelf} as we increase the number of eigenvalues.

Mathematically we are doing the following. Considering $2L$, the length of the domain with $L = \pi l$. If f is a function with period $2L = 2\pi l$, its (complex) Fourier series expansion is

$$f(x) = \sum_{k=-\kappa_{Max}}^{\kappa_{Max}} c_k e^{ik\frac{\pi}{L}x} \tag{3.51}$$

with $c_k = \frac{1}{2L} \int_{-L}^{L} f(x) e^{-ik\frac{\pi}{L}x} dt$.

From this formulae (3.51) it is clear that when we consider

$$k_{Max} = 2^8, \ k_{Max} = 2^9 \text{ and } k_{Max} = 2^{10}, \tag{3.52}$$

with

$$L = \pi 2^3, \ L = \pi 2^4, \text{ and } L = \pi 2^5 \tag{3.53}$$

respectively. We obtain

$$\frac{2^8 \pi}{\pi 2^4}, \ \frac{2^9 \pi}{\pi 2^5} \text{ and } \frac{2^{10} \pi}{\pi 2^6} \tag{3.54}$$

respectively. Keeping constant the maximal exponent with $\mu = \kappa_{Max} \frac{\pi}{L} = 2^4$.

Once we apply this enlargement of the the domain for the increasing value of k_{Max} we compute numerically the eigenvectors and the eigenvalues of the operator associated with these dimensions with the aim to give some insights on the nature of these functions and to analyse its asymptotic behaviour.

We will analyse the shape of the eigenfunctions and the picture of the whole spectrum of the operator associated to these particular geometries. The goal is to determine whether or not these eigenfunctions can be associate with trapped modes or in spectral terms whether the eigenvalue of this operator belongs to the discrete or continuum spectrum.

The second aim of this section is to give some accurate insights on the solutions that we compute with the operator in order to be able to compare qualitatively and quantitatively with the exact solutions we obtain from the shallow water model using the cross-sections $\beta_{\text{Off-Calif}}$ and $\beta_{\text{Off-Taiwan}}$ given by (3.49) and (3.50), respectively. That we will compute in the next section.

We study the shelves in three different length domains illustrated in Figure 3.13. The figure shows three shelves with the same deep in $h_2 = 0.12$ but, with computational lengths of different sizes: 64π, 128π and 256π, respectively. We will denote each shelf as $\beta_{blueshelf}$, $\beta_{blackshelf}$ and $\beta_{redshelf}$, respectively
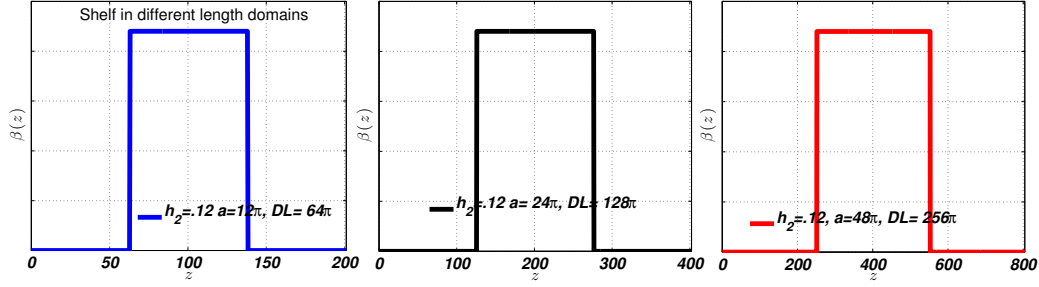
Figure 3.13: Continental shelf with $a = 12\pi$, $a = 24\pi$ and $a = 48\pi$ in different lengths domains. Blue shelf ($\beta_{blueshelf}$): Computational domain length of 64π. Black shelf ($\beta_{blackshelf}$): Computational domain length of 128π. Red shelf ($\beta_{redshelf}$): Computational domain length of 256π, (3.50).
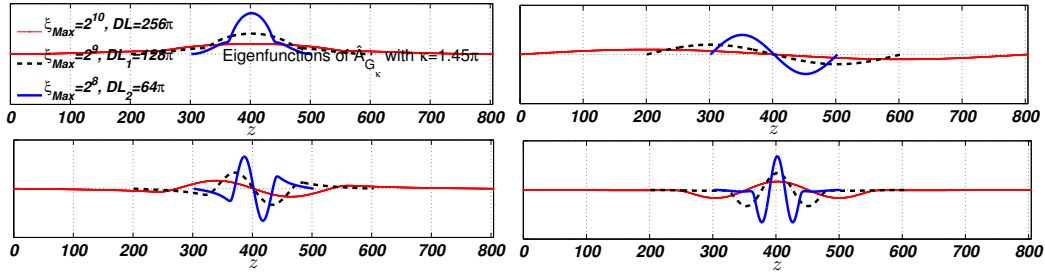
Figure 3.14: Eigenfunctions of operator $\hat{\mathcal{A}}_{G_\kappa}(\beta_{shelf})$ with $\kappa = 1.45\pi$. From the left in the top to the right in the bottom are the plots of Zero Mode (even and odd) and First mode (even and odd). Red: $\beta_{redshelf}$ in Figure 3.13. Black: $\beta_{blackshelf}$ in Figure 3.13. Blue: $\beta_{blueshelf}$ in Figure 3.13.

In Figure 3.14 and in Figure 3.15 we illustrate the first three eigenfunctions (the even and odd case for each n) of operator $\hat{\mathcal{A}}_{G_\kappa}(\beta_{shelf})$ computed for each different shelf in blue color as the name indicate are the modes obtained substituting $\beta_{blueshelf}$ in the operator, in black color are the modes obtained substituting $\beta_{blackshelf}$ in the operator and finally the same with shelf $\beta_{redshelf}$.

We point out that in each plot the eigenfunctions have the same number of flexions (thus nodes) and also all aigenfunctions decay out of the shelf.

Finally, we present the numerical spectrum of the operator $\hat{\mathcal{A}}_{G_\kappa}$ for different continental shelf profiles. In Figure 3.17 we plot the numerical spectrum of $\hat{\mathcal{A}}_{G_\kappa}(\beta_{shelf})$ for all the different shelves we have studied in this section. In the top of the figure we show the numerical spectra of $\hat{\mathcal{A}}_{G_\kappa}(\beta_{redshelf})$ using $\xi_{max} = 2^{10}$ with its associate computational domain. In the middle of the figure we show the numerical spectra of $\hat{\mathcal{A}}_{G_\kappa}(\beta_{blackshelf})$ using $\xi_{max} = 2^9$ with its associate compu-
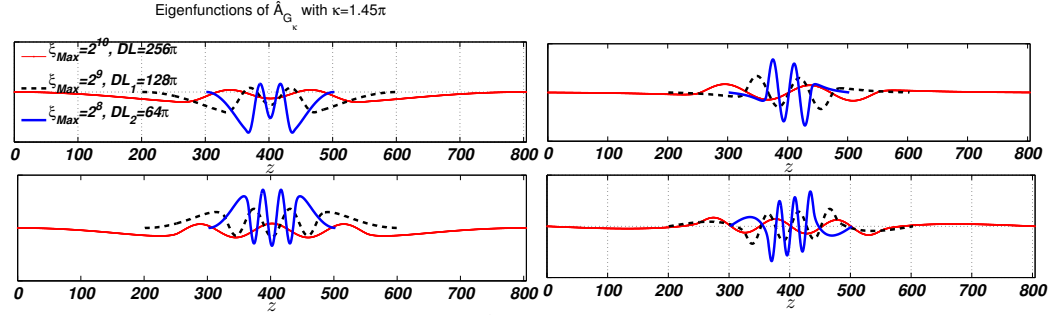
Figure 3.15: Eigenfunctions of operator $\hat{\mathcal{A}}_{G_\kappa}(\beta_{shelf})$ with $\kappa = 1.45 * pi$. From the left in the top to the right in the bottom are the plots of Second Mode (even and odd) and Third mode (even and odd). Red: $\beta_{redshelf}$ in Figure 3.13 and $\xi_{Max} = 2^{10}$. Black: $\beta_{blackshelf}$ in Figure 3.13 and $\xi_{Max} = 2^9$. Blue: $\beta_{blueshelf}$ in Figure 3.13 and $\xi_{Max} = 2^8$.

tational domain. In the bottom of the figure we show the numerical spectra of $\hat{\mathcal{A}}_{G_\kappa}(\beta_{blueshelf})$ using $\xi_{max} = 2^8$.

Broadly speaking, we see that the total spectrum of this operator includes a discrete spectrum and a continuous spectrum. It is hard to give strong conclussions from this preliminar analysis. Currently we are working on this. At this point we need more theorethical and analytical arguments to be sure about the specific nature of each element of the spectrum. The discretization of this pseudodifferential operator is very sensitive to the enlargement of the domain and a detailed analysis should be done on this behaviour before applying directly on the computation of this eigenfunctions in diferent lengths, in particular we remark two facts: i) the shape of the eigenfunction seem to have an asymptotic behavior but very slowly relative to the enlargement of the length domain. Also the hole picture that we obtain of the eigenvalues as we increase k_max and we readjust the length of the domain we do not see fixed elements of the discrete spectrum as we increase the number of eigenvalues, this is possible due because we have not try the exact factor of readjustement on the pseudo-differential operator once we increase the length domain and the size of the shelf. The aim is to use figures in Figure 3.17 and Figure 3.16 to give some insights on the behaviour of the spectra. There are many questions considering which eigenvalues correspond to the discrete spectrum of this operator and when from these spectra it is possible to clearly identify the trapped modes captured with this operator and distinguish them from the rest of the oscillatory modes corresponding to the continum spectrum.

There is a large literature on this see [48, 60, 4, 41], and it is well known that the discrete spectrum is finite for a continental shelf of finite length and it contains at least one trapped mode except in the limiting case of constant depth.
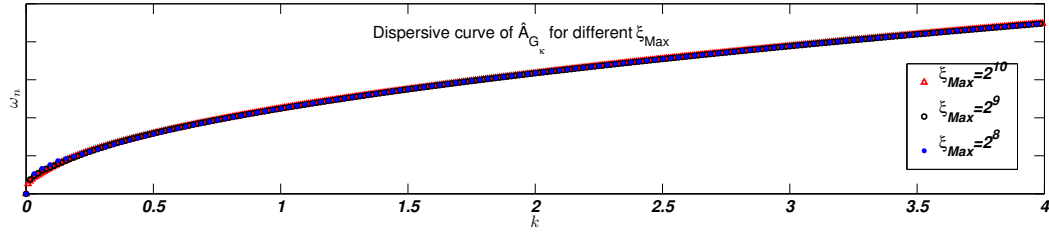
Figure 3.16: Generalized dispersive curve. Black line: $\xi_{Max} = 2^{10}$. Blue line: with $\xi_{Max} = 2^9$. Green line: with $\xi_{Max} = 2^8$.
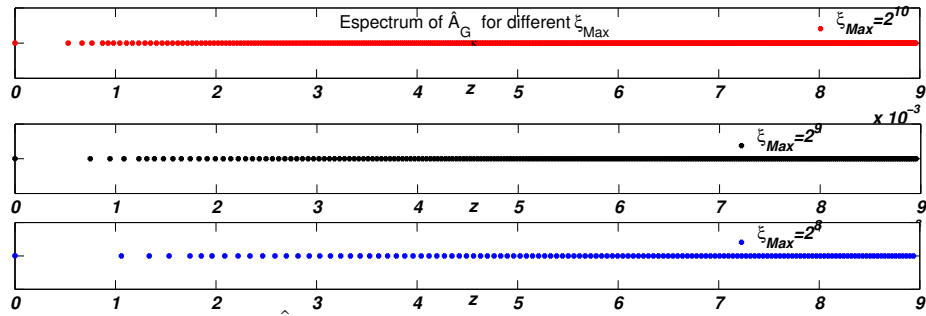
Figure 3.17: Spectra of operator $\hat{\mathcal{A}}_{G_\kappa}(\beta_{shelf})$ with $\kappa = 1.45\pi$. Top: $\beta_{redshelf}, \xi_{Max} = 2^{10}$ and computational domain 256π. Middle: $\beta_{blackshelf}, \xi_{Max} = 2^9$ and computational domain 128π. Bottom: $\beta_{blueshelf}, \xi_{Max} = 2^8$ and computational domain 64π (3.50).

3.3.2 Exact trapped modes solutions over continental shelves with shallow water theory.

The aim of this section is to give a detailed and simplified presentation of the linearized shallow water theory presented by Miles, [53], C.C. Mei et al. [52], and Lin et. al., [43].

   Before start with this presentation its convenient to motivate the relationship between our pseudodifferential approach and the shallow water theory. For that first let's examine the long wavelength limit of the operator $\mathcal{A}_{G_\kappa}(\beta)$ given in (3.17) for longitudinal modes of longitudinal wavelength κ.

   From (3.17) the symbol of $\mathcal{A}_{G_\kappa}(\beta)$

$$Sym[\sqrt{\kappa^2 + \xi^2}\tanh(h(z)\sqrt{\kappa^2 + \xi^2})], \tag{3.55}$$

where ξ is the Fourier variable for the transverse direction z. Expanding in Taylor series around $\xi = 0$ we have

$$
\begin{aligned}
Sym[\sqrt{\kappa^2 + \xi^2}\tanh(h(z)\sqrt{\kappa^2 + \xi^2})] &= Sym[\sqrt{\kappa^2 + \xi^2}h(z)\sqrt{\kappa^2 + \xi^2} + O(\xi^4)] \tag{3.56}\\
&= Sym[h(z)(\kappa^2 + \xi^2) + O(\xi^4)]. \tag{3.57}
\end{aligned}
$$

Longitudinal modes of the shallow water wave model of longitudinal wavelength κ are eigenfunctions of the lowest order operator $h(z)(-\partial_{zz} + \kappa^2)$ corresponding to the above symbol.

   Equivalently, we Taylor expand the symbol of the three dimensional approximate Dirichlet-Neumann operator of around the origin in Fourier space, keeping the lowest order terms in longitudinal and transverse Fourier variables κ and ξ respectively. Then equations at the free surface are approximated by

$$
\begin{cases}
\hat{\eta}_t(\kappa,\xi) = Sym[h(z)(\kappa^2 + \xi^2)]\hat{\phi}(\kappa,\xi)\\
\hat{\phi}_t(\kappa,\xi) = -g\hat{\eta}(\kappa,\xi)
\end{cases}
\tag{3.58}
$$

leading to

$$\eta_{tt} = gSym[h(z)(\partial_{xx} + \partial_{zz})]\eta. \tag{3.59}$$

The same equation is satisfied also by $f(x,z,t) = \phi(x,z,y,t)$ at $y = h_M$.

   The above equations are also considered by Mei [52], where shallow water equations are obtained following a different reasoning, assuming that the water motion in long waves is essentially horizontal, implying that the vertical variation is weak and the pressure is hydrostatic. One obtains

$$g\nabla \cdot (h(z)\nabla\eta) = \frac{\partial^2\eta}{\partial t^2}, \tag{3.60}$$

with $\nabla = (\partial_x, \partial_z)$, which is a hyperbolic partial differential equation with variable coefficients and the left hand side operator is symmetric.

Equation (3.60) can be expressed

$$g\nabla \cdot (h(z)\nabla\eta) \;\; = \;\; \frac{\partial^2\eta}{\partial t^2}, \tag{3.61}$$

$$g[\nabla h(z) \cdot \nabla\eta + h(z)(\nabla \cdot (\nabla\eta))] \;\; = \;\; \frac{\partial^2\eta}{\partial t^2}, \tag{3.62}$$

$$g[\partial_z(h(z)\partial_z\eta(z)) + h(z)\partial_{xx}\eta] \;\; = \;\; \frac{\partial^2\eta}{\partial t^2}, \tag{3.63}$$

We are looking for longitudinal wave solutions of the form

$$\eta(x, z, t) = V(z)\cos(\kappa x - \omega t). \tag{3.64}$$

Then substituting (3.64) on (3.61) we obtain

$$g\frac{\partial}{\partial z}\left(h(z)\frac{\partial V(z)}{\partial z}\right) + \omega^2 V(z) = h(z)\kappa^2 g V(z), \tag{3.65}$$

or

$$-\frac{\partial}{\partial z}\left(h(z)\frac{\partial V(z)}{\partial z}\right) + h(z)\kappa^2 V(z) = \frac{\omega^2}{g}V(z), \tag{3.66}$$

In further work we woul like to present an spectral analysis of this operator

$$-[\partial_z\left(h(z)\partial_z\right) - h(z)\kappa^2]V(z) = \frac{\omega^2}{g}V(z), \tag{3.67}$$

that in Fourier space with ξ the fourier variable of z its expressed as

$$\mathcal{F}\left\{-[\partial_z\left(h(z)\partial_z\right) - h(z)\kappa^2]V(z)\right\} = \mathcal{F}\left\{\frac{\omega^2}{g}V(z)\right\}, \tag{3.68}$$

$$-\mathcal{F}\left\{\partial_z h(z)\partial_z V(z)\right\} - \mathcal{F}\left\{h(z)\partial_{zz}V(z)\right\} + \mathcal{F}\left\{h(z)\kappa^2 V(z)\right\} = \mathcal{F}\left\{\frac{\omega^2}{g}V(z)\right\}, \tag{3.69}$$

$$-\mathcal{F}\left\{\partial_z h(z)\partial_z V(z)\right\} - \mathcal{F}\left\{h(z)\partial_{zz}V(z)\right\} + \kappa^2\mathcal{F}\left\{h(z)\right)V(z)\} = \frac{\omega^2}{g}\mathcal{F}\left\{V(z)\right\}, \tag{3.70}$$

$$-[\mathcal{F}\{\partial_z h(z)\} * \mathcal{F}\{\partial_z V(z)\}] - [\mathcal{F}\{h(z)\} * \mathcal{F}\{\partial_{zz} V(z)\}] \quad (3.71)$$

$$+ \quad \kappa^2[\mathcal{F}\{h(z)\} * \mathcal{F}\{V(z)\}] = \frac{\omega^2}{g}\mathcal{F}\{V(z)\}, \quad (3.72)$$

$$-[i\xi\hat{h}(\xi) * i\xi\hat{V}(\xi)] - [\hat{h}(\xi) * (i\xi)^2\hat{V}(\xi)] + \kappa^2[\hat{h}(\xi) * \hat{V}(\xi)] = \frac{\omega^2}{g}\hat{V}(\xi), \quad (3.73)$$

$$\xi^2[\hat{h}(\xi) * \hat{V}(\xi)] + \xi^2[\hat{h}(\xi) * \hat{V}(\xi)] + \kappa^2[\hat{h}(\xi) * \hat{V}(\xi)] = \frac{\omega^2}{g}\hat{V}(\xi), \quad (3.74)$$

$$2\xi^2[\hat{h}(\xi) * \hat{V}(\xi)] + \kappa^2[\hat{h}(\xi) * \hat{V}(\xi)] = \frac{\omega^2}{g}\hat{V}(\xi), \quad (3.75)$$

$$(2\xi^2 + \kappa^2)[\hat{h}(\xi) * \hat{V}(\xi)] = \frac{\omega^2}{g}\hat{V}(\xi), \quad (3.76)$$

$$[(2\xi^2 + \kappa^2)\hat{h}(\xi)] * \hat{V}(\xi) = \frac{\omega^2}{g}\hat{V}(\xi), \quad (3.77)$$

$$Op_\sigma[V](z) = \int_{\mathbb{R}} \sigma(z,\xi)\hat{V}(\xi)e^{i\xi z}d\xi. \quad (3.78)$$

In the formalism of pseudo-differential operators. The operator in (3.77) can be expressed considering a pseudodifferential operator $\mathcal{O}p_{\hat{g}}$ with symbol

$$\sigma(z,\xi) = \hat{g}(\xi) = (2\xi^2 + \kappa^2)[\hat{h}_\xi], \quad (3.79)$$

where the symbol depends only in the Fourier variable ξ.

Finally we obtain a new expression for the operator (3.77) as

$$Op_{\hat{g}}[V](z) = \mathcal{F}^{-1}(\hat{g}(\xi)\hat{V}(\xi)) = g * V \quad (3.80)$$

A discretization of this operator

$$Op_{\hat{g}}[V](z) = [(g*V)(z)] = \frac{1}{2L}\sum_{\xi\in\mathbb{Z}} \hat{g}(\xi)\hat{V}_\xi e^{i\xi\frac{\pi}{L}z}d\xi = \frac{1}{2L}\sum_{\xi\in\mathbb{Z}}(2\xi^2+\kappa^2)[\hat{h}_\xi]\hat{V}_\xi e^{i\xi\frac{\pi}{L}z}.$$
$$(3.81)$$

We also describe the Galerkin truncation of the equation (3.81). Let $J_M = 0, 1, ..., M$ and let $\hat{V}^M = (\hat{V}_1, ..., \hat{V}_M)$ and $\hat{g}^M = (\hat{g}_1, ..., \hat{g}_M)$

Assuming $h(z)$ is piece-wise constant, with

$$h(z) = \begin{cases} h_2 \text{ for } z \in [-a, a], \\ h_1 \text{ for } z \notin [-a, a]. \end{cases} \quad (3.82)$$

Then (3.67) leads to

$$gh\frac{\partial^2 V}{\partial z^2} + V\omega^2 = \kappa^2 ghV, \tag{3.83}$$

with $h = h_1$ or h_2 solved in [52] for ω fixed. At each constant depth we have

$$\frac{\partial^2 V}{\partial z^2} = (\kappa^2 - \lambda^2)V, \tag{3.84}$$

with $h = h_1$ or h_2 and $\lambda = \frac{\omega}{\sqrt{gh}}$, clearly, we have two kind of solutions:

1. *Oscillatory solutions.* Assuming $\lambda^2 \geq \kappa^2$ and denoting $\lambda^2 - \kappa^2 = \alpha^2$ we have

$$V(z) = Be^{i\alpha z} + Ce^{-i\alpha z} \text{ where } \alpha = \sqrt{\lambda^2 - \kappa^2} \tag{3.85}$$

2. *Exponentially growth/decaying solutions.* Assuming $\lambda^2 \leq \kappa^2$ and letting $\kappa^2 - \lambda^2 = \gamma^2$, we have

$$V(z) = Ae^{\gamma z} + De^{-\alpha z} \text{ where } \alpha = \sqrt{\alpha^2 - \lambda^2} \tag{3.86}$$

We then seek solutions that are oscilatory solutions on the top of the shelf and with exponential decay on both sides of the shelf. We fix the geometry designed by the constants h_1, h_2, a and ω. We will then seek k for which we can have solution η that are oscillatory at $z \in [-a, a]$, depth h_2, and decay exponentially for $z \notin [-a, a]$, depth h_1

We will assume the shelf lift over the domain $[-a, a]$.This traslation of the domain does not affect the surface profile of the trappaed wave.

In order to find the trapped wave solutions for our physical picture of trapped waves over a shelf we seek for real solutions, we assume that over the shelf the even solutions are

$$\eta(z) = f(z)\cos(\kappa x - \omega t) \tag{3.87}$$

that are oscillatory solutions on the top of the shelf and with exponential decay on both sides of the shelf. For sake of simplicity we will assume the shelf lift over the domain $-a < 0 < a$. This translation of the domain does not affect the surface profile of the trapped wave.

In order to simplify the computations and to find the trapped modes profiles, we will separate the solutions η in two cases the even solutions and the odd solutions.

For the even case

$$f(z) = B\cos(\alpha_2 z) \text{ at } z \in [-a, a] \text{ and } h(z) = h_2 \tag{3.88}$$

where

$$\alpha_2 = \sqrt{\lambda_2^2 - \kappa^2} \tag{3.89}$$

with

$$\lambda_2 = \frac{\omega}{\sqrt{gh_2}}, \tag{3.90}$$

we will also assume, that the solution attenuates to zero at infinity on either side of the ridge, as it is the nature of this kind of trapped waves solutions so,

$$f(z) = Ae^{-\gamma_1(|z|-a)} \ \text{ at } z \notin [-a, a] \text{ and } h(z) = h_1 \tag{3.91}$$

where

$$\gamma_1 = \sqrt{\kappa^2 - \lambda_1^2} \tag{3.92}$$

with

$$\lambda_1 = \frac{\omega}{\sqrt{gh_1}}, \tag{3.93}$$

The functions described above are real and even functions. The even modes can be regarded alternatively as the trapped modes on an idealized continental shelf of width a with $z = 0$ being the coastline.

For the odd case

$$f(z) = B' \sin(\alpha_2 z) \ \text{ at } z \in [-a, a] \text{ and } h(z) = h_2 \tag{3.94}$$

where $\alpha_2 = \sqrt{\lambda_2^2 - \kappa^2}$ with

$$\lambda_2 = \frac{\omega}{\sqrt{gh_2}}, \tag{3.95}$$

we will also assume, that the solution attenuates to zero at infinity on either side of the ridge, as it is the nature of this kind of trapped waves solutions so,

$$f(z) = -A'e^{-\gamma_1(|z|-a)} \ \text{ at } z \notin [-a, 0] \text{ and } h(z) = h_1 \tag{3.96}$$

and

$$f(z) = A'e^{-\gamma_1(|z|-a)} \ \text{ at } z \notin [0, a] \text{ and } h(z) = h_1 \tag{3.97}$$

where $\gamma_1 = \sqrt{\kappa^2 - \lambda_1^2}$ with

$$\lambda_1 = \frac{\omega}{\sqrt{gh_1}}, \tag{3.98}$$

The functions described above are real and odd functions.

We now want to match the boundary conditions in order to find the relation over the quantities α_2 and γ that should be accomplished. That is a restricction on the solutions we are looking for. The coefficients A (and thus B) and A' (and thus B') respectively will find later once we normalice the eigenfunctions.

Assuming continuity of η and $h(z)\frac{\partial \eta}{\partial z}$ (this condition guaranties the solution is weakly differentiable function), en each case is enough to consider the boundary matching condition only at $z = a$,

For the even case: The two equations we get are

$$B \cos(\alpha_2 a) = A \tag{3.99}$$

$$-h_2 B \alpha_2 \sin(\alpha_2 a) = -h_1 \gamma_1 A \tag{3.100}$$

Substituting the first equation into the second we find:

$$\tan(\alpha_2 a) = \frac{h_1 \gamma_1}{h_2 \alpha_2} \tag{3.101}$$

Then we obtain an equation not for the coefficient A but a constraint on the eigenvalues α_2 and γ_1

This equation cannot be solved analytically, we thus search for a solution graphically (it could be done of course numerically). To do so, we first make a change of variable, setting

$$\chi = a\sqrt{\lambda_2^2 - \kappa^2} = a\alpha_2 \tag{3.102}$$

Then we can rewrite the equation for χ

$$\tan(\chi) = \frac{\sqrt{\kappa^2 - \lambda_1^2}}{h\alpha_2}$$

It will be convenient to introduce the dimensionless parameter

$$h = \frac{h_2}{h_1} \tag{3.103}$$

and to notice that $\lambda_1^2 = h\lambda_2^2$.

Then

$$\tan(\chi) = \frac{a\sqrt{\kappa^2 - h\lambda_2^2}}{h\chi}$$

Notice that

$$a\sqrt{\kappa^2 - h\lambda_2^2} = \sqrt{a^2\kappa^2 - a^2 h\lambda_2^2} = \sqrt{a^2\kappa^2 - a^2 h\lambda_2^2 - \lambda_2^2 a^2 + \lambda_2^2 a^2} \tag{3.104}$$

$$= \sqrt{\lambda_2^2 a^2(1-h) - a^2(\lambda_2^2 - \kappa^2)} \tag{3.105}$$

$$= \sqrt{\lambda_2^2 a^2(1-h) - \chi^2} \tag{3.106}$$

Finally, equation (3.3.2) can be rewrited as,

$$\tan(\chi) = \frac{\sqrt{\chi_*^2 - \chi^2}}{h\chi}$$

setting

$$\chi_*^2 = \lambda_2^2 a^2 (1-h) = \frac{(\omega a)^2}{g h_2}(1-h). \tag{3.107}$$

Hence,

$$\cot(\chi) = \frac{h\chi}{\sqrt{\chi_*^2 - \chi^2}} \tag{3.108}$$

This is a trascendental equation for χ. To find solutions we plot both sides of equation and look for crossings.

For the odd case: The two equations we get are

$$B' \sin(\alpha_2 a) = A' \tag{3.109}$$

$$h_2 B' \alpha_2 \cos(\alpha_2 a) = -h_1 \gamma_1 A' \tag{3.110}$$

Substituting the first equation into the second we find:

$$\cot(\alpha_2 a) = -\frac{h_1 \gamma_1}{h_2 \alpha_2} \tag{3.111}$$

Again, this equation cannot be solved analytically, we thus search for a solution graphically. To do so, applied the same change of variable in (3.102) using also the identities in (3.103) for λ_1 and (3.103) we can rewrite the equation for χ Finally equation (3.111) can be rewrited as,

$$\tan(\chi) = -\frac{h\chi}{\sqrt{\chi_*^2 - \chi^2}} \tag{3.112}$$

Again we get a trascendental equation for χ. To find solutions we plot both sides of equation and look for crossings.

3.3.3   Trapped modes on idealized shelves on California and Taiwan

I. Coast of California In order to get the trapped modes for this continental shelf represented in (3.11), we will consider the even modes obtained from the idealized continental shelf described by (3.49) and represented in Figure 3.18. This shelf has been studied and reported first in Mile's paper, [53], and later in Mei's book [52] . We will consider the data reported in those sources in order to compute the trapped modes profiles for the *Off Coast of California*. We find there that $\chi_* = 6.8801 \approx 2.19\pi$. From the graphic solutions showed in the lower plot of Figure 3.18 for $n = even$ it is clear that for $\chi_* = 2.9\pi$, there are three points of intersection between $y_1 = \cot(\chi)$ and (3.108); $0 < \chi_0 < \pi$, $\pi < \chi_2 < 2\pi$ and $2\pi < \chi_4 < \chi_* < 3\pi$.
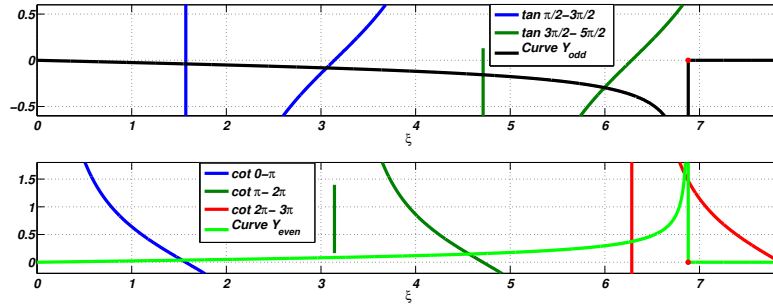
Figure 3.18: Graphic solution of roots of (3.112) and (3.108) for example I. *Off Coast of California*. Upper side, $n = odd$. Lower side $n = even$. The red spot corresponding to $\chi_* = 2.9\pi$

Table 3.2: The roots ξ_n of equation (3.108) (3.112)

	χ_0	χ_1	χ_2	χ_3	χ_4
Even	1.5327		4.5656		6.8429
Odd		3.059		5.9954	

From graphical solution in the upper plo of the same figure for $n = odd$ it is clear that for $\chi_* = 2.9\pi$ there are two points of intersection between $y_3 = \tan(\chi)$ and (3.112); $\frac{\pi}{2} < \chi_1 < \frac{3\pi}{2}$ and $\frac{3\pi}{2} < \chi_3 < \frac{5\pi}{2}$. In Table 3.2 we summarize the values χ_i obtained from he intersection of the curves.

From formulae (3.107) we have that $\omega = 0.1582$. Using formulae (3.98) and (3.95), we obtain $\lambda_1 = 0.3978$ and $\lambda_2 = 0.6225$. In Table 3.3 we summarize the eigenwavenumbers α_{2_n} that we get from formulae (3.102) for $n = 0, 1, 2, 3, 4$. We also summarize in this table each value of κ_n and γ_{1_n} that we obtain from (3.89) and (3.92) respectively. With all this data its then possible to compute the surface profile of each mode given by equations (3.87), (3.88) and (3.94). From Table 3.3 we find all the elements necessary to obtain the surface profile of the normal modes.

Finally, replacing values α_{2_n} κ_n and γ_{1_n} for $n = 0, 1, 2, 3, 4$ on $\eta(z)$ given by

Table 3.3: The eigenwavenumbers α_n associated with root χ_n of equation (3.102)

	$n = 0$	$n = 1$	$n = 2$	$n = 3$	$n = 4$
$\alpha_{2_n} = \frac{\chi_n}{a}$	0.0788	0.1573	0.2348	0.3083	0.3519
$\kappa_n = \sqrt{\lambda_2^2 - \alpha_{2_n}^2}$	0.7957	0.7840	0.7643	0.7378	0.7180
$\gamma_{1_n} = \sqrt{\kappa_n^2 - \lambda_1^2}$	0.7256	0.7128	0.6911	0.6616	0.6395

Values α_2 κ and γ_1 for $n = 0, 1, 2, 3$ and 4 associated with the *Coast of California*.

(3.58) for even and off functions profiles for

Figure 3.19 shows the surface profiles of the lowest, first, second,third and fourth mode. The nodal points for channel can be seen in this figure.. We note that the nodes for all modes are symmetric about the center of the channel. The profile for the lowest mode has no nodes and the second mode has a symmetric profile with two nodal points. The fourth mode has symmetric profile with four nodal points. The nodal points moves toward the channel walls with increasing value of n.

3.3.4   Comparison of trapped modes computed with $\mathcal{A}_{G_\kappa}$ and shallow water model

There are some remarks that we need to state before show the results:

  i In (3.17), we have fixed the wavenumer κ in order to solve the eigenvalue problem stated in *Section 3.1* to obtain the appropiate eigenfrequencies associated with each eigenfunction derived from this operator.

  ii In the analisys of Mei and stated in detail in the previous section we find that for a given eigenfrequency, i.e. fixed ω, and geometry we can find the wavenumber associate with each mode.

With this is mind and with the aim of computing modes for our operator that we can compare with the modes derived by the previous analysis, we do the following:

We have ω fixed for all modes and we know from the previous computations summarized in Table 3.3 the value of each wavenumber k_n. So, to compute *mode 0* we will compute the first eigenfunction associate with the operator with κ_0 fixed in the symbol operator. To compute *mode 1* we will compute the corresponding eigenfunction associate with the operator (3.17) with κ_1 fixed in the symbol operator. To compute *mode 2* we will compute the corresponding eigenfunction associate with the operator (3.17) with κ_2 fixed in the symbol operatorand and so on.

In Figure ((3.20)), ((3.21)), ((3.22)), ((3.23)) and ((3.24)) we show as dot-dash lines the modes computed from Mei's analysis and as a continuous blue line the eigen modes computed with the operator (3.17) with the corresponding κ_n and choosing the appropriate eigenfunction derived from the spectral analysis of this operator.

II. Off coast of Taiwan To the study of this study we will use the same estimations for χ_*, thus,ω and the dimensions of h_1, h_2 and a used in [43]. The data reported in that paper, uses $\chi_* \approx 1.618$. From the graphical solution plotted in Figure 3.19 there is only one even mode, with $\chi_0 = 1.4647$.

In analogy with the previous case **I.** once we have χ_* and using the geometry of the shelf, we can compute values $\omega = 0.0185$, $\lambda_1 = 0.0059$ and $\lambda_2 = 0.0264$.
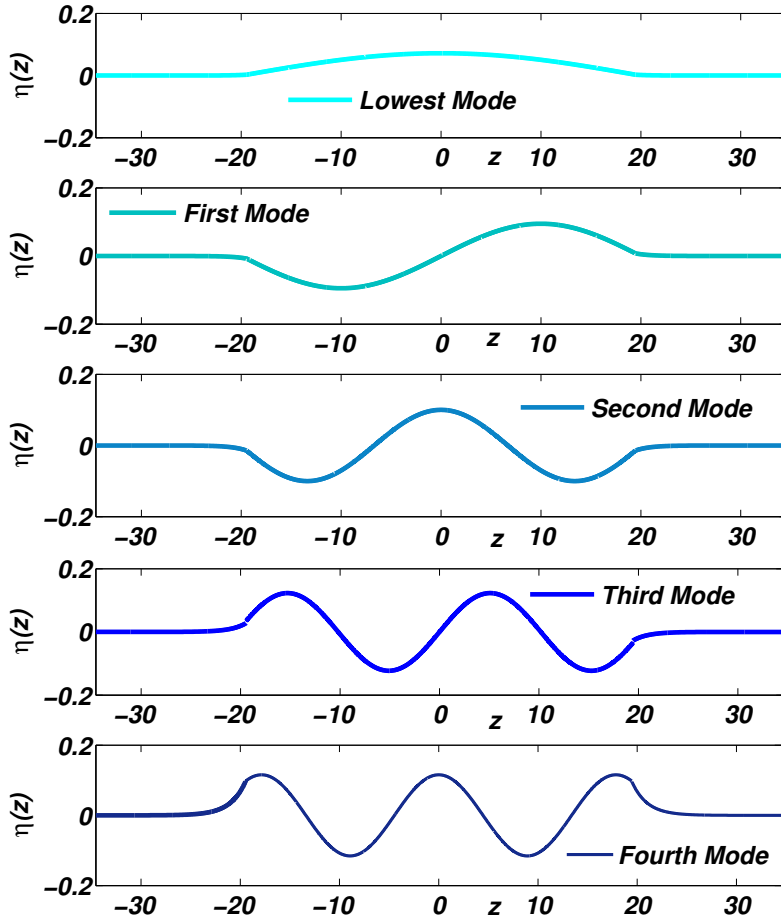
Figure 3.19: Surface profiles of trapped modes for the Coast of California given by profile (3.49) and represented in Figure 3.11. In blue line we plot the modes computed with $\mathcal{A}_{G_\kappa}(\beta_{OffCalif})$ and in dashed lines are the surface waves derived by Mei in formulas (3.87) (3.88) and (3.94)
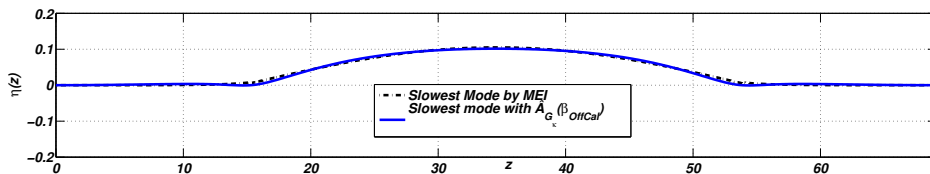
Figure 3.20: Surface profile of the slowest mode given by (3.88) and (3.91) for $n = 0$ with $\omega = 1.0220$, $\kappa_0 = 0.7957$ and $\epsilon = 0.32$. In blue line we plot the slowest mode computed with $\mathcal{A}_{G_\kappa}(\beta_{OffCalif})$

.
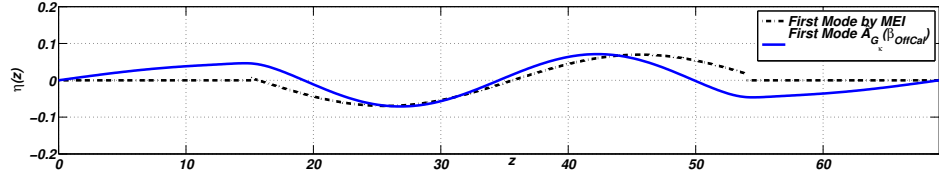
Figure 3.21: Surface profile of the first mode given by (3.94), (3.96) and (3.97) for $n = 1$ with $\kappa_2 = 0.7840$ and $\epsilon = 0.32$. In blue line we plot the first mode computed with $\mathcal{A}_{G_\kappa}(\beta_{OffCalif})$

.
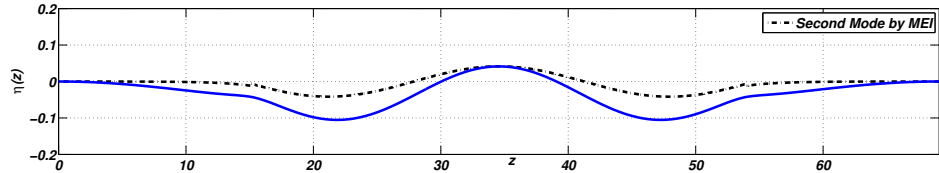
Figure 3.22: Surface profile of the second mode given by (3.88) and (3.91) for $n = 2$ with, $\kappa_2 = 0.7643$ and $\epsilon = 0.32$. In blue line we plot the second mode computed with $\mathcal{A}_{G_\kappa}(\beta_{OffCalif})$

.
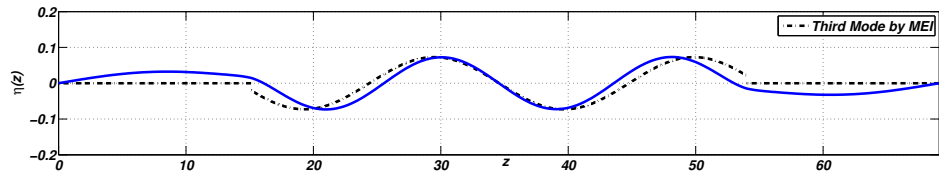
Figure 3.23: Surface profile of the third mode given by (3.94), (3.96) and (3.97) for $n = 3$, $\kappa_3 = 0.7378$ and $\epsilon = 0.32$. In blue line we plot the third mode computed with $\mathcal{A}_{G_\kappa}(\beta_{OffCalif})$

.
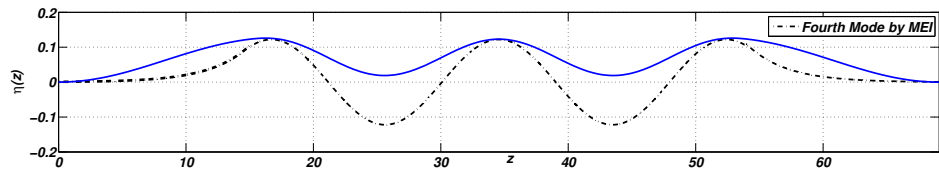
Figure 3.24: Surface profile of the fourth mode given by (3.88) and (3.91) for $n = 4$, $\kappa_4 = 0.7180$ and $\epsilon = 0.32$. In blue line we plot the fourth mode computed with $\mathcal{A}_{G_\kappa}(\beta_{OffCalif})$

.
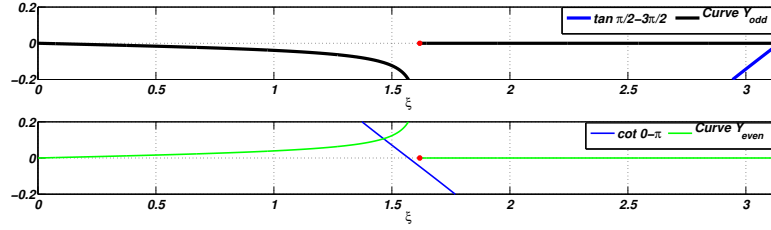
Figure 3.25: Graphic solution roots of (3.108) and (3.112) for example **II.** *Off Coast of Taiwan*. Upper side for $n = odd$. Lower side for $n = even$. The red spot corresponding to $\chi_* = 1.68$.

Table 3.4: The eigenwavenumbers α_0 associated with root ξ_0 of equation (3.102)

|	α_{2_0}	κ_0	γ_{1_0}	B_0	A_0
$n = 0$	0.0233	0.7813	0.7812	0.027	0.0057

Values associated with the *Off Coast of Taiwan.*

The Figure 3.3.4 shows the surface profile of the only mode associated for this topography.

We plot in colored and continous lines the modes computed with operator (3.13) for each continental shelf ploted in Figure 3.26 and that correspond with several idealized continental shelfs with the same length of Taiwan's shelf but with different heights.

$$\beta_{Taiwan_{h_{2_i}}}(z) = \begin{cases} 0 \text{ in } 0 \leq z < 25\pi \\ h_{2_i} \text{ in } 25\pi \leq z \leq 65\pi \\ 0 \text{ in } 65\pi \leq z < 90\pi \end{cases} \tag{3.113}$$

with $h_{2_a} = 0.86, h_{2_b} = 0.92, h_{2_c} = 0.95$, each one is a different height of the shelf.

and we compare this plots with the mode derived from equation (3.88) to (3.91) using the corresponding values ranged in Table 3.4. In this case we use this variational approach for different heights and different values for the nonlinear nondimensional parameter ϵ because the fit as we can see in Figure 3.3.4 is not as good as in the case of Case **I.**
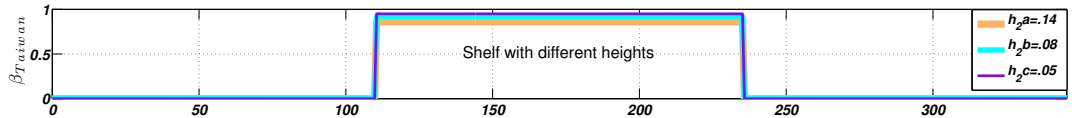
Figure 3.26: Taiwan shelf (3.50). Variational approach with different highs, and considering $\epsilon = 0.0185$
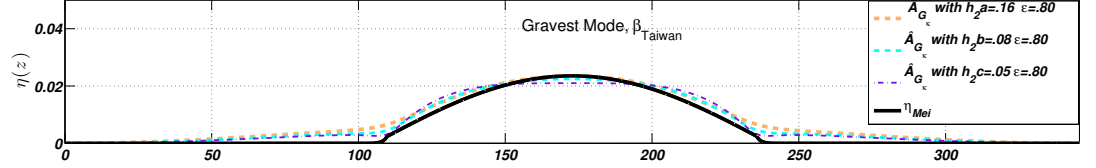
Figure 3.27: In colored and doted lines are the Gravest Mode computed with operator $\hat{\mathcal{A}}_{G_\kappa}$. In black and continuos line is the Gravest Mode using equations (3.88) and (3.91).

Appendix A

The aim of this appendix is to present the self-adjoint operaytor associated with the discretized operator $a(z, D)$ in the Fourier space. In order to do that First we compute the adjoint of operator

$$a(z, D)[f](z) = \frac{1}{2\pi} \sum_{\lambda \in \mathbb{Z}} a(z, \lambda) \hat{f}_\lambda e^{i\lambda z}. \tag{3.114}$$

following straigforward computation we obtain the adjoint of this operator as

$$\left[(a\widehat{(x, D)}f)_k \right]^* = \frac{1}{2\pi} \sum_{\lambda \in \mathbb{Z}} \hat{f}_\lambda^* \hat{a}_{k-\lambda}^*(\lambda) \tag{3.115}$$

So, the desired operator is composed using (3.117) and (3.115) as the operator $B_{k\lambda} := B$ where the fourier coefficient of this operator are defined by

$$\hat{b}_{k\lambda} = \frac{1}{4\pi} \left[\hat{a}_{k-\lambda}(\lambda) + \hat{a}_{\lambda-k}^*(k) \right] \tag{3.116}$$

Let define operator $B_{\kappa\lambda}$ as $B_{k\lambda} = \frac{1}{2}(A_{\kappa\lambda} + A_{\lambda\kappa}^*)$ where $A_{\kappa\lambda} = \frac{1}{2\pi}\hat{a}_{\kappa-\lambda}(\lambda)$ and $A_{\lambda\kappa}^* = \frac{1}{2\pi}\hat{a}_{\lambda-\kappa}^*(\kappa)$ Hence $B_{\lambda k} = \frac{1}{2}(A_{\lambda k} + A_{k\lambda}^*) = \frac{1}{2}(A_{k\lambda}^* + A_{\lambda k}) = B_{k\lambda}^*$ so we get the self-adjoint operator of (3.117),

$$B[f](z) = \frac{1}{8\pi^2} \sum_{\kappa, \lambda \in \mathbb{Z}^2} \left[\hat{a}_{k-\lambda}(\lambda) + \hat{a}_{\lambda-k}^*(k) \right] \hat{f}_\lambda \tag{3.117}$$

We also describe the Galerkin truncations of operator $B_{\kappa\lambda}$. Let $I_M = -M, ..., -1, 0, 1, ...M$ where M is the cut-off of this truncatiuon. Let denote $J_M = 0, 1, ..., M$ and $\overline{J}_M = 0, -1, ..., -M$. Let $\hat{\xi}^M = (\hat{\xi}_0, ..., \hat{\xi}_M)$.

$$H_B^M = \frac{1}{8\pi^2} \sum_{[\kappa, \lambda] \in I_M \times I_M} \hat{\xi}_\kappa \hat{\xi}_\lambda^* \left[\hat{a}_{k-\lambda}(\lambda) + \hat{a}_{\lambda-k}^*(k) \right] \tag{3.118}$$

Then

$$H_B^M \;=\; \frac{1}{8\pi^2} \sum_{[k,\lambda]\in J_M^2} [\hat{\xi}_k \hat{\xi}_\lambda^* b_{\lambda k} + \hat{\xi}_k \hat{\xi}_\lambda b_{-\lambda k} + \hat{\xi}_k^* \hat{\xi}_\lambda^* b_{-\lambda k} + \hat{\xi}_k^* \hat{\xi}_\lambda b_{\lambda k}] \quad (3.119)$$

From the first summation of equation (3.119) $\sum_{[k,\lambda]\in J_M^2} \hat{\xi}_k \hat{\xi}_\lambda^* b_{\lambda k}$ we obtain the matrix B1

$$B1 = \begin{pmatrix} [\hat{a}_{0-0}(0)+\hat{a}_{0-0}^*(0)] & [\hat{a}_{1-0}(0)+\hat{a}_{0-1}^*(1)] & [\hat{a}_{2-0}(0)+\hat{a}_{0-2}^*(2)] & [\hat{a}_{3-0}(0)+\hat{a}_{0-3}^*(3)] & [\hat{a}_{4-0}(0)+\hat{a}_{0-4}^*(4)] \\ [\hat{a}_{0-1}(1)+\hat{a}_{1-0}^*(0)] & [\hat{a}_{1-1}(1)+\hat{a}_{1-1}^*(1)] & [\hat{a}_{2-1}(1)+\hat{a}_{1-2}^*(2)] & [\hat{a}_{3-1}(1)+\hat{a}_{1-3}^*(3)] & [\hat{a}_{4-1}(1)+\hat{a}_{1-4}^*(4)] \\ [\hat{a}_{0-2}(2)+\hat{a}_{2-0}^*(0)] & [\hat{a}_{1-2}(2)+\hat{a}_{2-1}^*(1)] & [\hat{a}_{2-2}(2)+\hat{a}_{2-2}^*(2)] & [\hat{a}_{3-2}(2)+\hat{a}_{2-3}^*(3)] & [\hat{a}_{4-2}(2)+\hat{a}_{2-4}^*(4)] \\ [\hat{a}_{0-3}(3)+\hat{a}_{3-0}^*(0)] & [\hat{a}_{1-3}(3)+\hat{a}_{3-1}^*(1)] & [\hat{a}_{2-3}(3)+\hat{a}_{3-2}^*(2)] & [\hat{a}_{3-3}(3)+\hat{a}_{3-3}^*(3)] & [\hat{a}_{4-3}(3)+\hat{a}_{3-4}^*(4)] \\ [\hat{a}_{0-4}(4)+\hat{a}_{4-0}^*(0)] & [\hat{a}_{1-4}(4)+\hat{a}_{4-1}^*(1)] & [\hat{a}_{2-4}(4)+\hat{a}_{4-2}^*(2)] & [\hat{a}_{3-4}(4)+\hat{a}_{4-3}^*(3)] & [\hat{a}_{4-4}(4)+\hat{a}_{4-4}^*(4)] \end{pmatrix}$$

$$HB1 = (\hat{\xi}_1,\hat{\xi}_2,\hat{\xi}_3,\hat{\xi}_4) \begin{pmatrix} [\hat{a}_0(0)+\hat{a}_0^*(0)] & [\hat{a}_1(0)+\hat{a}_1(1)] & [\hat{a}_2(0)+\hat{a}_2(2)] & [\hat{a}_3(0)+\hat{a}_3(3)] & [\hat{a}_4(0)+\hat{a}_4(4)] \\ [\hat{a}_1^*(1)+\hat{a}_1^*(0)] & [\hat{a}_0(1)+\hat{a}_0^*(1)] & [\hat{a}_1(1)+\hat{a}_1(2)] & [\hat{a}_2(1)+\hat{a}_2(3)] & [\hat{a}_3(1)+\hat{a}_3(4)] \\ [\hat{a}_2^*(2)+\hat{a}_2^*(0)] & [\hat{a}_1^*(2)+\hat{a}_1^*(1)] & [\hat{a}_0(2)+\hat{a}_0^*(2)] & [\hat{a}_1(2)+\hat{a}_1(3)] & [\hat{a}_2(2)+\hat{a}_2(4)] \\ [\hat{a}_3^*(3)+\hat{a}_3^*(0)] & [\hat{a}_2^*(3)+\hat{a}_2^*(1)] & [\hat{a}_1^*(3)+\hat{a}_1^*(2)] & [\hat{a}_0(3)+\hat{a}_0^*(3)] & [\hat{a}_1(3)+\hat{a}_1(4)] \\ [\hat{a}_4^*(4)+\hat{a}_4^*(0)] & [\hat{a}_3^*(4)+\hat{a}_3^*(1)] & [\hat{a}_2^*(4)+\hat{a}_2^*(2)] & [\hat{a}_1^*(4)+\hat{a}_1^*(3)] & [\hat{a}_0(4)+\hat{a}_0^*(4)] \end{pmatrix} \begin{pmatrix} \hat{\xi}_1^* \\ \hat{\xi}_2^* \\ \hat{\xi}_3^* \\ \hat{\xi}_4^* \end{pmatrix}$$

From the second summation of equation (3.119)

$$\sum_{[k,\lambda]\in J_M^2} \hat{\xi}_k \hat{\xi}_\lambda b_{-\lambda k}$$

we obtain the matrix $B2$

$$B2 = \begin{pmatrix} [\hat{a}_{0+0}^*(0)+\hat{a}_{0+0}^*(0)] & [\hat{a}_{1+0}^*(0)+\hat{a}_{0+1}^*(-1)] & [\hat{a}_{2+0}^*(0)+\hat{a}_{0+2}^*(-2)] & [\hat{a}_{3+0}^*(0)+\hat{a}_{0+3}^*(-3)] & [\hat{a}_{4+0}^*(0)+\hat{a}_{0+4}^*(-4)] \\ [\hat{a}_{0+1}^*(1)+\hat{a}_{1+0}^*(0)] & [\hat{a}_{1+1}^*(1)+\hat{a}_{1+1}^*(-1)] & [\hat{a}_{2+1}^*(1)+\hat{a}_{1+2}^*(-2)] & [\hat{a}_{3+1}^*(1)+\hat{a}_{1+3}^*(-3)] & [\hat{a}_{4+1}^*(1)+\hat{a}_{1+4}^*(-4)] \\ [\hat{a}_{0+2}^*(2)+\hat{a}_{2+0}^*(0)] & [\hat{a}_{1+2}^*(2)+\hat{a}_{2+1}^*(-1)] & [\hat{a}_{2+2}^*(2)+\hat{a}_{2+2}^*(-2] & [\hat{a}_{3+2}^*(2)+\hat{a}_{2+3}^*(-3)] & [\hat{a}_{4+2}^*(2)+\hat{a}_{2+4}^*(-4)] \\ [\hat{a}_{0+3}^*(3)+\hat{a}_{3+0}^*(0)] & [\hat{a}_{1+3}^*(3)+\hat{a}_{3+1}^*(-1)] & [\hat{a}_{2+3}^*(3)+\hat{a}_{3+2}^*(-2)] & [\hat{a}_{3+3}^*(3)+\hat{a}_{3+3}^*(-3)] & [\hat{a}_{4+3}^*(3)+\hat{a}_{3+4}^*(-4)] \\ [\hat{a}_{0+4}^*(4)+\hat{a}_{4+0}^*(0)] & [\hat{a}_{1+4}^*(4)+\hat{a}_{4+1}^*(-1)] & [\hat{a}_{2+4}^*(4)+\hat{a}_{4+2}^*(-2)] & [\hat{a}_{3+4}^*(k)+\hat{a}_{4+3}^*(-3)] & [\hat{a}_{4+4}^*(4)+\hat{a}_{4+4}^*(-4)] \end{pmatrix}$$

$$HB2 = (\hat{\xi}) \begin{pmatrix} [\hat{a}_0^*(0)+\hat{a}_0^*(0)] & [\hat{a}_1^*(0)+\hat{a}_1^*(-1)] & [\hat{a}_2^*(0)+\hat{a}_2^*(-2)] & [\hat{a}_3^*(0)+\hat{a}_3^*(-3)] & [\hat{a}_4^*(0)+\hat{a}_4^*(-4)] \\ [\hat{a}_1^*(1)+\hat{a}_1^*(0)] & [\hat{a}_2^*(1)+\hat{a}_2^*(-1)] & [\hat{a}_3^*(1)+\hat{a}_3^*(-2)] & [\hat{a}_4^*(1)+\hat{a}_4^*(-3)] & [0 \\ [\hat{a}_2^*(2)+\hat{a}_2^*(0)] & [\hat{a}_3^*(2)+\hat{a}_3^*(-1)] & [\hat{a}_4^*(2)+\hat{a}_4^*(-2] & 0 & 0 \\ [\hat{a}_3^*(3)+\hat{a}_3^*(0)] & [\hat{a}_4^*(3)+\hat{a}_4^*(-1)] & 0 & 0 & 0 \\ [\hat{a}_4^*(4)+\hat{a}_4^*(0)] & 0 & 0 & 0 & 0 \end{pmatrix} \begin{pmatrix} \hat{\xi}_1 \\ \hat{\xi}_2 \\ \hat{\xi}_3 \\ \hat{\xi}_4 \end{pmatrix}$$

From the third summation of equation (3.119) $\sum_{[k,\lambda]\in J_M^2} \hat{\xi}_k^* \hat{\xi}_\lambda^* b_{-\lambda k}$ we obtain the matrix $B3$

$$HB3 = \begin{pmatrix} [\hat{a}_{0+0}(0)+\hat{a}_{0+0}(0)] & [\hat{a}_{1+0}(0)+\hat{a}_{0+1}(1)] & [\hat{a}_{2+0}(0)+\hat{a}_{0+2}(2)] & [\hat{a}_{3+0}(0)+\hat{a}_{0+3}(3)] & 0 \\ [\hat{a}_{0+1}(-1)+\hat{a}_{1+0}(0)] & [\hat{a}_{1+1}(-1)+\hat{a}_{1+1}(1)] & [\hat{a}_{2+1}(-1)+\hat{a}_{1+2}(2)] & [\hat{a}_{3+1}(-1)+\hat{a}_{1+3}(3)] & 0 \\ [\hat{a}_{0+2}(-2)+\hat{a}_{2+0}(0)] & [\hat{a}_{1+2}(-2)+\hat{a}_{2+1}(1)] & [\hat{a}_{2+2}(-2)+\hat{a}_{2+2}(2)] & 0 & 0 \\ [\hat{a}_{0+3}(-3)+\hat{a}_{3+0}(0)] & [\hat{a}_{1+3}(-3)+\hat{a}_{3+1}(1)] & 0 & 0 & 0 \\ 0 & 0 & 0 & 0 \end{pmatrix}$$

$$HB3 = (\hat{\xi}^*) \begin{pmatrix} [\hat{a}_0(0)+\hat{a}_0(0)] & [\hat{a}_1(0)+\hat{a}_1(1)] & [\hat{a}_2(0)+\hat{a}_2(2)] & [\hat{a}_3(0)+\hat{a}_3(3)] & 0 \\ [\hat{a}_1(-1)+\hat{a}_1(0)] & [\hat{a}_2(-1)+\hat{a}_2(1)] & [\hat{a}_3(-1)+\hat{a}_3(2)] & [\hat{a}_4(-1)+\hat{a}_4(3)] & 0 \\ [\hat{a}_2(-2)+\hat{a}_2(0)] & [\hat{a}_3(-2)+\hat{a}_3(1)] & [\hat{a}_4(-2)+\hat{a}_4(2)] & 0 & 0 \\ [\hat{a}_3(-3)+\hat{a}_3(0)] & [\hat{a}_4(-3)+\hat{a}_4(1)] & 0 & 0 & 0 \\ 0 & 0 & 0 & 0 \end{pmatrix} \begin{pmatrix} \hat{\xi}_1^* \\ \hat{\xi}_2^* \\ \hat{\xi}_3^* \\ \hat{\xi}_4^* \end{pmatrix}$$

From the fourth summation of equation (3.119) $\sum\limits_{[k,\lambda]\in J_M^2} \hat{\xi}_k^* \hat{\xi}_\lambda b_{\lambda k}$ we obtain the matrix $B4$

$$B4 = \begin{pmatrix} [\hat{a}_{0+0}(0) + \hat{a}_{0+0}^*(0)] & [\hat{a}_{-1+0}(0) + \hat{a}_{0+1}^*(-1)] & [\hat{a}_{-2+0}(0) + \hat{a}_{0+2}^*(-2)] & [\hat{a}_{-3+0}(0) + \hat{a}_{0+3}^*(-3)] & [\hat{a}_{-4+0}(0) + \hat{a}_{0+}^* \\ [\hat{a}_{0+1}(-1) + \hat{a}_{-1+0}^*(0)] & [\hat{a}_{-1+1}(-1) + \hat{a}_{-1+1}^*(-1)] & [\hat{a}_{-2+1}(-1) + \hat{a}_{-1+2}^*(-2)] & [\hat{a}_{-3+1}(-1) + \hat{a}_{-1+3}^*(-3)] & [\hat{a}_{-4+1}(-1) + \hat{a}_{-1}^* \\ [\hat{a}_{0+2}(-2) + \hat{a}_{-2+0}^*(0)] & [\hat{a}_{-1+2}(-2) + \hat{a}_{-2+1}^*(-1)] & [\hat{a}_{-2+2}(-2) + \hat{a}_{-2+2}^*(-2)] & [\hat{a}_{-3+2}(-2) + \hat{a}_{-2+3}^*(-3)] & [\hat{a}_{-4+2}(-2) + \hat{a}_{-2}^* \\ [\hat{a}_{0+3}(-3) + \hat{a}_{-3+0}^*(0)] & [\hat{a}_{-1+3}(-3) + \hat{a}_{-3+1}^*(-1)] & [\hat{a}_{-2+3}(-3) + \hat{a}_{-3+2}^*(-2)] & [\hat{a}_{-3+3}(-3) + \hat{a}_{-3+3}^*(-3)] & [\hat{a}_{-4+3}(-3) + \hat{a}_{-3}^* \\ [\hat{a}_{0+4}(-4) + \hat{a}_{-4+0}^*(0)] & [\hat{a}_{-1+4}(-4) + \hat{a}_{-4+1}^*(-1)] & [\hat{a}_{-2+4}(-4) + \hat{a}_{-4+2}^*(-2)] & [\hat{a}_{-3+4}(-4) + \hat{a}_{-4+3}^*(-3)] & [\hat{a}_{-4+4}(-4) + \hat{a}_{-4}^* \end{pmatrix}$$

$$HB4 = (\hat{\xi}^*) \begin{pmatrix} [\hat{a}_0(0) + \hat{a}_0(0)] & [\hat{a}_1^*(0) + \hat{a}_1^*(-1)] & [\hat{a}_2^*(0) + \hat{a}_2^*(-2)] & [\hat{a}_3^*(0) + \hat{a}_3^*(-3)] & [\hat{a}_4^*(0) + \hat{a}_4^*(-4)] \\ [\hat{a}_1(-1) + \hat{a}_1(0)] & [\hat{a}_0(-1) + \hat{a}_0^*(-1)] & [\hat{a}_1^*(-1) + \hat{a}_1^*(-2)] & [\hat{a}_2^*(-1) + \hat{a}_2^*(-3)] & [\hat{a}_3^*(-1) + \hat{a}_3^*(-4)] \\ [\hat{a}_2(-2) + \hat{a}_2(0)] & [\hat{a}_1(-2) + \hat{a}_1(-1)] & [\hat{a}_0(-2) + \hat{a}_0^*(-2)] & [\hat{a}_1^*(-2) + \hat{a}_1^*(-3)] & [\hat{a}_2^*(-2) + \hat{a}_2^*(-4)] \\ [\hat{a}_3(-3) + \hat{a}_3(0)] & [\hat{a}_2(-3) + \hat{a}_2(-1)] & [\hat{a}_1(-3) + \hat{a}_1(-2)] & [\hat{a}_0(-3) + \hat{a}_0^*(-3)] & [\hat{a}_1^*(-3) + \hat{a}_1^*(-4)] \\ [\hat{a}_4(-4) + \hat{a}_4(0)] & [\hat{a}_3(-4) + \hat{a}_3(-1)] & [\hat{a}_2(-4) + \hat{a}_2(-2)] & [\hat{a}_1(-4) + \hat{a}_1(-3)] & [\hat{a}_0(-4) + \hat{a}_0^*(-4)] \end{pmatrix} \begin{pmatrix} \hat{\xi}_1 \\ \hat{\xi}_2 \\ \hat{\xi}_3 \\ \hat{\xi}_4 \end{pmatrix}$$

Chapter 4

Discussion and future work

I.

The operator $\mathcal{A}_{G_0} = Sym(Dtanh(h(x)D))$ offers a simple and compact approximation to the variable depth Dirichlet-Neumann operator $G_0(\beta)$. Our numerical simulations using the Whitham-Boussinesq model suggest that variable depth has significant effects on the dynamics of the long-wave model we considered. Also, the model is simple enough to motivate some further studies. For instance, [1] suggested the possibility of singularity, see Whitham [68], formation at higher amplitudes, and the existence of solitons with a cusped profile. These are features introduced by the weaker dispersion, and can be studied in the presence of stronger depth effects that could not be captured by the system of H_1 in [1]. The new Whitham-Boussinesq model can be also used to study other effects of interest in nonlinear wave equations with spatial inhomogeneity, e.g. analogues of traveling waves. On the other hand, the relevance of our model to the water wave problem is tentative. This question requires comparisons with more detailed approximations of the full system.

Another issue is the efficiency of the numerical evaluation of

$$\mathcal{A}_{G_0} = Sym(Dtanh(h(x)D)).$$

The present work did not emphasize efficiency. However the question becomes important with possible practical applications, for instance considering the three dimensional analogue of $\mathcal{A}_{G_0}$, with D replaced by $|D|$. Through *Section* 2.4 and *Appendix A* in 2.5, the evaluation of $\mathcal{A}_{G_0}$ in Fourier variables requires $O(M^2)$ operations, where M is the number of Fourier modes. The three dimensional analogue would require $O(M^4)$ operations. The cost is therefore comparable to the cost of evaluating the quadratic nonlinearity in spectral variables. The nonlinearity can, however be evaluated with $O(M \log M)$ operations using the Fast Fourier transform (and $O(M^2 \log M)$ operations in three dimensions). The structure of $\mathcal{A}_{G_0}$

does not suggest any simplification in the nodal representation. We remark, however, that the plots of the spectral truncations $\mathcal{A}_{G_0}$, e.g. in Figure 2.2, suggest that a full matrix multiplication may not be necessary, since the matrix decays rapidly away from the diagonal, especially for large wavenumbers. Thus, a scheme where we use a banded matrix up to a certain wavelength, and a diagonal matrix for larger wavelengths may give satisfactory results. A banded structure would require at most $O(MR)$ and $O(M^2R)$ operations in two and three dimensions respectively, where R would be the width of the band. This would make the cost of the evaluation of $\mathcal{A}_{G_0}$ comparable to the cost of the pseudospectral method. The number R depends on the depth variation β, e.g. its smoothness, and can be determined numerically.

Note that Guyenne and Nicholls approximate $G_0(\beta)$ in two and three dimensions using the expansion of $L(\beta)$ in powers of β, see [23, 24, 12]. The terms L_j of this expansion only involve products in space and in Fourier space, see e.g. (2.21) for L_1, and can be evaluated at a cost of $O(M\log M)$, $O(M^2\log M)$ operations in two and three dimensions, respectively. A possible drawback is the presence of higher derivatives in L_j as j increases, as and the authors P. Guyenne and D.P. Nicholls in [23, 24] and W. Craig, P. Guyenne, D.P. Nicholls and C. Sulem in [12] use high frequency truncations of the derivatives. The question of whether the particular $\mathcal{A}_{G_0}$, or other approximations of the Dirichlet-Neumann operator that avoid expansions in the depth variation, can be evaluated with an efficiency that is comparable to that of pseudospectral methods is an interesting problem for further study.

II.

The operator
$$\hat{\mathcal{A}}_{G_\kappa} = \mathsf{Sym}[\sqrt{\kappa^2 + D^2}\tanh(h(z)\sqrt{\kappa^2 + D^2})] \tag{4.1}$$

offers a simple way to compute transverse modes (with $\kappa = 0$) for classical straight channels and and trapped modes for a simplified continental shelf, that also have been studied in the literature, [19, 22, 53, 4, 42, 41, 51, 43, 52, 58].

The revealing results presented in this thesis for the geometries given by (3.30), (3.43), (3.49) and (3.50) give us enought confidence to apply the same method to other geometries.

Results presented in Figure 3.5 also sugests good quantitative agreement for the even modes. For the odd modes presented in Figure 3.6 we see that the wave amplitudes differ at the boundary, representing the sloping beach. In particular the odd eigenvectors of $\mathcal{A}_{G_\kappa}(\beta)$ have nodes at $z = 0$, $b = 2\pi$, while the exact odd modes do not. It appears that the procedure for obtaining the exact odd modes is

obtained from a flow that satisfies the rigid wall boundary condition, and it appears that they do not require of that η be defined in a fixed interval of the variable z. This leads to a more realistic motion of the surface at the sloping beach. In contrast, the odd modes of $\mathcal{A}_{G_\kappa}(\beta)$ correspond to pinned boundary conditions that are not realistic. It should be investigate an appropriate approach for odd modes in the straight channels, particularly to improve the fitting on the boundaries of the channel, one issue that we have started to explore is about the Γ and Y_0 functions.

Another issue that we have started to explore is on the discrete spectrum of the operator $\hat{\mathcal{A}}_{G_\kappa}$ with κ a fixed value. With the aim to obtain some insights on the specific nature of each mode.

In further work we woul like to present an spectral analysis of operator

$$- [\partial_z \left(h(z)\partial_z \right) - h(z)\kappa^2]V(z) = \frac{\omega^2}{g}V(z), \tag{4.2}$$

with the aim to compare the spectra of this operator with the spectra derived the operator (4.2).

The simplicity of the computation of transverse modes and trapped modes with our pseudodifferential approach motivates further studies in this field and opens the possibility to extend this pseudodifferential approach to the study of many questions concerning the existence of trapped modes and the exact number of them given any particular geometry. There are several problems relevant to oceanagraphy, ocean engineering and fluid mechanics related to the mass transport of fluid and flow in rivers, coastal regions.

There is also a large scope for the analysis of the discrete spectrum of operator (4.1) for the existence of trapped modes. All these problems are of interest in mathematics and there are many researchers working on the spectra of different kinds of coastal geometries.

In conclusion regarding the results obtained here agree with well known exact analytical solutions, shows the relevance to continue working with this pseudodifferential approach and continuing to apply this approach to water waves and other fields when this approach is an option.

Bibliography

[1] P. Aceves- Sánchez, A. A. Minzoni, and P. Panayotaros. Numerical study of a nonlocal model for water - waves with variable depth, *Wave Motion* 50(1):80-93, 2013.

[2] W. J. D. Bateman, C. Swan, P. H. Taylor. On the efficient numerical simulation of directionally spread surface water waves, *J. Comp. Phys.,* 174(1): 277-305, 2001.

[3] T. B. Benjamin, and P. J. Olver, Hamiltonian structure, symmetries and conservation laws for water waves. *Journal of Fluid Mechanics*, 125, 137-185, 1982.

[4] A. S. Bonnet, and P. Joly. Mathematical and numerical study of trapping waves. In Fifth Zntl. *Workshop on Water Waves and Floating Bodies*, pp. 25-28, 1990.

[5] L. J. F. Broer. On the Hamiltonian theory of surface waves. *Applied Scientific Research*, 29(1), 430-446 1974.

[6] R. Coifman, Y. Meyer, Nonlinear harmonic analysis and analytic dependence. Pseudodifferential operators and applications (Notre Dame, Indiana), 71-78. *Proc. Sympos. Pure Math.*, Amer. Math. Soc., Providence, RI, 43, 1985.

[7] W. Craig and M. D. Groves. Hamiltonian long-wave approximations of the water-wave problem. *Wave Motion,* 19(4):376-389, 1994.

[8] W. Craig, P. Guyenne, D. P. Nicholls and C. Sulem. Hamiltonian long-wave expansions for water waves over a rough bottom. In *Proceedings of the Royal Society of London A: Mathematical,Physical and Engineering Sciences,* volume 461, pages 839-887.The Royal Society, 2005.

[9] W. Craig and C. Sulem. Numerical simulation of gravity waves *J. Comp. Phys.,* 108(1): 73-83, 1993.

[10] W. Craig and C. Sulem. Numerical simulation of gravity waves *Journal of Computational Physics,* 108(1): 73-83, 1993.

[11] W. Craig, and M. D. Groves. Hamiltonian long-wave approximations to the water-wave problem. *Wave motion*, 19(4), 367-389, 1994.

[12] W. Craig, P. Guyenne, D.P. Nicholls and C. Sulem. Hamiltonian long-wave expansions for water waves over a rough bottom. In *Proceedings of the Royal Society of London A: Mathematical,Physical and Engineering Sciences,* volume 461, pages 839-887.The Royal Society, 2005.

[13] D. V. Evans and C. M. Linton. Sloshing frequencies. *The Quarterly Journal of Mechanics and Applied Mathematics*, 46(1), 71-87, 1993.

[14] J. W. Dold. An efficient surface-integral algorithm applied to unsteady gravity waves, *J. Comp. Phys.* 103:90-115, 1992.

[15] B. Fornberg. A numerical method for conformal mapping, *SIAM Journal on Scientific and Statistical Computing* 1(3): 386-400, 1980.

[16] C. S. Gardner. Korteweg - de Vries equation and generalizations. IV. The Korteweg - de Vries equation as a Hamiltonian system. Journal of Mathematical Physics, 12(8), 1548 - 1551 (1971).

[17] R.M. Garipov. Nonsteady waves above an underwater ridge. *Soviet Physics Doklady*, 10, p. 194, 1965.

[18] M. Gouin, G. Ducrozet and P. Ferrant, Development and validation of a highly nonlinear model for wave propagation over a variable bathymetry. In *ASME 2015 34th International Conference on Ocean, Offshore and Artic Engineering,* pages 41213-41223. American Society of Mechanical Engineers, 2015.

[19] A. G. Greenhill. Wave Motion in Hydrodynamics (Continued). *American Journal of Mathematics*, 97-112, 1887.

[20] R. Grimshaw, Edge waves: a long-wave theory for oceans of finite depth. *Journal of Fluid Mechanics*, 62:(4), 775-791, 1974.

[21] E. Van Groesen and S.R. Pudjaprasetya. Uni - directional waves over slowly varying bottom. Part I: Derivation of kdv - type of equation. *Wave Motion* 18(4): 345 - 370, 1993.

[22] M. D. Groves. Hamiltonian long-wave theory for water waves in a channel. *Quarterly journal of mechanics and applied mathematics*, 47, 367-404, 1994.

[23] P. Guyenne and D. P. Nicholls. Numerical simulations of solitary waves on plane slopes. *Mathematics and Computers in Simulation*, 69(3):269-281, 2005.

[24] P. Guyenne and D. P. Nicholls. A high-order spectral method for nonlinear water waves over moving bottom topography. *SIAM Journal on Scientific Computing*, 30(1):81-101, 2007.

[25] T. S. Haut, and M. J. Ablowitz. A reformulation and applications of interfacial fluids with a free surface. *Journal of Fluid Mechanics*, 631, 375 - 396, 2009.

[26] L. Hormander. Pseudo - differential operators. Communications on Pure and Applied Mathematics, 18(3), 501- 517, 1965.

[27] R. S. Johnson. On the development of a solitary wave moving over an uneven bottom. *Mathematical Proceedings of the Cambridge Philosophical Society,* 73, 183 -203,1973.

[28] J. T Kirby. Nonlinear, dispersive long waves in water of variable depth. *Technical report, DTIC Document*, 1996.

[29] J. J. Kohn, and L. Nirenberg. An algebra of pseudo - differential operators. Communications on Pure and Applied Mathematics, 18(1-2), 269 - 305, 1965.

[30] J. Klapp, L. D. G. Sigalotti, A. Medina, A. López, and G. Ruiz - Chavarría. Recent Advances in Fluid Dynamics with Environmental Applications. Environmental science, 2016.

[31] P. Kelland. On waves. *Philos. Trans. Roy. Soc. Edinburgh*, 7, p. 87, 1839.

[32] J. T. Kirby. Nonlinear, dispersive long waves in water of variable depth. *Technical report, DTIC Document*, 1996.

[33] D. J. Korteweg and De Vries, G. XLI. On the change of form of long waves advancing in a rectangular canal, and on a new type of long stationary waves. *The London, Edinburgh, and Dublin Philosophical Magazine and Journal of Science*, 39(240), 422-443, 1895.

[34] J. Boussinesq, Théorie de l'intumescence liquide appelée onde solitaire ou de translation se propageant dans un canal rectangulaire. *Comptes Rendus Acad. Sci* (Paris), 72, 755-759, 1871.

[35] T. B. Benjamin, J. L. Bona and J. J. Mahony. Model equations for long waves in nonlinear dispersive systems. *Philosophical Transactions of the Royal Society of London A: Mathematical, Physical and Engineering Sciences*, 272(1220), 47-78, 1972.

[36] F. Serre, Contribution à l'étude des Ã©coulements permanents et variables dans les canaux. *La Houille Blanche*, (6), 830-872, 1953.

[37] A. E. Green and P. M. Naghdi. A derivation of equations for wave propagation in water of variable depth. *Journal of Fluid Mechanics*, 78(02), 237-246, 1976.

[38] R. Camassa and D.D. Holm. An integrable shallow water equation with peaked solitons. *Physical Review Letters*, 71(11), 1661, 1993.

[39] B. B. Kadomtsev and V. I. Petviashvili. On the stability of solitary waves in weakly dispersing media. *In Sov. Phys. Dokl* (Vol. 15, No. 6, pp. 539-541), 1970.

[40] N. Kuznetsov, V. Maz'ya, and B. Vainberg. *Linear water waves: a mathematical approach.* Cambridge University Press, 2002.

[41] D. S. Kuznetsov. A spectrum perturbation problem and its applications to waves above an underwater ridge. *Siberian Mathematical Journal*, 42(4), 668-684, 2001.

[42] Lamb, H. (1932). Hydrodynamics. *Cambridge university press.*

[43] M. C. Lin, W. J. Juang and T. K. Tsay. Anomalous amplifications of semidiurnal tides along the western coast of Taiwan. *Ocean Engineering*, 28(9), 1171-1198, 2001.

[44] M. S. Longuet-Higgins. On the trapping of wave energy round islands. *Journal of Fluid Mechanics*, 29(4), 781-821, 1967.

[45] P. H. LeBlond and L. A. Mysak. Waves in the Ocean. Elsevier, Vol 20, 1981.

[46] D. Lewis, J. Marsden, R. Montgomery, and T. Ratiu, . The Hamiltonian structure for dynamic free boundary problems. *Physica D: Nonlinear Phenomena*, 18(1), 391 - 404, 1986.

[47] F. Magri. A simple model of the integrable Hamiltonian equation. *Journal of Mathematical Physics*, 19(5), 1156 - 1162, 1978.

[48] A.M. Marín, R.D. Ortíz, R. D. and P. Zhevandrov. Waves Trapped by Submerged Obstacles at High Frequencies. *Journal of Applied Mathematics*, 2007.

[49] D. Moldabayev, H. Kalisch, and D. Dutykh. The Whitham equation as a model for surface water waves, *Physica D* 309, 99-107, 2014.

[50] A. Nachbin and G.C. Papanicolaou. Water waves in shallow channels of rapidly varying depth, *Journal of Fluid Mechanics,* 241:311-332, 1992.

[51] H. M. Macdonald, Waves in canals. *Proceedings of the London Mathematical Society*, 1(1), 101-113, 1893.

[52] C. C. Mei, M. Stiassnie and D. K. P. Yue. Theory and applications of ocean surface waves: nonlinear aspects. *World scientific.* 23, 2005.

[53] J. W. Miles. Wave propagation across the continental shelf. *Journal of Fluid Mechanics*, 54(01), 63-80, 1972.

[54] J. W. Miles. On Hamilton's principle for surface waves, *Journal of Fluid Mechanics,* 83(01):153-158, 1977.

[55] A. A. Minzoni, and G. B. Whitham. On the excitation of edge waves on beaches. Journal of Fluid Mechanics, 79(02), 273-287, 1977.

[56] W. Munk, F. Snodgrass and F. Gilbert. Long waves on the continental shelf: an experiment to separate trapped and leaky modes. Journal of Fluid Mechanics, 20(4), 529-554, 1964.

[57] A. Nachbin and G. C. Papanicolaou. Water waves inshallow channels of rapidly varying depth, *Journal of Fluid Mechanics,* 241:311-332, 1992.

[58] B. A. Packham. Small-amplitude waves in a straight channel of uniform triangular cross-section. *The Quarterly Journal of Mechanics and Applied Mathematics*, 33(2), 179-187, 1980.

[59] A. C. Radder. An explicit Hamiltonian formulation of surface waves in water of finite depth, *Journal of Fluid Mechanics*, 237:435 - 455, 1992.

[60] M. I. Romero Rodríguez and P. Zhevandrov. Trapped modes and resonances for water waves over a slightly perturbed bottom. Russian Journal of Mathematical Physics, 17(3), 307-327, 2010.

[61] M. A. Shubin. Pseudodifferential operators and spectral theory (Vol. 200, No. 1). Berlin: Springer - verlag, 1987.

[62] G. G. Stokes. Report on recent researches in hydrodynamics. *Brit. Ass. Rep*, 1, 1-20, 1846.

[63] M.E. Taylor. . Pseudodifferential operators. In Partial Differential Equations II (pp. 1 - 73). Springer New York, 1996.

[64] F. Ursell. Edge waves on a sloping beach. In Proceedings of the Royal Society of London A: Mathematical, Physical and Engineering Sciences, 214:1116, 79-97, 1952.

[65] R. M. Vargas-Magaña and P. A. Panayotaros, Whitham-Boussinesq long-wave model for variable topography *Wave Motion* 65(1):156-174, 2016.

[66] J. Vint. Surface waves on limited sheets of water. *Proceedings of the London Mathematical Society*, 2(1), 1-14, 1924.

[67] J.V., Wehausen, and E-. V. Laitone. Surface waves. In Fluid Dynamics/Stromungsmechanik. Springer Berlin Heidelberg, pp. 446 - 778, 1960.

[68] G. B. Whitham, *Linear and Nonlinear Waves*, vol. 42. John Wiley & Sons, 2011.

[69] S. B. Yoon and P. L-F. Liu. A note on hamiltonian for long water waves in varying depth, *Wave Motion* 20(4):359 -370, 1994.

[70] V. E. Zakharov, Stability of periodic waves of finite amplitude on the surface of a deep fluid, *Journal of Applied Mechanics and Technical Physics,* 9(2):190-194, 1968.

[71] V. E. Zakharov, Weakly nonlinear waves on the surface of an ideal finite depth fluid, *American Mathematical Society Translations* , pages 167-197, 1998.